

PHYSIOLOGICAL CLASSIFICATION OF RETINAL GANGLION  
CELLS IN THE SALAMANDER RETINA

Dissertation  
for the award of the degree  
"Doctor rerum naturalium"  
of the Georg-August-Universität Göttingen

within the doctoral program  
Theoretical and Computational Neuroscience  
of the Georg-August University School of Science (GAUSS)

submitted by  
FERNANDO OHLWEILER ROZENBLIT

from Recife, Brazil  
Göttingen 2015

THESIS COMMITTEE

FIRST REFEREE AND SUPERVISOR

Prof. Dr. Tim Gollisch,  
*Dept. of Ophthalmology, University Medical Center Göttingen*

SECOND REFEREE

Prof. Dr. Fred Wolf,  
*Dept. of Theoretical Neurophysics,  
Max Planck Institute for Dynamics and Self-organization, Göttingen*

Dr. Robert Gütig,  
*Dept. of Theoretical Neuroscience,  
Max Planck Institute for Experimental Medicine, Göttingen*

OTHER MEMBERS OF THE EXAMINATION BOARD

Prof. Dr. Alexander Gail,  
*German Primate Center, Göttingen*

Dr. Marion Silies,  
*European Neuroscience Institute Göttingen*

Prof. Dr. Florentin Wörgötter,  
*Third Institute of Physics, Georg-August-Universität Göttingen*

Date of oral examination: 25 September 2015

AFFIDAVIT

Here I declare that my doctoral thesis entitled "Physiological Classification of Retinal Ganglion Cells in the Salamander Retina" has been written independently with no other sources or aids than quoted.

---

Fernando Ohlweiler Rozenblit  
Göttingen, July 2015



To my parents and grandparents,  
for the most important lessons in life...

*[...] it is well known that a vital ingredient of  
success is not knowing that what you're  
attempting can't be done.*

— TERRY PRATCHETT, *Equal Rites*



## ABSTRACT

---

The retina is a complex neural network, responsible for breaking down the visual scene into its distinctive features such as local contrast, motion and color. The retinal ganglion cells form the output layer of this network, and a typical vertebrate retina may contain more than 10 different ganglion cell types. These cells can be separated based on their anatomical or physiological properties, and each type is expected to relay information about distinct visual features to specific areas in the brain. Separating these channels of information is crucial for understanding how the visual scene is encoded, and much effort is put into classifying retinal ganglion cells. From the different strategies used to classify a ganglion cell, the physiological one – based on the responses of the cell to light stimulation – may be the most challenging, because physiological properties do not always discriminate between different cell types. For the salamander, previous attempts to classify retinal ganglion cells were based on their temporal filtering properties, and were successful in separating ganglion cells into coarse temporal response types. But surprisingly, only one of the types showed tiling (a mosaic arrangement) of its receptive fields. Because tiling is considered a strong signature of single cell types, I ask here whether a refined classification is possible – and whether it yields tiling by further ganglion cell types.

Spiking activity was recorded from isolated axolotl retinas using multi-electrode arrays, and more than 200 cells could be simultaneously recorded in a typical experiment. The retina was stimulated with an uncorrelated noise (white-noise) stimulus, which was used to estimate via reverse correlation the receptive field properties of the ganglion cells. Together with the autocorrelation of the spike-trains, the receptive field extent and temporal filtering properties were used to characterize the ganglion cells. While a single property did not easily distinguish between cell types, a spectral clustering algorithm was able to classify the ganglion cells into putative types based on a combination of their properties. The identified types were then matched across retinas.

At least two tiling types were consistently observed across retinas, with the remaining types showing few violations of tiling. Cell types with similar physiological properties, whose distinction would be blurred if analyzed within a single property, could be distinguished by a combination of properties. The results suggest that salamander ganglion cells can be classified when their physiological features are taken in tandem, and that tiling is a fundamental feature of ganglion cells types – also in the salamander retina.





## ACKNOWLEDGMENTS

---

I thank the members of the Gollisch lab for all the happy memories over the years: Jian Liu, Michael Weick, Norma Kühn, Vidhyasankar Krishnamoorthy, Helene Schreyer, Mohammad Khani, Sebastian Bemme, Larissa Lauterbach, Daisuke Takeshita, Omar Diaz and Christiane Westermann. Those late-night snacks were great, but the scientific discussions were even better. I learned a lot from this lab.

I also thank Tim Gollisch for the opportunity to work in his lab, and I am grateful for all the support and time you dedicated to me.

I thank the members of my thesis committee, Fred Wolf and Robert Gütig, for all the great and constructive criticism during our meetings. I also would like to thank Alexander Gail, Marion Silies and Florentin Wörgötter, for accepting to join my thesis examination board.

Many thanks to the friends I made after coming to Göttingen, whose names may be too many to fit in here, but in special to my first flatmates: Corinna, Felix, Norman, Nina and Klara, who helped me tremendously after I arrived here. To the many friends I left in Brazil. In special to Rafael Stern, for showing me that reviewing is an art.

To Mechthild and Helmuth for all the Christmas and good times together, and especially to Angelika Beneke for telling me the things I should have known (but didn't).

To my parents, Helio and Gyslaine, and grandparents, José, Dora and Therezinha, for enticing my curiosity and helping me to become who I am today.



## CONTENTS

---

1	INTRODUCTION	1
1.1	Overview of the retina . . . . .	1
1.2	A brief history of physiological classification . . . . .	3
1.2.1	Receptive fields . . . . .	4
1.2.2	Feature detection . . . . .	5
1.2.3	Physiological types and morphology . . . . .	5
1.2.4	Mosaics of functional types . . . . .	6
1.3	Aim of this study . . . . .	6
2	EXPERIMENTAL METHODS	9
2.1	Animal model . . . . .	9
2.2	Tissue preparation . . . . .	11
2.3	Recording and stimulation . . . . .	11
2.4	Spike-sorting . . . . .	13
2.4.1	Dealing with duplicate units . . . . .	15
2.5	Estimating receptive fields . . . . .	15
2.5.1	Linear-Nonlinear-Poisson Model . . . . .	16
2.5.2	Reverse correlation . . . . .	17
2.6	Decomposing the spatiotemporal receptive field . . . . .	17
2.7	Measuring direction selectivity . . . . .	19
2.8	Measuring properties of the spike-trains . . . . .	21
2.8.1	Autocorrelation of the spike-trains . . . . .	21
2.8.2	Coefficient of variation . . . . .	21
2.8.3	Local variation coefficient . . . . .	22
3	CLUSTERING	23
3.1	The clustering problem . . . . .	24
3.2	K-means . . . . .	25
3.3	Gaussian mixture . . . . .	26
3.4	Spectral clustering . . . . .	28
3.4.1	Building a similarity matrix . . . . .	29
3.4.2	Partitioning the similarity graph . . . . .	29
3.4.3	Clustering using graph partitions . . . . .	32
3.4.4	An algorithm for spectral clustering . . . . .	33
3.5	Heuristics for the number of clusters . . . . .	35
3.5.1	Gap statistic . . . . .	36
3.5.2	Akaike and Bayesian information criteria . . . . .	38
3.5.3	Eigenvalues of the graph Laplacian . . . . .	39
4	FUNCTIONAL TYPES OF RETINAL GANGLION CELLS	41

## CONTENTS

4.1	Assessing classification quality with tiling . . . . .	42
4.1.1	Measuring tiling . . . . .	43
4.1.2	Modeling a mosaic . . . . .	44
4.1.3	Normalizing distances . . . . .	46
4.2	Physiological classification of ganglion cells . . . . .	47
4.3	Features of Ganglion cells . . . . .	47
4.3.1	Autocorrelation function . . . . .	48
4.3.2	Spatiotemporal receptive field . . . . .	50
4.3.3	Receptive field size . . . . .	51
4.3.4	Temporal filters . . . . .	51
4.3.5	Combined temporal and spatial components . . . . .	52
4.4	Finding putative types . . . . .	53
4.4.1	Representing ganglion cells in a feature space . . . . .	54
4.4.2	Putative types of ganglion cells . . . . .	55
4.5	Properties of the putative types . . . . .	55
4.5.1	Sorted similarity matrix . . . . .	55
4.5.2	Receptive field properties . . . . .	57
4.5.3	Differences between the putative types . . . . .	57
4.6	Comparing three OFF types . . . . .	60
4.6.1	Differences between functional properties . . . . .	60
4.6.2	Mosaics which independently tiled the retina . . . . .	63
4.7	Homogeneity of properties in a cluster . . . . .	65
4.7.1	Regularity of the spike-trains . . . . .	65
4.7.2	Direction selectivity . . . . .	66
4.8	Comparing types across retinas . . . . .	69
4.9	Summary . . . . .	72
5	DISCUSSION . . . . .	75
5.1	Cell types in the salamander retina . . . . .	75
5.2	Scope for improvements . . . . .	77
5.3	Tiling in physiological classifications . . . . .	78
5.4	Importance of classification . . . . .	79
	BIBLIOGRAPHY . . . . .	81
	ACRONYMS . . . . .	89

## LIST OF FIGURES

---

Figure 1.1	Classes of neurons and their layers in the retina . . . . .	2
Figure 2.1	Overview of electrophysiological setup . . . . .	12
Figure 2.2	Reverse correlation . . . . .	18
Figure 2.3	Decomposed receptive field . . . . .	20
Figure 3.1	K-means . . . . .	26
Figure 3.2	Gaussian mixture . . . . .	28
Figure 3.3	Spectral clustering . . . . .	35
Figure 3.4	Similarity matrix . . . . .	36
Figure 3.5	Spectral clustering procedure . . . . .	37
Figure 4.1	Mosaics of receptive fields . . . . .	45
Figure 4.2	Normalized distance between receptive fields . . . . .	46
Figure 4.3	Spike-train autocorrelations from a single experiment . . . . .	49
Figure 4.4	Diversity of temporal filters from a single experiment . . . . .	50
Figure 4.5	Receptive field features . . . . .	52
Figure 4.6	Similarity matrix and eigenvalues of graph Laplacian . . . . .	56
Figure 4.7	Grouped cells from a single retina . . . . .	58
Figure 4.8	Matrix of classification features . . . . .	59
Figure 4.9	Comparing three similar OFF types . . . . .	61
Figure 4.10	Temporal filters from temporal white-noise . . . . .	61
Figure 4.11	Differences between three OFF types . . . . .	62
Figure 4.12	Combining clusters increases overlaps . . . . .	64
Figure 4.13	Measurements of spike-train regularity . . . . .	67
Figure 4.14	Direction selectivity . . . . .	68
Figure 4.15	Fast ON type across retinas . . . . .	69
Figure 4.16	Fast OFF types across retinas . . . . .	70
Figure 4.17	Medium OFF types across retinas . . . . .	71

## LIST OF TABLES

---

Table 4.1	Possible direction-selective types . . . . .	72
Table 4.2	Summary of observed types . . . . .	73
Table 5.1	Observed cell types and their temporal counterparts . . . . .	76



## INTRODUCTION

---

*The scientist does not study nature because it is useful to do so. He studies it because he takes pleasure in it; and he takes pleasure in it because it is beautiful.*

— HENRI POINCARÉ, *Science and Method*

Our eyes are fantastic. Unlike a camera, our eyes can see at various light levels, constantly adjusting their sensitivity to the incoming light (for review, see Hurley 2002; Dowling 1987; Rodieck 1998). The differences to a camera do not stop there, however. The eyes do not send to the brain a unique view of the world. After an image is projected onto the back of the eye, it is broken down into color, outlines, motion – all are separately relayed to the brain. These parallel views of the world are created by a very thin and delicate tissue on the back of the eye – the retina (for review, see Wässle 2004; Masland 2012).

In the retina, an image is processed via five major classes of neurons: photoreceptors, horizontal, bipolar, amacrine and ganglion cells. Together, these cell classes combine into a complex neural network which decomposes the image into its distinct components. The ganglion cells form the output layer of the retina, and are very diverse: more than ten sub-classes (or types) are described in the vertebrate retina. Because all visual information that the brain receives must originate from the ganglion cells, it is expected that each of those ganglion cell types is responsible to encode specific features of the visual scene (see Gollisch and Meister 2010), giving a distinct view of the world (see Masland 2012). Hence, to understand the features encoded by the retina, much effort has been put into classifying ganglion cells based on their anatomical or physiological properties (see, e.g., Sanes and Masland 2015).

Before moving onto the properties of ganglion cells, it is worth reviewing the organization of the retina, and how the morphology of retinal cells relates to their physiology.

### 1.1 OVERVIEW OF THE RETINA

The retina has five classes of neurons which are interconnected to decompose the visual scene. Photoreceptors are the light-sensitive cells in the retina, and encode the light level as a graded chemical signal (high glutamate when dark, low when bright). Bipolar cells process the graded signal and relay it to the ganglion cells.

INTRODUCTION

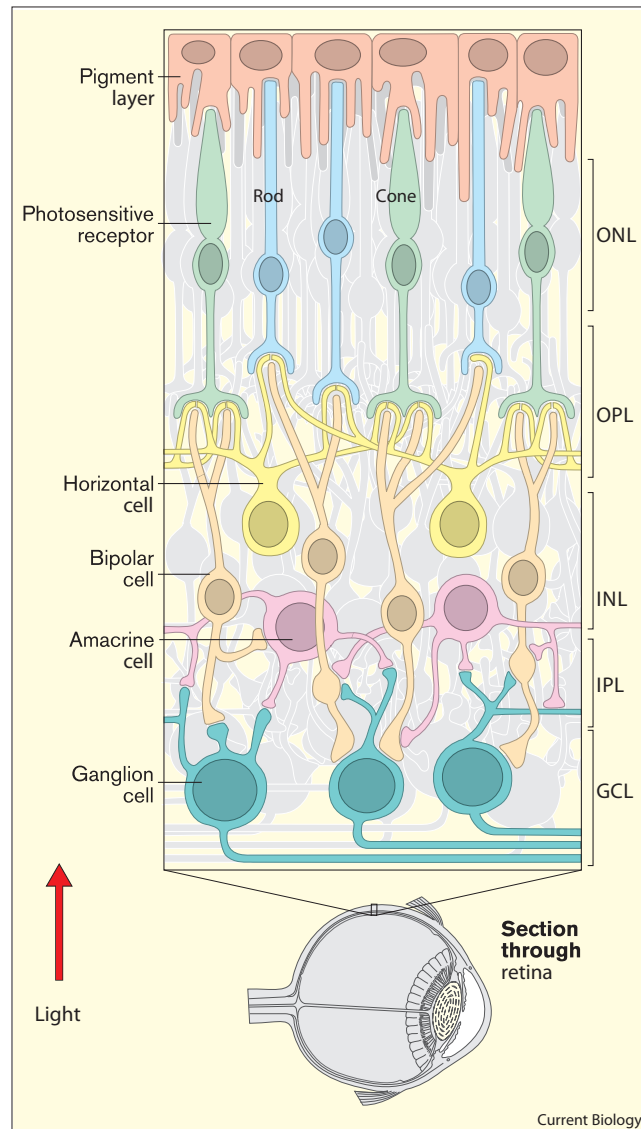


Figure 1.1: CLASSES OF NEURONS AND THEIR LAYERS IN THE RETINA. The retina is organized into either somatic (*nuclear or cell*) or synaptic (*plexiform*) layers. Photoreceptor somas are in the Outer Nuclear Layer (ONL); Synapses between photoreceptors, bipolar and horizontal cells take place in the Outer Plexiform Layer (OPL); Horizontal, bipolar and amacrine somas are in the Inner Nuclear Layer (INL); Synapses between bipolar, amacrine and ganglion cells take place in the Inner Plexiform Layer (IPL); Ganglion cells are in the Ganglion Cell Layer (GCL). Note that light enters most vertebrate retinas through the GCL. (see, e.g., Dowling 1987; Rodieck 1998)

Image: Reprinted from Current Biology, Vol. 8, Charles F. Stevens, "Neuronal diversity: Too many cell types for comfort?", R708-R710, Copyright (1998), with permission from Elsevier.



The signal from the bipolar cells is collected and compared by ganglion cells, which transmit the visual information to the brain through their axons. The remaining classes, horizontal and amacrine cells, perform lateral signaling and feedback within the retina. The retina is organized into five layers, each containing either somas or synapses.<sup>1</sup> A scheme of the organization of the retina is shown in Figure 1.1.

This simple model, however, must be adapted to the reality of the retina. To give a taste of reality, at least 12 bipolar cell types are reported in the mouse retina (Masland 2012). From those, one is a rod bipolar and eleven types are cone bipolar. Each cone bipolar can be coarsely classified into either ON or OFF bipolar. OFF bipolar cells are hyperpolarized by light, while ON bipolar cells are depolarized. The main difference between the two lies in their glutamate receptors: OFF bipolar expresses ionotropic (AMPA and kainate) receptors, while ON bipolar expresses metabotropic receptors. The axons of the bipolars terminate at the Inner Plexiform Layer, and are spatially segregated. OFF bipolars terminate closer to the Inner Nuclear Layer, while ON bipolars terminate closer to the Ganglion Cell Layer. Each different type of bipolar, however, may stratify to a different sub-layer (see, e.g., Wässle 2004). The intuition is that each bipolar already filters the visual scene in some special way: ON, OFF, transient, sustained, and so on; those channels of visual information are then provided at a specific depth in the Inner Plexiform Layer (see, e.g., Masland 2012). Ganglion cells arborize their dendrites in the Inner Plexiform Layer and are a diverse population, with 10-15 ganglion cells often reported in vertebrate retinas. Depending on their arborization, the ganglion cells will receive distinct information from the bipolar cells, and can have their response modified by amacrine cells (of which there are many types, but little is known of their effects). (see Sanes and Masland 2015)

Morphology then plays an important role for determining the response of ganglion cells. By studying their different responses, one may be able to grasp this complexity. But how to understand the responses of a ganglion cell?

## 1.2 A BRIEF HISTORY OF PHYSIOLOGICAL CLASSIFICATION

Recording from the optic nerve of an Eel, Adrian and Matthews (1927) observed an increased activity whenever light was presented or withdrawn. Because of the experimental conditions, however, they were limited to recording from many axons simultaneously. The recording of a single ganglion cell was only possible after improvements on the technique by Hartline (1938).

---

<sup>1</sup> If one is not familiar with the nomenclature, it can be hard to remember what is in each retinal layer. A tip, as seen in Rodieck (1998), is that each layer in the retina contains either cell bodies (*nuclear* or *cell* layer) or synaptic processes (*plexiform* layers). Inner layers are closer to the center of the eye, outer layers closer to the outside.

1.2.1 *Receptive fields*

Reporting on how a single fiber of the optic nerve of frogs responded to light, Hartline (1938) observed an “extreme and unmistakable” diversity, and could discern three response types: cells which responded to increments of light (ON), those that responded to decrements (OFF), and those that responded to both (ON-OFF). Hartline (1938) further observed that a cell would only respond if light was presented to a specific region on the retina – the receptive field. To account for a surrounding region that was observed to suppress the action of the receptive field center, the concept of a receptive field was extended in the cat by Kuffler (1953) (and in the frog by Barlow 1953) to include all regions which could functionally affect a ganglion cell.

To understand the effect of this surrounding region on the ganglion cell, Rodieck (1965) suggested a linear model of the receptive field, consisting of two components: an excitatory center and an inhibitory surrounding region, each independently filtering the incoming light. In this model, for each component, the pattern of light on the retina is weighted by its spatial sensitivity and convolved by its temporal response curve. The ganglion cell activity would then be determined by the combined output of center and surround.<sup>2</sup>

While studying the (spatial) contrast sensitivity of ganglion cells in the cat retina, Enroth-Cugell and Robson (1966) observed that ganglion cells responded differently to a grating pattern that varied sinusoidally along one direction in space, perpendicular to the bars. By shifting the position of this grating, some cells would not respond to presentations of the grating. This silence was assumed to happen because they linearly collected what was presented to their photoreceptors, and hence it was possible to find a position where the dark and bright segments negate each other, evoking no response from the cell. Those linear cells were referred to as X cells. Surprisingly, other cells did not sum their receptive fields linearly, and responded to the presentation of the grating at any position – those were called Y cells. This non-linearity was independent of whether the cell responded preferably to increments (ON) or decrements (OFF) of light. Later, a method to measure this non-linearity was devised by Hochstein and Shapley (1976). This suggested a division of ganglion cells in the cat retina based on non-linearity (X and Y) and polarity of response (ON, ON-OFF and OFF).

---

<sup>2</sup> Rodieck (1965) suggests that a non-linear function could account for second-order effects in the response, and observed that a supra-linear function best matches the experimental data. In the cat, using parameters of the receptive field obtained from flashing spots (Rodieck and Stone 1965a), this model was used to explain the average firing rate of cells to moving bars (Rodieck and Stone 1965b). Note also that this linear model is similar to the linear-nonlinear-Poisson model, which will be discussed in Section 2.5.1.

1.2.2 *Feature detection*

Meanwhile, evidence of more complex features in the retina started accumulating. Barlow (1953), for example, observed that the center-surround structure could aid the retina of the frog to reject useless information from the image, passing on only the features relevant for the animal behavior; that is, he suggested that the retina should be viewed as a feature detector (see also Barlow 1961). This idea was explored by Lettvin et al. (1959), who showed that the frog retina had at least four ganglion cell types which could be distinguished based on their behaviors (sustained contrast detection, net convexity detection, moving edge detection and net dimming detection).

In the rabbit, Barlow and Hill (1963) observed direction-selective units (cells which respond to a moving stimulus with a preferred direction). A survey of response types of rabbit ganglion cells by Barlow et al. (1964) showed that besides the classical receptive fields and direction-selective cells, there were cells which were selective to the speed of movement. This reinforced the idea of “trigger features”, features which a ganglion cell type would preferably encode. A more thorough survey of the rabbit retina by Levick (1967) showed a rich repertoire of feature detection: ganglion cells could now also be classified as orientation-selective, uniformity-detectors or local-edge-detectors.

1.2.3 *Physiological types and morphology*

These ganglion cells with complicated receptive fields, however, had properties which could not be accounted for by the simple center-surround model, and did not fit into either the X or the Y class. In the retina of cats, these neurons were collected into a new class, the W cells (see Stone and Fukuda 1974; Rodieck 1979).<sup>3</sup> From the X, Y and W classification, only the X and Y cells could be matched to morphological types that had been recently identified in the cat retina (Boycott and Wässle 1974). The Y cells were found to be  $\alpha$ -cells, cells with large dendritic fields, while the X cells were found to be  $\beta$ -cells, with small dendritic fields (Wässle and Boycott 1991). This correlation between morphology and physiology was strengthened by Peichl and Wässle (1981), who observed that the center of the receptive fields of Y cells matched the location of  $\alpha$ -cell somas.

In these morphological types, a curious pattern emerged. The somas of  $\alpha$ -cells were not randomly spread, but instead avoided one another, so that their dendrites resembled a mosaic (Wässle and Riemann 1978; Wässle, Peichl, et al. 1981). A similar pattern was observed for the somas of  $\beta$ -cells (Wässle, Boycott, and Illing

<sup>3</sup> Later, the W cells were found to be too diverse, and it was suggested that each distinct ganglion cell type should be named on its own. Hence, X (or brisk-sustained) and Y (brisk-transient) cells remained, but were joined by at least 10 more types (Rodieck 1979).

1981). It was not clear, however, if this spatial organization would apply to other ganglion cell types.

#### 1.2.4 *Mosaics of functional types*

Because of its regularity, this mosaic organization of cells was called tiling. Wässle and Boycott (1991) suggested that tiling was important to ensure that a population of cells in a type is equally sensitive to light spots anywhere in the retina, minimizing blind spots.

To investigate the generality of tiling, DeVries and Baylor (1997) recorded simultaneously the electrical activity from ganglion cells in a rabbit retina using a multi-electrode array. The ganglion cells were grouped according to the statistics of their spike-trains and time-courses of their mean effective stimulus (also known as spike-triggered average, see Chapter 2). From the 11 types described by DeVries and Baylor (1997), 8 of those tiled the retina.

Tiling was further observed in the monkey retina, where Field et al. (2007) grouped ganglion cells based on their response to light (mean effective stimulus). Then, they assigned the grouped cells to morphological types by comparing their light responses to those reported in the literature. They observed mosaics in at least 5 types. Using a similar method, Gauthier et al. (2009) observed that receptive fields of ganglion cells from the same type, while irregularly shaped, would organize to uniformly tile the visual space.

For the salamander, Segev et al. (2006) grouped cells by either the statistics of their spike-trains (autocorrelation functions), receptive field size or temporal properties – one at a time, because the grouping was found to be worse by combining features. Tiling was reported only when cells were classified by their temporal properties, yet for only 1 of the 5 proposed types. Segev et al. (2006) further suggested that this absence of tiling could be a property of the salamander retina, given the known redundancy in this retina (Puchalla et al. 2005).

### 1.3 AIM OF THIS STUDY

The classification of ganglion cells is important for understanding how visual information is transmitted to the brain. However, because properties which can be used for characterizing cells do not always clearly distinguish between types, the physiological classification of ganglion cells is a challenging problem. Manual classification of ganglion cells is possible (DeVries and Baylor 1997; Field et al. 2007), but does not scale as datasets grow (Stevenson and Kording 2011; Armañanzas and Ascoli 2015).

Tiling is also considered a fundamental property of retinal cell types, and is key to identify types in morphological studies (see, e.g., Cook and Chalupa 2000; Rock-

hill et al. 2000; Masland 2012). Hence, one may wonder whether the presence of a single tiling type in the salamander retina, as observed by Segev et al. (2006), comes from the classification method which was chosen or a fundamental difference in the organization of its retina.

In this thesis, I suggest an improvement on the current physiological classification of ganglion cells in the salamander retina. Using a multi-electrode array, I record simultaneously from hundreds of ganglion cells in the same retina. These ganglion cells are characterized based on a simple stimulus – an uncorrelated noise. This stimulus provides information on the ganglion cell receptive field size and temporal filtering properties, which together with the autocorrelation of spike-trains are used to characterize a ganglion cell. I investigate whether it is possible to classify retinal ganglion cells based on a combination of these features, using a spectral clustering algorithm, and if an improved classification would recover tiling from more than a single ganglion type.

In Chapter 2, I describe the experimental methods required to obtain a large enough dataset for classification and the methods used to characterize a ganglion cell. In Chapter 3, I consider different clustering techniques and their advantages and limitations. Because clustering is an involved problem in itself, I consider it separately from cell classification. In Chapter 4, I classify ganglion cells in the salamander retina, using a spectral clustering algorithm. The putative types from clustering are tested for their quality based on the homogeneity of their properties, and whether they tile. Tentative names are given to the clusters based on their properties. In Chapter 5, I compare the results from the classification shown here with previous results for the salamander, the implications of tiling for functional classification and how the retina can be used for illuminating aspects of the organization of the brain.



EXPERIMENTAL METHODS

---

*“Data! data! data!” he cried impatiently. “I can’t make bricks without clay.”*

— SIR ARTHUR CONAN DOYLE, *The Adventure of the Copper Beeches*

To classify retinal ganglion cells based on their physiology, one must first gather data from a large population of cells. Preferably, one would simultaneously record these cells to avoid variance caused, for example, by the animal development (age, diseases, or mutations), or preparation quality. One technique for recording from multiple cells is to use a multi-electrode array (MEA), which records the neuronal activity extracellularly. In this chapter, I will describe how to mount the retina on a multi-electrode array. Because it is not known a priori from which neuron a recorded spike originated, the spikes must be grouped according to the similarity of their waveforms (spike-sorting). These groupings are referred to as units and considered to contain most of the spikes originating from a single cell. Of course, this method has limitations. I will explain how these limitations affect the goal of classifying retinal ganglion cells (RGCs) and how to best overcome them. Finally, I show how to analyze properties from the recorded neurons such as their receptive field dynamics, direction selectivity and temporal structure of their spike-trains. These properties will be important for classifying as well as evaluating the possible retinal ganglion cell types.

## 2.1 ANIMAL MODEL

For the experiments in this thesis, isolated retinas from axolotl salamanders (*Ambystoma mexicanum*, pigmented wild type) were used. The axolotl is an amphibian which becomes sexually mature while retaining its larval morphology (neoteny), with only few reported cases of successful metamorphosis (see Taurog 1974; Taurog et al. 1974). Because of its ability to regrow limbs, it is known as a model in regeneration and aging research (for a review, see McCusker and Gardiner 2011). But why use axolotls in vision research?

Amphibians, being cold-blooded vertebrates, are more forgiving to harsh experimental conditions and have a long history in retinal studies. Frogs were used for the first recordings of single fibers in the optic nerve (Hartline 1938), leading to the first description of receptive fields (Hartline 1940b; Hartline 1940a). Later, it was observed that salamanders possessed large retinal neurons (larger than many

other vertebrates), which were more easily recorded with microelectrodes. The mudpuppy (*Necturus maculosus*), an aquatic salamander, was used for understanding the structure and function of photoreceptors (Brown et al. 1963) and had an important role in mapping the synaptic organization of the retina (Dowling and Werblin 1969; Werblin and Dowling 1969; Miller and Dacheux 1976).

A close relative to the axolotl, the tiger salamander (*Ambystoma tigrinum*) is frequently studied in retina research. It was used for describing the connections between retinal cells (Lasansky 1973; Wong-Riley 1974) and for identifying the synaptic input received by ganglion cells, according to their response classes (Wunk and Werblin 1979; Asari and Meister 2014). The tiger salamander's retina was a model to understand contrast adaptation (Baccus and Meister 2002) and to find, for example, that the separation of objects from the scene background can already be performed by the retina (Ölveczky et al. 2003). More recently, a new form of plasticity was identified using the tiger salamander, where a ganglion cell sensitizes – instead of adapting – when presented with a high-contrast stimulus.<sup>1</sup> The ganglion cells were found to divide into two populations according to their responses after a change in the stimulus contrast: the adapting and sensitizing cells (Kastner and Baccus 2011; Kastner and Baccus 2013). There were recent attempts to automatically classify ganglion cells in the tiger salamander retina using either their morphological (Costa and Velte 1999) or temporal filtering properties (Segev et al. 2006; Marre et al. 2012), with reasonable success.

The axolotl is not a new model in vision research either. Axolotls were used in one of the first observations of gap junctions between photoreceptors (Custer 1973) and for understanding adaptation in rods (Grabowski et al. 1972). They have also been used for research on the role of glial cells in the retina (Brew and Attwell 1987; Mobbs et al. 1988), membrane properties of the bipolar cell (Attwell et al. 1987; Tessier-Lavigne et al. 1988), and the study of subfields in the retina (Bölinger and Gollisch 2012; Garvert and Gollisch 2013; Takeshita and Gollisch 2014).

Salamanders have thus been proven as a useful model for retinal research. The most recent works in the field have focused on tiger salamanders and axolotls. There are no reported (nor expected) differences in the organization of their retinas, and the decision between both species boils down, mostly, to local availability. The recordings using salamander retinas can last 6-8 hours, with anecdotal evidence of retinas whose neurons were still reliably responding to stimuli after 12 hours of recordings. The ease of preparation is also an advantage compared to mammals, due to the salamander retina's robustness to changes of temperature or oxygen concentration.

---

<sup>1</sup> This sensitization supposedly helps overcome the loss of information during changes of contrast, in the brief period before short-term adaptation. (Kastner and Baccus 2011)



## 2.2 TISSUE PREPARATION

The axolotl was anesthetized and dark-adapted by placing it in an ice bath, in a dark room, for at least 30 minutes. After the cold anesthesia, the animal was decapitated and double-pithed through the spinal cord to stop the contraction reflexes. The eyes were enucleated and kept in Ringer's solution (110 mM NaCl, 2.5 mM KCl, 1.0 mM CaCl<sub>2</sub>, 1.6 mM MgCl<sub>2</sub>, 22 mM NaHCO<sub>3</sub>, and 10 mM D-Glucose). The Ringer solution was continuously bubbled with Carbogen (5% CO<sub>2</sub>, 95% O<sub>2</sub>), for a minimum of 30 minutes before use, to maintain a pH of 7.4. The eyes were hemisected and the halves containing the retinas were stored in Ringer solution, at room temperature, until further use.

The whole procedure was performed in the dark to avoid bleaching the retina and ensure it remained responsive to a variety of light intensities for longer times. The tissue was prepared under infrared illumination, with infrared goggles adapted to the oculars of a microscope. The eyes of salamanders are small, with a diameter of about 3 mm, and the retina is a very fragile tissue. The retina must be gently detached from the eye cup using forceps. The vitreous humor, an insulating transparent sticky substance that fills the inside the eye, was removed. The forceps were inserted and delicately slid between the retina and the pigmented epithelium until the retina was completely free. The remaining pigmented epithelium was picked away and small incisions were made at the retina's border to flatten it. Any vitreous humor still attached to the ganglion cell-side was carefully removed until the retina could lay mostly flat.

## 2.3 RECORDING AND STIMULATION

For classifying RGCs, it is important to record from as many cells as possible in the same retina. The larger number of ganglion cells increases the chance of finding more cells in each putative type, thus improving the statistics for assessing the quality of the found types. But that is not all. Recording from the same retina avoids variations in the ganglion cell response properties due to animal age, diseases, genetic background, and preparation quality. While it is reasonable to expect cell types to be conserved in animals of the same species, it is safer to assume that experimental variations could blur the distinction between cell types when the data from multiple retinas is taken together. An overview of the experimental setup used for these large-scale recordings is shown in Figure 2.1.

An isolated axolotl retina was recorded with a 252-electrode array (MEA; Multichannel Systems), with 30  $\mu\text{m}$  electrode diameter and 100  $\mu\text{m}$  spacing between electrodes.<sup>2</sup> In order to mount the retina on the array, the retina was moved with

<sup>2</sup> A higher density MEA model, with 60  $\mu\text{m}$  distance and 10  $\mu\text{m}$  electrodes, was used initially but yielded only 80 – 100 cells per recording. The arrays used for the experiments in this thesis, with

## EXPERIMENTAL METHODS

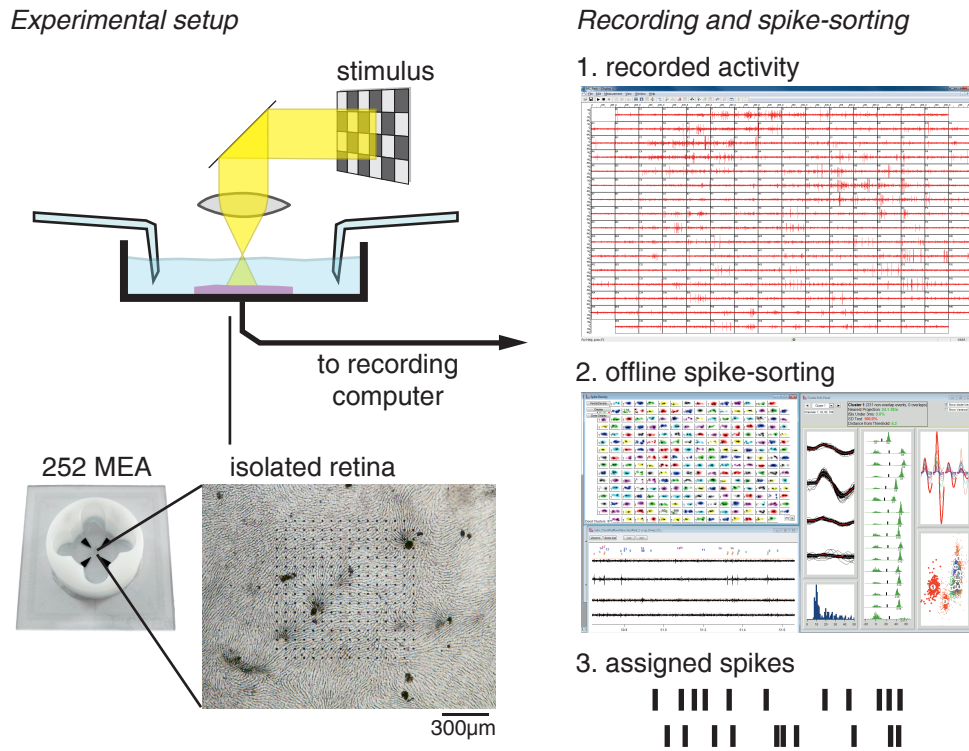


Figure 2.1: OVERVIEW OF ELECTROPHYSIOLOGICAL SETUP. The retina was laid with the ganglion cell layer down on a 252-electrode array and stimulated with an OLED, whose image is focused on the photoreceptor layer. The extracellular potential recorded at each electrode is band-pass filtered (300 Hz to 5 KHz) and digitized at 10 KHz. Offline spike-sorting assigned detected spikes (within groups of up to four electrodes) to putative units (see Section 2.4). The black spots on the retina are from the remaining pigmented epithelium, but do not significantly affect the recording.

a pipette onto a semipermeable membrane (dialysis membrane), which was held taut on a plastic support. Excess solution was removed until the retina could lay flat with the ganglion cell side up. A multi-electrode array was pressed from above against the retina, so that the electrodes were in contact with the ganglion cell layer. The combination was then placed onto the amplifier for recording. Oxygenated Ringer solution (pH 7.4; bubbled with Carbogen) was continuously supplied at a rate of 3 – 5 mL/min.

Stimuli were generated by a computer with custom-made C++ software using the OpenGL library for graphics generation. The image was presented with an OLED display (eMagin, resolution of  $800 \times 600$  pixels at 60 Hz) and projected onto the retina via a telecentric lens (Edmund Optics). The projected image was focused on the photoreceptor layer and optically reduced to a constant size of  $7.5 \mu\text{m}/\text{pixel}$ .

The electrical activity of the ganglion cells was sensed by the MEA electrodes. The signal at each electrode was band-pass filtered from 300 Hz to 5 KHz, digitized at 10 KHz and stored in the recording computer for offline analysis. The MEA detected the extracellular activity close to the ganglion cell layer, where each electrode recorded the combination of extracellular potentials from cells in its neighborhood. At the same time, the spikes from individual cells could be detected in multiple electrodes. The spikes were sorted offline and assigned to single units.

## 2.4 SPIKE-SORTING

Spike-sorting is the procedure of assigning spikes from the recorded population activity to the single cells which produced them. Because one does not have direct access to the original cells, spike-sorting uses the fact that spikes from the same cell are stereotypical and can be grouped according to their shapes (for a review, see Lewicki 1998). The amplitude of the spikes depends on the distance of the cell to the recording electrode, so the signal from multiple electrodes can be pooled to differentiate between spikes with similar waveforms but generated by spatially separated cells.

To classify retinal ganglion cells, it is important that spikes which are grouped together indeed originate from the same cell. Similarly, one would presume that the spikes from a single cell are not split into two groups.

However, no method is perfect. Spikes can be wrongly assigned, so it is common to refer to those clusters of spikes as units or candidate cells. Good units are clusters with well separated spikes and which respect the refractory period (i.e., no spikes less than 1 ms apart, very few below 3 ms). While one might be confident that good units are single cells, there is the lurking possibility of a spike sorting artifact that must be in mind at all time (see, for e.g., Lewicki 1998; Pillow et al.

---

larger inter-electrode spacing and electrodes, consistently recorded from 150 – 300 cells at a time, depending on the preparation quality.

2013). For simplicity, the good units in this thesis which are not artifacts – to the best of my knowledge – will be referred to as cells.

Using a custom-made spike-sorting software (Pouzat et al. 2002; written in IgorPro 6, 64-bit), the electrodes from the MEA were joined into groups of up to four electrodes according to the cross-correlations of their recorded signals (Pouzat et al. 2002). For each electrode group, spikes were detected when the filtered signal at any electrode crossed a threshold  $Thr$  defined as

$$Thr = 4\sigma_x, \sigma_x = \text{median} \left\{ \frac{|x(t)|}{0.6745} \right\} \quad (2.1)$$

where  $\sigma_x$  is the estimated background noise level and  $x(t)$  the band-pass filtered signal. The median absolute deviation<sup>3</sup> was used instead of the standard deviation, as the latter could be biased by the high amplitude of the spike events and cause an artificially high threshold (Quiroga et al. 2004; Donoho and Johnstone 1994). Each spike was represented by a 2.1 ms waveform (21 sample points) extracted from the filtered signal of all channels belonging to the same group. The spike peaks were aligned at the 7th sample, so that information from the rising phase of the action potential could also be considered. The waveforms in each channel group were clustered using a Gaussian mixture model (see Section 3.3) and the units ranked according to their quality (Pouzat et al. 2002).

The resulting clusters from unsupervised sorting were inspected and manually split (or joined) to improve the sorting quality. Each unit was graded according to its spike amplitudes, how well separated its spikes were from other units, and its refractory period. The quality of the refractory period was used to tell whether a unit contained spikes from a single cell (if a unit is composed of two cells, spikes would not necessarily respect the refractory period); this quality was assessed by the fraction of spikes that happened within 3 ms of each other. Violations up to 3% of the inter-spike intervals were still accepted, as long as the unit had large amplitude spikes and appeared to be well-separated. Those were mostly the case for bursting cells.<sup>4</sup> The grades ranged from 1 (best quality) to 5 (should be ignored in analysis, e.g., when amplitudes are too low or the cluster has poor separation). Axonal spikes were few, but could be identified in this step because of their stereotypical triphasic shape (see, e.g., Li et al. 2015) and only removed if the same neuron had already been recorded in another group of electrodes (Section 2.4.1).

- 
- <sup>3</sup> The median absolute deviation is defined as  $MAD\{x(t)\} = \text{median}\{|x(t) - \text{median}\{x(t)\}|\}$  and can be used to approximate the standard deviation of a signal. As the signal  $x(t)$  was high-pass filtered and the noise is considered Gaussian,  $\text{median}\{x(t)\}$  is small, which results in Equation 2.1. This assumption is often not explicitly mentioned in the literature, but is empirically found to hold true.
- <sup>4</sup> Roughly, half of the good units showed no refractory period violations (inter-spike intervals smaller than 3ms), while only 10% of units in an experiment have more than 1% violations in their inter-spike intervals; data not shown.

### 2.4.1 *Dealing with duplicate units*

Duplicates can be detected by cross-correlating the spike trains (binned in bins of 0.5 ms) for each cell pair. In the ideal case for duplicate cells, the cross-correlation would show a peak of unit amplitude at zero lag, as all spike times should be the same. However, spikes may not always be perfectly assigned, leading to peaks in the cross-correlation function which are less than unity (Field et al. 2007).

A pair of units are considered “suspicious” (possible duplicates) whenever their cross-correlations have a peak with an amplitude larger than a threshold, defined here to be four standard deviations above the average peak amplitude of all pairs. Besides showing a supra-threshold peak in the cross-correlation, a suspicious pair will be considered a duplicate only if the spatial components of both receptive fields (see Section 2.6) are similar,<sup>5</sup> with a cosine similarity larger than 0.8.

When the same units are found in two or more duplicate pairs, all units in those pairs are joined into a single group. From each group of duplicates, only the unit with largest number of spikes and best quality (best grade from Section 2.4) is kept for further analysis.

## 2.5 ESTIMATING RECEPTIVE FIELDS

The receptive field is the region of the visual space over which a retinal ganglion cell integrates a stimulus. The receptive field is known for having a center-surround structure, so that there exists a region outside its center which, when stimulated, typically suppresses the response of the ganglion cell. Because ganglion cells show temporal dynamics in the stimulus integration (e.g., by responding with different latencies to light flashes), it is common to attribute these dynamics to the receptive field. This extension of the receptive field is referred to as a spatiotemporal receptive field.

In single-cell recordings, the receptive field of a retinal ganglion cell is often stimulated by flashing dark and bright spots in the receptive field center. Using the flashed spots, one can coarsely separate ganglion cells into different response types, based on their polarity. There are ON cells, which respond to increments of light in the receptive field center. The OFF cells, which respond to decrements of light. Finally there are the ON-OFF cells, which respond to both increments and decrements of light. Moreover, the spatial extent of a receptive field can be mapped by varying the size of the flashed spots. As the spots initially grow in size, the number of evoked spikes also increases. When a spot is larger than the receptive field center, the surround will begin to suppress the ganglion cell’s activity. The

<sup>5</sup> In this work, most suspicious pairs showed also very similar spatial components (cosine similarities larger than 0.9), with only few exceptions. The exceptions were often suspicious pairs whose cross-correlation peaks were small, close to the threshold, but with clearly distinct spatial components.

spot size which elicits maximum activity is then taken as the size of the receptive field center.

While useful for characterizing ganglion cells, the method of flashing spots relies on knowing the location of the receptive field. This limitation is often a hindrance for experiments which record simultaneously from multiple cells. When dealing with multiple cells, one often simplifies the method by flashing the whole screen instead of a single spot. However, the stimulus is then not specific to the location of the cell's receptive field center. Besides losing information on the receptive field size, the response may mix center and surround properties, which is not always easy to disambiguate.

An alternative method, better suited for multiple-cell recordings, models the spiking output of each ganglion cell as resulting from a "black box", whose input is defined as the light arriving on the photoreceptors and is, somehow, processed in the circuit (i.e., horizontal, bipolar and amacrine cells) that precedes the ganglion cell (see, e.g., Chichilnisky 2001). The underlying model assumes that one or more linear filters are convolved with the input (see, e.g., Schwartz et al. 2006). The resulting linear output is transformed by a non-linear function and fed into a probabilistic process for spike generation. Then, the filters of the model can be adjusted until the generated spikes optimally match the recorded spikes from a ganglion cell (see, e.g., Paninski 2003). By fitting the model to approximate the recorded spikes, one finds not only an estimate for the latency and polarity of the cell, such as in the flashed spots, but also a fine description for the temporal dynamics of the receptive field. The receptive field extent can also be estimated directly, even if its location is a priori unknown, from this black box approach.

A simple model for this black box consists of a single filter, with a spike generator that follows a Poisson distribution, which is called a Linear-Nonlinear-Poisson model. I will briefly describe this model and show how its parameters can be estimated directly from the data, when one chooses the correct stimulus.

### 2.5.1 *Linear-Nonlinear-Poisson Model*

A stimulus can be represented by the brightness of each pixel on the screen  $S(\vec{x}, t)$ , where  $\vec{x} = (x, y)$  is the pixel location and  $t$  is the frame index. The linear-nonlinear-Poisson (LNP) model then assumes that a single spatiotemporal filter  $F(\vec{x}, t)$  of size  $N_{pixels} \times W$  is convolved over time with the stimulus, generating a linear signal

$$i(t) = \sum_{t'} \sum_{\vec{x}} F(\vec{x}, t') S(\vec{x}, t - t') , \quad (2.2)$$

which, assuming a non-linear function  $N(\cdot)$ , results in an instantaneous firing rate  $\lambda(t) = N(i(t))$ . If the spike generation is modeled by an inhomogeneous Poisson

process, then the probability of having at least one spike in a window between times  $t$  and  $t + dt$  is given, for small enough  $dt$ , by

$$P(\text{spike}; t) = \lambda(t)dt \quad (2.3)$$

The LNP model is useful because the estimation of its parameters do not require fitting, and can be directly obtained from the data.

### 2.5.2 Reverse correlation

By using an uncorrelated stimulus (white noise) as input, the linear filter of the LNP model can be estimated via reverse correlation (Chichilnisky 2001). The stimulus vector

$$\vec{s}_t = [S(\vec{x}, t - W + 1) \dots S(\vec{x}, t - 1) S(\vec{x}, t)] \quad (2.4)$$

represents the last  $W$  frames of stimulus that were observed by the model before a time  $t$ . If  $\vec{s}_t$  is collected whenever a spike occurs, one has an ensemble of spike-triggered stimuli  $\{\vec{s}_t | t = \text{spike}\}$ . The average of the spike-triggered ensemble is the spike-triggered average (STA), and is proportional to the linear filter of the LNP. This is true as long as the stimulus distribution is radially symmetric and the non-linearity is “sufficiently asymmetric” (Chichilnisky 2001; Paninski 2003). The reverse correlation can then be used to obtain a linear approximation for the receptive field of a ganglion cell; see for example the illustration in Figure 2.2.

The LNP model is surprisingly effective in estimating the instantaneous firing rate of ganglion cells. Despite being only a phenomenological model, composed of a single linear filter and an output non-linearity, it approximates the way the visual information is processed all the way from the photoreceptors to the ganglion cells. This model can also be extended, for example, to consider multiple filters (Sharpee et al. 2004; Schwartz et al. 2006) or even coupling between cells and spike-history dependence (Paninski et al. 2007). This increase in complexity improves the prediction of the spike generation, but makes the model harder to fit and requires longer recordings. For this work, I focused on the information captured by a single linear filter.

## 2.6 DECOMPOSING THE SPATIOTEMPORAL RECEPTIVE FIELD

Using singular value decomposition (SVD), the spatiotemporal receptive field  $F(\vec{x}, t)$  was approximated into spatial and temporal components,

$$F(\vec{x}, t) = X(\vec{x})T(t) \quad (2.5)$$

where  $X(\vec{x})$  represents the sensitivity of the receptive field center, while  $T(t)$  represents the temporal filtering performed by the receptive field center.

EXPERIMENTAL METHODS

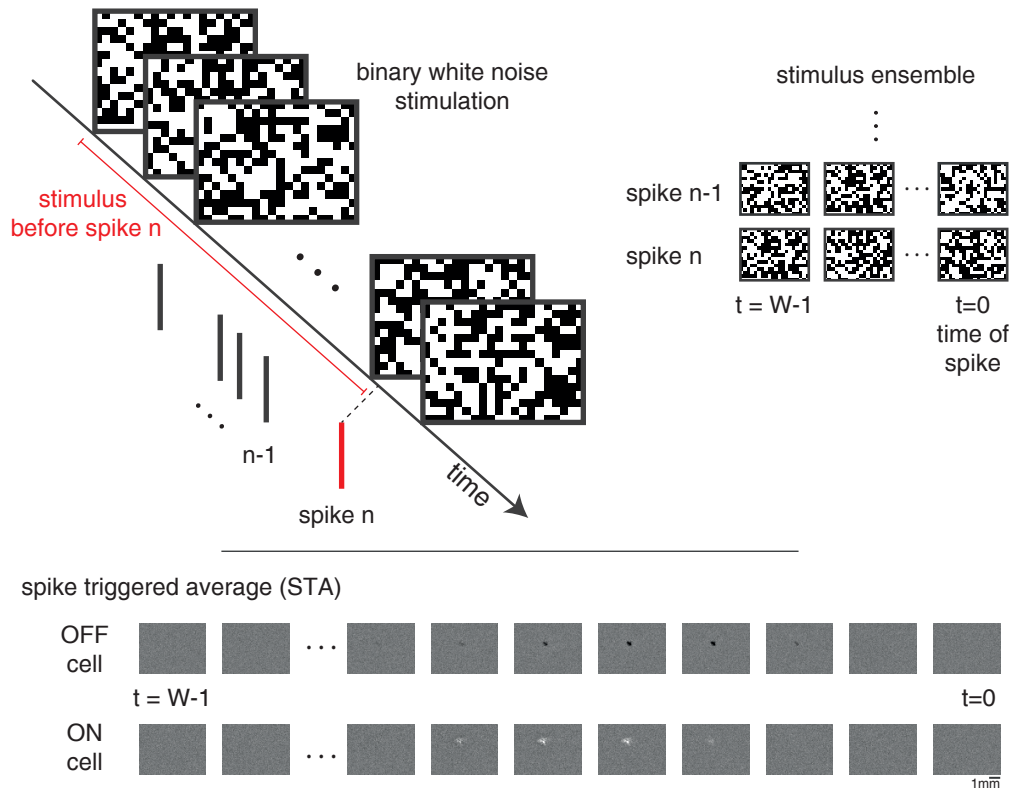


Figure 2.2: REVERSE CORRELATION. Frames of an uncorrelated stimulus (binary white noise) were presented to the cell. The stimulus which caused a spike are the last  $W$  frames before the neuron spiked ( $t = 0$ ) and can be collected, for each cell, in a stimulus ensemble. The average of the stimulus ensemble, also known as spike-triggered average (STA), is an estimate of the integration properties of the receptive field (see text in Section 2.5.2). For an OFF (ON) cell, the STA shows a darkening (brightening) of the region on the screen integrated by the receptive field center, as in the examples shown here.



In general, a ganglion cell receptive field is not separable.<sup>6</sup> However, the SVD offers a good approximation for its spatial extent and temporal filtering properties (see, e.g., Gauthier et al. 2009). An example of a decomposed receptive field is shown in Figure 2.3, where the temporal filter  $T(t)$  can be used to distinguish between an OFF and an ON cell.

The spatial component of the receptive field  $X(\vec{x})$  was approximated by a 2D-Gaussian function

$$X(\vec{x}) = A \exp\left(-\frac{1}{2}(\vec{x} - \vec{\mu})^T \Sigma^{-1}(\vec{x} - \vec{\mu})\right) \quad (2.6)$$

with

$$\Sigma = \begin{bmatrix} \sigma_x^2 & \rho\sigma_x\sigma_y \\ \rho\sigma_x\sigma_y & \sigma_y^2 \end{bmatrix}, \quad \vec{\mu} = \begin{bmatrix} x_c \\ y_c \end{bmatrix}. \quad (2.7)$$

The parameters  $A$ ,  $\sigma_x$ ,  $\sigma_y$ , and  $\rho$  represented the shape of the receptive field, while  $x_c$  and  $y_c$  represented the location of the receptive field center. The receptive field center was defined as the area enclosed by the ellipse at one standard deviation.<sup>7</sup> Defining  $\lambda_1$  and  $\lambda_2$  as the eigenvalues of  $\Sigma$ , the semi-axes of this ellipse were given by

$$\sigma_1 = \sqrt{\lambda_1}, \quad \sigma_2 = \sqrt{\lambda_2},$$

and the receptive field size  $D_{RF}$  was defined as the geometric mean

$$\begin{aligned} D_{RF} &= 2\sqrt{\sigma_1\sigma_2}, \\ &= 2(\lambda_1\lambda_2)^{1/4} = 2\det(\Sigma)^{1/4}, \\ &= 2(1 - \rho^2)^{1/4}\sqrt{\sigma_x\sigma_y}. \end{aligned} \quad (2.8)$$

which is the diameter of a circle needed to cover the same area as the receptive field center. Finally, the orientation  $\theta$  of the ellipse was obtained from the largest eigenvector  $\vec{m} = [m_x \ m_y]^T$  of  $\Sigma$  as

$$\theta = \arctan\left(\frac{m_y}{m_x}\right). \quad (2.9)$$

## 2.7 MEASURING DIRECTION SELECTIVITY

Direction selectivity is characterized by a special asymmetry in the response of a RGC to moving stimuli (most commonly, bars or gratings). A direction selective

<sup>6</sup> This is clear if one considers for example the receptive field surround, which is typically slower than the receptive field center. Because of the different speeds, the whole receptive field cannot be exactly described by a single temporal filter.

<sup>7</sup> That is,  $(\vec{x}_{RF} - \vec{\mu})^T \Sigma^{-1}(\vec{x}_{RF} - \vec{\mu}) \leq 1$  for every  $\vec{x}_{RF}$  located inside the receptive field center.

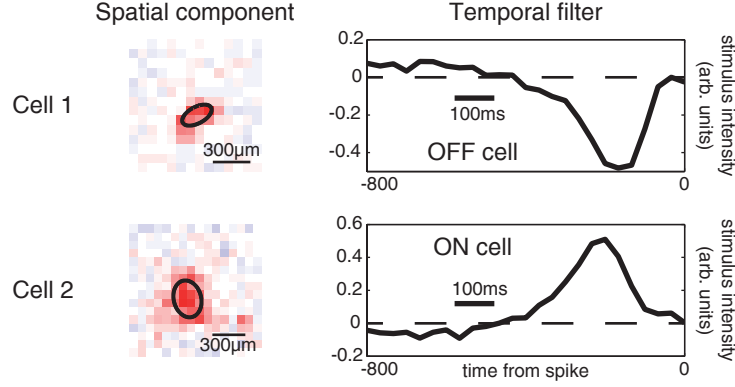


Figure 2.3: DECOMPOSED RECEPTIVE FIELD. The spatiotemporal receptive field is decomposed into spatial and temporal components. The ellipse at one standard deviation delimits the receptive field center. The temporal component incorporates the temporal filtering properties of the receptive field and can show, for example, if the cell responds preferentially to a decrease (OFF) or an increase (ON) in light intensity.

RGC responds only to movement in its preferred direction and shows no response to movements in the opposite direction (Barlow and Hill 1963; Barlow et al. 1964; Barlow and Levick 1965; Vaney et al. 2001).

One measures the direction selectivity of a cell by presenting a grating on the screen, which moves towards a direction  $\theta_d$  relative to the screen's center. For each direction, one counts the number of spikes  $R_d$  (where  $R_d \geq 0$ ) evoked by the stimulus presentation during a fixed time window. A retinal ganglion cell is then direction selective if there is a direction  $\theta_{max} = \theta_d$  for which the response  $R_{max}$  is maximum, while the opposite direction  $\theta_{null} = -\theta_{max}$  (also called null direction) has  $R_{null} \ll R_{max}$ .

Instead of dealing with the whole set of responses to the moving grating, it is common to extract a number that represents how selective a single cell is. The direction selectivity index (DSI) is useful in this regard, being defined as

$$\text{DSI} = \frac{1}{\sum_d R_d} \left| \sum_d R_d e^{i\theta_d} \right|, \quad (2.10)$$

where  $e^{i\theta} = \cos \theta + i \sin \theta$ ,  $i^2 = -1$  and  $|\cdot|$  is the norm of a complex number. By construction,  $0 \leq \text{DSI} \leq 1$ , and a larger DSI suggests a more direction-selective cell. The DSI equals unity only if all the spikes happen exclusively for a single direction ( $R_{max} = \sum_d R_d$ ), indicating a perfectly direction selective cell. Conversely, the DSI will be close to zero if there is no direction preference. The complex number

$$Z = \sum_d R_d e^{i\theta_d}, \quad (2.11)$$

which appears inside Equation 2.10, is named the direction bias. The reason for this name becomes clear if one visualizes the set of responses as vectors in the complex plane, with  $\vec{R}_d = R_d \exp(i\theta_d)$ . Then,  $Z = \sum_d \vec{R}_d$  will point towards the preferred direction with a norm proportional to the DSI.

## 2.8 MEASURING PROPERTIES OF THE SPIKE-TRAINS

Estimating direction selectivity and spike-triggered average are of course not the only uses for the spikes of a ganglion cell. The statistics of the spike-train can be useful for cell classification (Zeck and Masland 2007).

### 2.8.1 Autocorrelation of the spike-trains

The temporal autocorrelation of a spike-train, when properly normalized, is the probability of finding spikes at a time  $t + \tau$  after observing a spike at a time  $t$  – regardless of how many spikes happened in-between. Because the autocorrelation does not depend on a model, but on the spiking probability of a cell, it can be useful for neuronal classification (see, for e.g., Rieke et al. 1999).

When describing the temporal structure of the spike-train, one should be aware of the caveats of the autocorrelation function. For example, peaks in autocorrelation are often assumed to be an indication of bursts, but may be an effect of the refractory period on a cell with high spiking activity (Bar-Gad et al. 2001).

### 2.8.2 Coefficient of variation

If a spike-train is represented by its spike times  $\{t_i\}$ , where  $i$  is the index of a spike, then the inter-spike interval (ISI) can be defined as  $\Delta_i = t_{i+1} - t_i$ . To measure the variability of the ISIs, one can use the coefficient of variation

$$C_v = \frac{\sigma_\Delta}{\bar{\Delta}} = \frac{1}{\bar{\Delta}} \sqrt{\frac{1}{N-1} \sum_{i=1}^N (\Delta_i - \bar{\Delta})^2}, \quad (2.12)$$

where

$$\bar{\Delta} = \sum_{i=1}^N \Delta_i \quad (2.13)$$

is the average ISI and  $N$  is the number of inter-spike intervals. For long time-series, the coefficient of variation  $C_v$  equals unity when the spike times are Poisson-distributed (as  $\sigma_\Delta = \bar{\Delta}$ ). For a more regular time series,  $C_v$  will be very small.

### 2.8.3 *Local variation coefficient*

The coefficient of variation, however, does not take into account local variations in the temporal activity, assuming a stationary distribution of inter-spike intervals. To accommodate for those variations, Shinomoto et al. (2003) have proposed the local variation coefficient

$$L_v = \frac{1}{N-1} \sum_{i=1}^{N-1} \frac{3(\Delta_i - \Delta_{i+1})^2}{(\Delta_i + \Delta_{i+1})^2}. \quad (2.14)$$

The local variation coefficient takes into account the local regularity of the spikes. For spike-trains which change due to a stimulus or to adaptation, but whose local regularity is preserved, the  $L_v$  will stay small while  $C_v$  will grow large; therefore, the local variation coefficient is a better estimate of the “intrinsic spiking” properties of a cell (Shinomoto et al. 2003). Similar to  $C_v$ ,  $L_v$  will be unity if the spike-train is Poisson-distributed. The local variation coefficient will be small for more regular spike-trains, being zero when the spikes are perfectly regular.

CLUSTERING

---

*If somebody thinks they're a hedgehog, presumably you just give 'em a mirror and a few pictures of hedgehogs and tell them to sort it out for themselves.*

— DOUGLAS ADAMS, *So long, and thanks for all the fish*

The experimental methods described in the previous chapter provide a large amount of data, with often more than 200 ganglion cells recorded in a single experiment. When evaluating such large datasets, manual analysis does not scale well and techniques of machine learning become useful (for a review see, e.g., Armañanzas and Ascoli 2015). Machine learning is at the intersection of statistics and computer science, dedicated to the use of statistical methods to solve problems mechanically in a way that mimics human decisions (Hastie et al. 2009; Barber 2012).

Machine learning methods can be supervised or unsupervised, and their application depends on what is known about the dataset. If each element in a dataset is labeled by an expert<sup>1</sup>, a supervised method can be used to discover which features were important for the expert's decision and apply a similar decision to unlabeled elements of a similar dataset. Unsupervised methods are those used when the data was not previously labeled, but still one seeks structure in the dataset. Unsupervised methods can be used for dimensionality reduction, where one reduces the features needed to describe a dataset (e.g., principal component analysis; non-negative matrix factorization) by only keeping the most descriptive ones. Clustering is also an unsupervised method, where the data elements are grouped according to the similarity of their features. Members of a cluster are assumed to be more similar between themselves than to members of other clusters (Hastie et al. 2009).

The ganglion cells recorded in the experiments of this thesis have no labels, as there was no a priori knowledge to which classes they should belong. Thus, clustering may give insight on the possible ganglion cell classes by grouping cells based on the similarity of their features. For now, I will leave aside the problem of neuronal classification. Clustering is already an involved problem by itself, without

---

<sup>1</sup> An expert, by definition, is someone with an expert knowledge of the problem, trained to solve it. It does not need to be a human being; an algorithm sometimes does the role of an expert. For many techniques, the expert does not need to have perfect knowledge either (Liao 2005; Hastie et al. 2009).

the specifics of neuronal classification; I will return to the ganglion cells in the next chapter.

In this chapter, I will describe the clustering problem from a statistical point of view and the different methods to solve it. Each method has its own assumptions of what constitutes a cluster. As such, different methods are suited for different datasets, according to the expected structure in the data. In other words, the best case for each method is when the natural groups present in the data can be described by the method's own definition of a group. Conversely, there are datasets where these methods will fail. I will provide a short description of common clustering procedures, their assumptions and their shortcomings. For describing the methods, I will assume that the expected number of clusters in a dataset is known. This is not always true. Towards the end of the chapter, I will discuss heuristics which may be used to estimate the number of clusters in a dataset.

### 3.1 THE CLUSTERING PROBLEM

There is no single clustering method, just as there is no single way of describing why elements belong together. The intuitive feeling that two elements should be grouped has to be defined objectively, and each definition will lead to a different method. There are methods which attempt to minimize the dispersion of the data points (e.g., K-means), while others assume that the points are generated by a mixture of probability distributions (e.g., Gaussian mixture). Additionally, there are methods which transform the dataset to improve the separation of the data before the points are grouped (e.g., spectral clustering).

Formally, a dataset contains  $N$  elements which can be labeled with an index  $i = 1, 2, \dots, N$ . The goal of clustering is to assign for each element a label  $\lambda_i = 1, 2, \dots, K$ , where  $K$  is the total number of clusters. Each element  $i$  in the dataset has  $n$  features  $x_1^i, x_2^i, \dots, x_n^i$  and can be represented by a vector

$$\vec{X}_i = [x_1^i, x_2^i, \dots, x_n^i]^T. \quad (3.1)$$

The dissimilarity between two elements  $i$  and  $j$  is defined as the dissimilarity (or distance) between their features. When the features are numeric, the *squared* Euclidean distance

$$d(i, j) = \|\vec{X}_i - \vec{X}_j\|^2 = \sum_m (x_m^i - x_m^j)^2 \quad (3.2)$$

is often taken due to its simplicity (Hastie et al. 2009). Other distances may be more appropriate depending on the features in consideration and expected structure of the data; finding a good (dis-)similarity measure for a problem is sometimes an art (Gordon 1990; Hastie et al. 2009).

For a given configuration of labels  $\{\lambda_i\}$ , the dispersion  $D(k)$  of a cluster  $k$  is defined (Hastie et al. 2009) as the sum of the pairwise distances of its elements. That is,

$$D(k) = \frac{1}{2} \sum_{\lambda_i=k} \sum_{\lambda_j=k} d(i, j), \quad (3.3)$$

and the total dispersion

$$D^* = \sum_{k=1}^K D(k) = \frac{1}{2} \sum_{k=1}^K \sum_{\lambda_i=k} \sum_{\lambda_j=k} d(i, j). \quad (3.4)$$

### 3.2 K-MEANS

Maybe one of the most popular clustering methods, K-means assumes that clusters are compact: their dispersion should be minimal (Hastie et al. 2009). In this way, K-means searches for a collection of labels  $\lambda^* = \{\lambda_i\}$  such that the total dispersion (Eq. 3.4) is minimized:

$$\lambda^* = \arg \min_{\{\lambda_i\}} \frac{1}{2} \sum_{k=1}^K \sum_{\lambda_i=k} \sum_{\lambda_j=k} d(i, j). \quad (3.5)$$

In principle, this equation could be solved by brute-force, testing all the possible labels  $\{\lambda_i\}$  until a minimal dispersion is found. In practice, the number of possible assignments grows too fast with the input parameters. For instance, for  $K = 2$  clusters the number of possible assignments<sup>2</sup>  $S(N, K) \propto 2^N$ , which quickly becomes impractical.

To avoid sampling the whole solution space, K-means is often implemented as an iterative descent algorithm (Hastie et al. 2009, p.510); labels are randomly assigned at the start and exchanged at each step to reduce the total dispersion, until a minimum is found. The algorithm has guaranteed convergence, but may reach a local minimum. To avoid local minima (suboptimal solutions), the procedure is repeated several times with different initial conditions; the final label assignment is taken from the repeat with smallest total dispersion.

The algorithm of K-means runs fast and can be found in most scientific computing packages; for this thesis, I used the implementation of K-means already present in MATLAB<sup>3</sup>. Because K-means minimizes the total dispersion, it is better suited for finding spherical (or ellipsoidal) clusters, and often fails for non-convex clusters such as those shown in Figure 3.1.

<sup>2</sup> For a formula for  $S(N, K)$ , see Hastie et al. 2009, p.508.

<sup>3</sup> Method `kmeans`; MATLAB and Statistics Toolbox Release 2012a, The MathWorks, Inc., Natick, MA.

## CLUSTERING

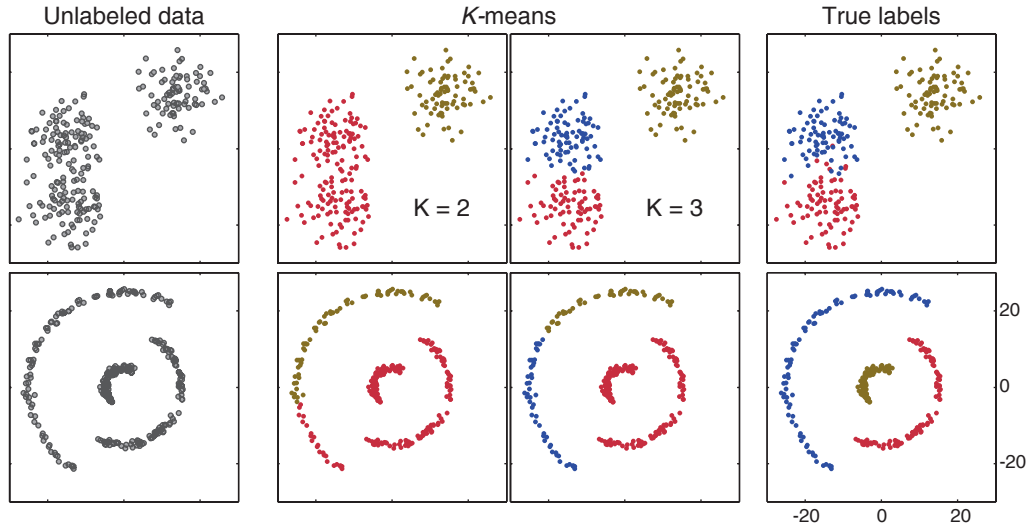


Figure 3.1: K-MEANS. The unlabeled dataset (left column) is classified via K-means for  $K = 2$  and  $K = 3$  clusters (center columns). The right column shows the original labels of the dataset. Points with the same color belong to the same cluster. Notice how K-Means classifies convex clusters well (top row) but fails to classify non-convex clusters (bottom row).

### 3.3 GAUSSIAN MIXTURE

The definition of K-means is not sensitive to the probability distribution of the features in the dataset. A mixture model (Hastie et al. 2009), on the other hand, attempts to explain the observed probability density of the  $n$ -dimensional feature vector  $\vec{X} = [x_1, x_2, \dots, x_n]^T$  in the dataset. A mixture model assumes the existence of  $k$  components with their own probability distributions  $P(\vec{X}|\lambda = k)$ , so that

$$P(\vec{X}) = \sum_k^K a_k P(\vec{X}|\lambda = k), \quad (3.6)$$

where  $a_k$  is the weight of component  $k$  in the mixed distribution and  $\sum_k a_k = 1$ .

If the probability distributions of the components were known, one could estimate the probability of membership for a data point  $i$  in component  $k$  as

$$P(\lambda = k|\vec{X}_i) = \frac{P(\vec{X}_i|\lambda = k)}{\sum_l^K a_l P(\vec{X}_i|\lambda = l)}. \quad (3.7)$$

This probability of membership incorporates the uncertainty which is inherent to the clustering process, and differently from K-means, leads to a “soft” classifica-



tion (Hastie et al. 2009). If, instead, a sharp classification is desired, the point  $i$  is assigned to its most likely component

$$\lambda_i = \arg \max_k P(\lambda = k | \vec{X}_i) . \quad (3.8)$$

However, one still needs to find the underlying probability distributions. Mixture models are usually built as a Gaussian mixture. As the name suggests, in a Gaussian mixture the probability distribution of the features from a component  $k$  is assumed Gaussian with mean  $\vec{\mu}_k$  and covariance matrix  $\Sigma_k$ , so that

$$P(\vec{X} | \lambda = k; \vec{\mu}_k, \Sigma_k) = \frac{1}{(2\pi)^{n/2} (\det \Sigma_k)^{1/2}} \exp \left( -\frac{1}{2} (\vec{X} - \vec{\mu}_k)^T \Sigma_k^{-1} (\vec{X} - \vec{\mu}_k) \right) . \quad (3.9)$$

To estimate the parameters of a Gaussian mixture, one defines the likelihood of the dataset as

$$\mathcal{L}(\theta) = \prod_i \sum_k a_k P(\vec{X}_i | \lambda_i = k; \vec{\mu}_k, \Sigma_k) , \quad (3.10)$$

where  $\theta = (\{a_k\}, \{\vec{\mu}_k\}, \{\Sigma_k\})$  is the set of parameters of the model. Then, the most likely parameters for the mixture are given by

$$\theta_{ML} = \arg \max_{\theta} \mathcal{L}(\theta) , \quad (3.11)$$

which can be solved via an expectation maximization (EM) algorithm (see Barber 2012, pp.439–442).

Similarly to K-means, a Gaussian mixture separates convex clusters well (Figure 3.2). Indeed, K-means can be shown (Hastie et al. 2009; Barber 2012) to be a special case of a Gaussian mixture, and hence both methods are related. If one restricts all components in a mixture to have the same covariance matrix  $\sigma^2 I$  (where  $I$  is the identity matrix), then the probability that a data point belongs to a component (Equation 3.7) will depend mostly on the distance of that point to the center of the mixture components. Moreover, in the limit  $\sigma \rightarrow 0$ , the Gaussian mixture reduces to K-means as each data point will be strictly assigned to a single cluster; that is, the membership function for a given data point will be either 1 or 0 (Hastie et al. 2009).

But differently from K-means, Gaussian mixtures have the advantage of estimating the probability distribution of the cluster features, as can be seen by the iso-probability curves in Figure 3.2. The dependence on Gaussian-distributed features, though, leads a Gaussian mixture model to still be a poor choice when non-convex clusters are expected, as exemplified by the bottom row of Figure 3.2.

## CLUSTERING

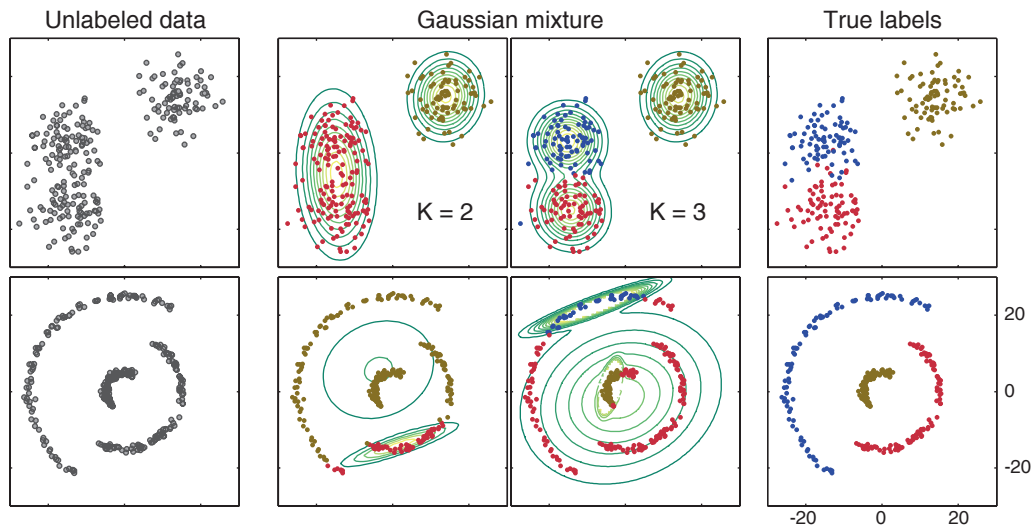


Figure 3.2: GAUSSIAN MIXTURE. The unlabeled dataset (left column) is classified via Gaussian mixture using  $K = 2$  and  $K = 3$  components, with the points labeled according to their most likely component. The original labels are shown in the right column. Lines are iso-probability curves of the mixture. Gaussian mixtures classify convex clusters well (top row) but are also not suited to classify non-convex clusters (bottom row).

### 3.4 SPECTRAL CLUSTERING

K-means and Gaussian mixtures are reasonable clustering methods, both being relatively fast and simple. Gaussian mixtures improved on K-means by modeling the distribution of features in the data, but did not remove the assumption that clusters should be convex, which is implicit in the use of the Euclidean distance (Hastie et al. 2009).

Spectral clustering, on the other hand, takes into account the local structure of the data by mapping the clustering problem into a graph partition problem (Luxburg 2007; Hastie et al. 2009). A similarity graph is built by considering the data points as nodes in a graph, where two nodes  $i$  and  $j$  are connected by an edge that has a non-negative weight  $w_{ij} \geq 0$ , given by the similarity between the two points. When  $w_{ij} = 0$ , the nodes are unconnected. The similarity measure is considered symmetric, so that  $w_{ij} = w_{ji}$ . The similarity matrix  $W = \{w_{ij}\}$  is then also symmetric and can be seen as the adjacency matrix of an undirected similarity graph.

Once a similarity graph is defined (from the adjacency matrix  $W$ ), the clustering problem reduces to the problem of finding groups of nodes which are highly connected between themselves, while having few connections to nodes in other groups. There are different ways of implementing this intuitive description, which

leads to a diversity of spectral clustering methods (Shi and Malik 2000; Meila and Shi 2001; Ng et al. 2002; Luxburg 2007). The common thread among those methods is the reliance on eigenvectors of matrices derived from the similarity matrix  $W$  (Ng et al. 2002).

#### 3.4.1 Building a similarity matrix

Similarity matrices can be built in many ways (Luxburg 2007). If one has a distance measure  $d(i, j)$ , a simple procedure is to connect points  $i$  and  $j$  whose distances  $d(i, j) < \epsilon$  (where  $\epsilon$  is a constant chosen to represent the typical distances in the data). Another procedure involves connecting the closest  $k$  neighbors of a point  $i$  and assign  $w_{ij} = w_{ji} = 1$  (for all  $j$  in the neighborhood). Finally, one can also build a fully-connected graph, where the weights  $w_{ij}$  can be arbitrarily small and defined based on a similarity measure. So far, no theoretical guidelines exist for knowing which similarity matrix construction works best for typical problems (Luxburg 2007); for simplicity, I considered a fully connected graph<sup>4</sup> for the classification of ganglion cells, which will be shown in Chapter 4.

To create a fully-connected similarity graph, one first defines an appropriate similarity measure between the nodes  $i$  and  $j$ . Choosing a good similarity measure is not always easy (and sometimes an art; see Gordon 1990). A common choice (Shi and Malik 2000; Ng et al. 2002; Luxburg 2007) is to use the Gaussian similarity

$$w_{ij} = \exp\left(-\frac{\|\vec{X}_i - \vec{X}_j\|^2}{\sigma^2}\right), \quad (3.12)$$

where  $\vec{X}_i$  and  $\vec{X}_j$  are the feature vectors of  $i$  and  $j$ , and  $\sigma$  is a scaling parameter. The Gaussian similarity transforms the Euclidean distance into a similarity measure via a Gaussian kernel. If all the features of the nodes coincide (that is,  $d(i, j) = 0$ ), then the two nodes are similar and  $w_{ij} = 1$ . This similarity decreases as the Euclidean distance increases, with a characteristic length controlled by the parameter  $\sigma$ . The parameter  $\sigma$  is usually fine-tuned for each dataset, and in Section 3.4.4 I show a way to optimize it.

#### 3.4.2 Partitioning the similarity graph

Given an adjacency matrix  $W$  of a graph, there are many eigenvector-based methods which are proposed to partition the graph into subsets with highly connected nodes. Often, most of these methods have no supporting theoretical background (Ng

<sup>4</sup> The use of other construction methods for the similarity graph did not seem to improve on the overall classification of ganglion cells, though no exhaustive study was performed in this regard.

et al. 2002; Luxburg 2007). Two main approaches have been used to formalize spectral clustering, using either normalized minimal cuts of the graph (Shi and Malik 2000), or random walks on a graph (Meila and Shi 2001). While these methods seem unrelated at first, they were shown to be equivalent (Meila and Shi 2001) and complement each other in clarifying how spectral clustering works.

If a graph is partitioned into two disjoint sets of nodes  $A$  and  $B$  by removing edges, the sum of the disconnected weights will be given by

$$\text{cut}(A, B) = \sum_{i \in A} \sum_{j \in B} w_{ij} . \quad (3.13)$$

A minimal cut searches for a partition where  $\text{cut}(A, B)$  is minimal (Shi and Malik 2000; Luxburg 2007). Because this definition could easily lead to sets where only a single node is separated, it has been proposed that minimal normalized cuts should be used instead (Shi and Malik 2000). Normalized cuts are defined as

$$\text{Ncut}(A, B) = \text{cut}(A, B) \left( \frac{1}{\text{vol}(A)} + \frac{1}{\text{vol}(B)} \right) \quad (3.14)$$

where  $\text{vol}(A) = \sum_{i \in A} \sum_j w_{ij}$  is the total sum of weights connecting nodes of set  $A$  to all nodes in the graph. Thus, a minimal normalized cut is the procedure of finding  $A$  and  $B$  such that  $\text{Ncut}(A, B)$  is minimal. The minimal normalized cut is more parsimonious, as it takes into account the relative weight of the severed edges.

However, there is no known efficient algorithm to minimize a normalized cut exactly<sup>5</sup>, and an approximation has been proposed (Shi and Malik 2000). This approximation is based on the eigenvectors of the graph Laplacian. Defining the degree of a node  $i$  as

$$g_i = \sum_m w_{im} , \quad (3.15)$$

and the diagonal matrix

$$D = \begin{bmatrix} g_1 & 0 & \cdots & 0 \\ 0 & g_2 & \cdots & 0 \\ \vdots & \vdots & \ddots & \vdots \\ 0 & 0 & 0 & g_n \end{bmatrix} , \quad (3.16)$$

the graph Laplacian is given by

$$L = D - W . \quad (3.17)$$

<sup>5</sup> Indeed, the minimal normalized cut problem was shown to be NP-complete (Shi and Malik 2000). NP-complete is a class of problems for which no polynomial-time algorithms are expected to exist.

The approximate minimal normalized cut is obtained (Shi and Malik 2000) by solving the generalized eigenvector problem

$$L\vec{v} = \lambda D\vec{v}, \quad (3.18)$$

and taking the second smallest generalized eigenvector  $\vec{v}^{(2)}$  as an indicator vector for the partition; that is, for a given node  $i$ , the coordinate  $v_i^{(2)}$  will specify to which side of the partition the node belongs.

Intuitively, if the transition probability between two nodes is proportional to the weight of the edge connecting them, a random walker will likely visit a region of highly connected nodes. In this region, the random walker will visit the same nodes over and over. If there are few connections to other nodes in other groups, the random walker might take a long time to reach another group of highly connected nodes. One can formalize this intuition by defining the transition probability between nodes  $i$  and  $j$  as

$$p_{ij} = \frac{w_{ij}}{\sum_m w_{im}}, \quad (3.19)$$

which is the stochastic matrix  $P = \{p_{ij}\} = D^{-1}W$ . If  $P$  represents a Markov process, the eigenvectors and eigenvalues of  $P$  can be used to describe the dynamics of a random walk, with a convergence to a stationary state (if it converges) with a rate controlled by the eigenvalues. Note that by left-multiplying (3.18) by  $D^{-1}$ , one obtains

$$\begin{aligned} D^{-1}L\vec{v} &= (I - D^{-1}W)\vec{v} = \lambda\vec{v}, \\ P\vec{v} &= (1 - \lambda)\vec{v}. \end{aligned} \quad (3.20)$$

Thus, an eigenvector  $\vec{v}$  of the stochastic matrix  $P$  with eigenvalue  $(1 - \lambda)$  is also an eigenvector of  $L$  with eigenvalue  $\lambda$ . As before, the second *largest* eigenvector of  $P$  is also an indicator vector and partitions the graph. The equivalence between the random walk and the minimal normalized cuts is not a coincidence; the minimal normalized cuts separate the graph into two regions  $A$  and  $B$ , where the chance of transiting from a node in  $A$  to a node in  $B$  is minimal (Meila and Shi 2001; Luxburg 2007). That is, a random walk starting in  $A$  will tend to stay in it for a long time.

The graph Laplacian has an interesting property. Given a vector  $\vec{a}$ ,

$$\begin{aligned} \vec{a}^T L\vec{a} &= \vec{a}^T (D - W)\vec{a} = \vec{a}^T D\vec{a} - \vec{a}^T W\vec{a}, \\ &= \sum_i g_i a_i^2 - \sum_{i,j} w_{ij} a_i a_j, \\ &= \frac{1}{2} \sum_{i,j} w_{ij} (a_i - a_j)^2. \end{aligned} \quad (3.21)$$

From this equation, it is easy to see that  $\vec{1} = [1, 1, \dots, 1]^T$  is an eigenvector of  $L$  with eigenvalue 0, and the multiplicity of the eigenvalue 0 will indicate the number of

connected components<sup>6</sup> in the graph (see, e.g., Luxburg 2007). This is consistent with the random walk interpretation, as  $P\vec{1} = \vec{1}$  is always true for an stochastic matrix because the rows are normalized to one. Moreover, if  $\vec{a}^T L \vec{a} = 0$ , this result implies that for  $w_{ij} \neq 0$ ,  $a_i = a_j$  and all nodes in the same connected component will have the same constant. If the value of  $\vec{a}^T L \vec{a} \neq 0$  but small, with the nodes  $i$  and  $j$  connected ( $w_{ij} > 0$ ), then the difference between  $a_i$  and  $a_j$  must also be small. This suggests an intuitive reason for why the coordinates of the second smallest eigenvector of  $L$  can be used for partitioning the similarity graph, if its eigenvalue is very small or zero (for a proof, see Shi and Malik 2000).

### 3.4.3 Clustering using graph partitions

Based on the second smallest eigenvector of the graph Laplacian  $L$ , a similarity graph can be partitioned into two disjoint sets of nodes. For clustering a dataset, though, one often seeks a specific number  $K$  of groups (Section 3.1). In principle, the similarity graph could be recursively split until a desired number of groups is reached (Shi and Malik 2000; Meila and Shi 2001). However, the next smallest eigenvectors of  $L$  may already contain the information required to group similar nodes, as suggested by (3.21) above.

For instance, if the graph consists of  $K$  connected components, both the similarity matrix  $W$  and the graph Laplacian  $L$  can be block-diagonalized. The  $K$  eigenvalues  $\lambda_{1,2,\dots,K} = 0$  of  $L$  will lead to  $K$  orthogonal eigenvectors  $\vec{v}_{1,2,\dots,K}$ . The indicator vectors of the connected components are eigenvectors of  $L$  (Luxburg 2007). But note also that any rotation of the  $K$  eigenvectors still spans the same subspace. As such, the smallest eigenvectors  $\vec{v}_{1,2,\dots,K}$  will cover the same subspace as the indicator vectors, but rotated, which could hinder the interpretation of any single eigenvector as an indicator vector. (Ng et al. 2002).

Nevertheless, as the eigenvectors span the same subspace, then the eigenvector coordinates  $v_m^i = v_m^j$  (for every  $m = 1, 2, \dots, K$ ) for nodes  $i$  and  $j$  in the same connected component. In this  $K$ -dimensional space, the nodes form compact clusters; thus, any simple clustering algorithm – such as K-means or Gaussian mixtures – can be used to easily separate the  $K$  components. (Meila and Shi 2001; Ng et al. 2002; Luxburg 2007)

Of course, having a block-diagonal similarity matrix  $W$  is an ideal case. In practice, this is not always the case. Weak connections between different components do exist, sometimes by noise, and should be taken into account. Hence, it is important to know whether spectral clustering methods still work for “real” datasets. If the ideal block-diagonal matrix is  $\tilde{W}$ , one can treat the difference  $E = W - \tilde{W}$  as a perturbation. Ng et al. (2002) shows, using matrix perturbation theory, that if there

<sup>6</sup> In a connected component, a path can be found between any pair of nodes.

is at least one eigenvalue  $\lambda_{K+1} = \delta > 0$ , and the perturbation is small compared to  $\delta$ , then spectral clustering can still be used to find  $K$  partitions in the similarity graph. (for a formal proof, see Ng et al. 2002; Luxburg 2007)

#### 3.4.4 An algorithm for spectral clustering

So far, I have shown how and why spectral partitioning of a graph works. While there are many choices of spectral clustering methods (Shi and Malik 2000; Meila and Shi 2001; Ng et al. 2002), they are closely related (Luxburg 2007). For this thesis, I use the algorithm of spectral clustering as proposed by Ng et al. (2002), as it directly recovers  $K$  clusters. This will be the algorithm that I refer from now on as spectral clustering, and it is performed as follows.

Recall that the goal is to find  $K$  clusters in a dataset. A dataset contains  $N$  data points, each having  $n$  features. The features of a node  $i$  are organized as an  $n$ -dimensional vector  $\vec{X}_i$ . A similarity matrix  $W$  for this dataset is built as described in Section 3.4.1. In short, the similarity graph is fully-connected and the weight of an edge between a pair of nodes  $i$  and  $j$  is given as

$$w_{ij} = \exp(-\|\vec{X}_i - \vec{X}_j\|^2 / \sigma^2), \quad (3.22)$$

which is a Gaussian similarity with  $\sigma$  as a scale parameter.

Given a similarity matrix  $W$ , the degree of a node  $i$  is defined as  $g_i = \sum_j w_{ij}$  and a diagonal matrix  $D$  is constructed with the values  $g_i$  in its diagonal. A normalized graph Laplacian<sup>7</sup> is then given by

$$\begin{aligned} L_{\text{sym}} &= I - D^{-\frac{1}{2}} L D^{-\frac{1}{2}}, \\ &= D^{-\frac{1}{2}} W D^{-\frac{1}{2}}. \end{aligned} \quad (3.23)$$

The  $K$  largest eigenvalues of  $L_{\text{sym}}$  are  $\lambda_{1,\dots,K} \leq 1$ , with respective eigenvectors  $\vec{v}_{1,\dots,K}$ . If any repeated eigenvalues exist, the eigenvectors are chosen to be orthogonal. The  $K$  largest eigenvectors are then collected in a matrix

$$\begin{aligned} V &= [\vec{v}_1 \vec{v}_2 \cdots \vec{v}_K], \\ &= \begin{bmatrix} v_1^1 & v_2^1 & \cdots & v_K^1 \\ v_1^2 & v_2^2 & \cdots & v_K^2 \\ \vdots & \vdots & \ddots & \vdots \\ v_1^N & v_2^N & \cdots & v_K^N \end{bmatrix}. \end{aligned} \quad (3.24)$$

<sup>7</sup> The results in the previous section for the unnormalized graph Laplacian  $L$  still apply to the normalized graph Laplacian  $L_{\text{sym}}$ , with the distinction that one now must find the  $K$  largest eigenvectors  $\vec{v}_{1,\dots,K}$ , whose eigenvalues  $\lambda_{1,\dots,K} \leq 1$ . (see, e.g., Ng et al. 2002; Luxburg 2007)

The matrix  $V$  can be normalized so the rows have unit length, resulting in a new matrix  $Y = \{y_{ij}\}$  whose elements are

$$y_{ij} = \frac{v_j^i}{\sqrt{\sum_m (v_m^i)^2}}. \quad (3.25)$$

The matrix  $Y$  has size  $N \times K$  and a row  $i$  can be taken as coordinates of the original data point  $i$  in a transformed  $K$ -dimensional space. Because of the properties of the graph Laplacian shown in the previous section, the coordinates  $y_m^i$  and  $y_m^{i'}$  (for every  $m = 1, \dots, K$ ) should be numerically close if  $i$  and  $i'$  belong in the same cluster. So, in this transformed space, the data should consist of many compact clusters, which are more amenable to any simple clustering methods.

Finally, K-means is used to find  $K$  clusters in the transformed data, with the rows of  $Y$  taken as  $N$  data points, each containing  $K$  features. The labels  $C = \{c_i\}$  returned by K-means are directly used to label the original dataset. Because the new features should form convex and tight clusters, K-means is expected to easily find the clusters. K-means was repeated 3000 times and only the best repeat, the one with smallest dispersion, was considered.

Ng et al. (2002) also suggests a way to optimize the scaling parameter  $\sigma$ . After clustering, the dispersion of the data can be measured (e.g., from Equation 3.4) and the  $\sigma$  adjusted until a minimal dispersion is found. That is, until the clusters are as compact as possible.

An example of this method is shown in Figure 3.3. A toy dataset used throughout this chapter contains non-convex clusters, which foiled every attempt to cluster it based on K-means or Gaussian mixture. Spectral clustering not only is able to find convex clusters, just as the other methods, but also works for non-convex clusters – differently from K-means and Gaussian mixtures.

The similarity matrix for the toy dataset with complicated clusters is shown in Figure 3.4. While the original similarity matrix shows no apparent structure, spectral clustering is used to find groups of very similar data points. Once the data points are sorted according to their assigned labels (for the  $K = 3$  case), the similarity matrix is shown to be organized in blocks of highly similar elements (center of Figure 3.4), with almost no similarity between points in different blocks.

Finally, Figure 3.5 illustrates how spectral clustering works ( $K = 3$ ). On the bottom of Figure 3.5, the three largest eigenvectors of  $L_{\text{sym}}$  are shown. Note how the eigenvector coordinates are piecewise constant, as expected from (3.21). Each coordinate represents one point in the dataset, and the difference between two coordinates should be small if the points should belong together. The coordinates of the eigenvectors are used to transform the points into a 3-dimensional space, whose projections are shown on the top. The transformed dataset shows very tight and easily classifiable clusters. In this example, the non-convex clusters have been transformed into well-separated compact clusters, and it is clear that these clusters



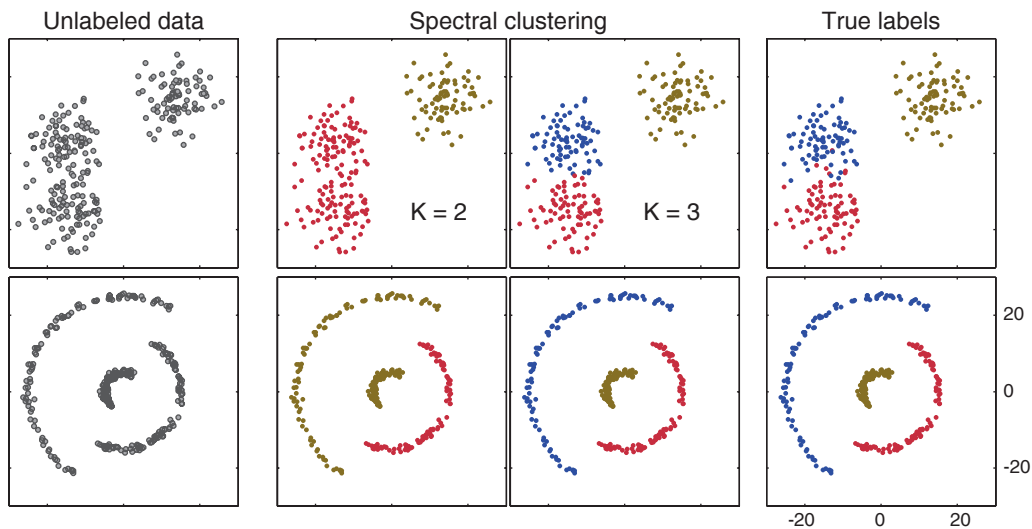


Figure 3.3: SPECTRAL CLUSTERING. The unlabeled dataset (left) is classified via spectral clustering using  $K = 2$  and  $K = 3$  clusters (center). The original labels are shown in the right. Besides classifying convex clusters well (top), spectral clustering is well suited to classify non-convex clusters because it considers the local structure (bottom).

should be found by any reasonable clustering method. Although this fact may not hold true for every dataset, spectral clustering can be a useful method for teasing out clusters when complicated cluster shapes are expected.

### 3.5 HEURISTICS FOR THE NUMBER OF CLUSTERS

The clustering methods defined in this chapter require as input the number of clusters that are sought. So far, nothing was said on how to find this crucial parameter. Estimating the number of clusters is not an easy problem; it can be specially challenging when there is no prior knowledge to guide the estimation. Before venturing, finally, into the classification of ganglion cells, I will show how to estimate the number of classes in a dataset, in the context of a general clustering problem. Techniques which apply only to the classification of ganglion cells will be explained in the next chapter.

Clustering is straightforward when the clusters are clearly separated and their number is known. Even if the correct number of clusters in a dataset is unknown, clustering still may be used to provide an estimate. An expert in the problem at hand (be it classifying shopping preferences of consumers, animal species, or neuronal cells) may use their intuition and previous knowledge for finding the number that best explains the data. Unfortunately, real data is messy. The intuition

## CLUSTERING

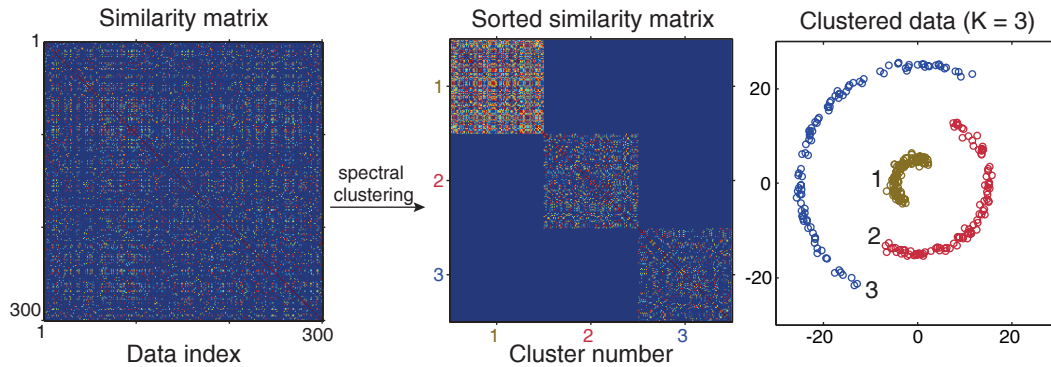


Figure 3.4: SIMILARITY MATRIX. (left, center) The similarity matrix of the dataset (left) is created from the pairwise Gaussian similarity of data points (see text). Pixel brightness indicates the similarity of a pair, with brighter pixels showing higher similarity (dark blue means no similarity). If data points are ordered by assigned cluster (right; from spectral clustering with  $K = 3$ ), one observes blocks of similarity (center).

of what constitutes a class may not be sufficient if the data is unclear. Even in good datasets, different experts might disagree on how many clusters should be present. In this case, it could be useful to have an objective procedure that substitutes or complements the expert knowledge.

A naive algorithm could assign each data point to its own class, but nothing could be generalized from that classification. At the other extreme, the whole dataset could be lumped as a single class; and nothing new would be learned<sup>8</sup>. Of course, the correct number of clusters must be between those extremes; but how to find it? Over time, many heuristics have been developed, each depending on the properties of the chosen clustering algorithm.

### 3.5.1 *Gap statistic*

For K-means, a common approach is to observe the sum of intra-cluster distances (the dispersion, as defined by Equation 3.4) as it changes with increasing number of clusters. When new clusters are added, they are created by rearranging the old clusters and the total dispersion will reduce. This could go on until each data point is in its own cluster, which is not desired. Thus, the hypothesis is that once the new clusters are formed only by splitting tight clusters, there should be a noticeable slow-down in the decay of the intra-cluster distances. The number of clusters just

<sup>8</sup> In fact, the task would become much easier, but the result boring.

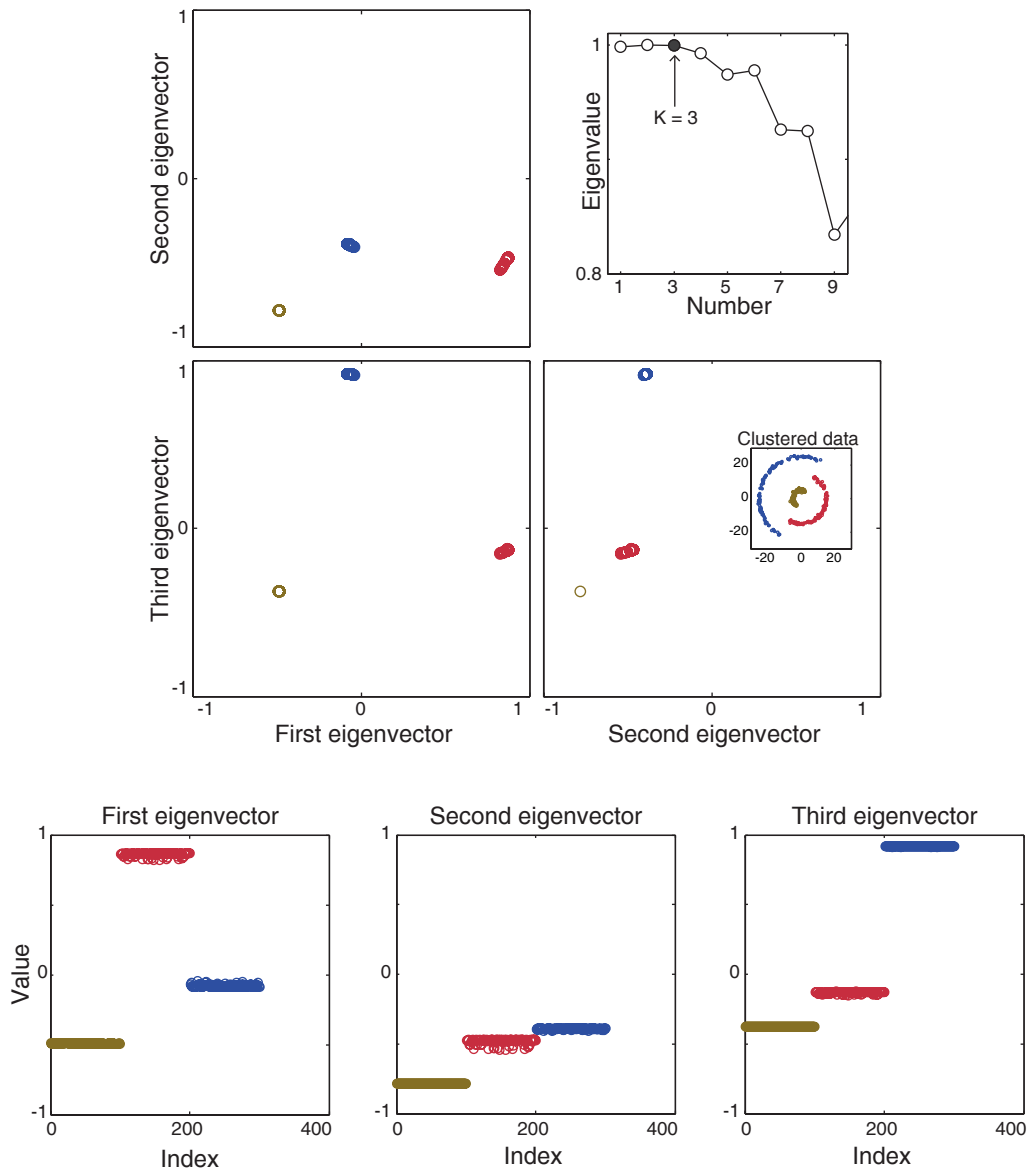


Figure 3.5: SPECTRAL CLUSTERING PROCEDURE. The spectral clustering uses the eigenvectors of the normalized graph Laplacian for improving data separation. For  $K = 3$  clusters, the first three eigenvectors are selected and shown in the bottom. Each eigenvector coordinate represents a single data point and can be used together to separate the data points (top center). Finally, because the transformed data is typically well separated and compact, simple clustering methods (such as K-means, or Gaussian mixture) work well in the transformed dataset and can be used for classification.

before the decay rate changes is then considered the number of clusters of the dataset.

This method as described is a subjective, but often suggested, rule-of-thumb. Indeed, it has already been proposed for a long time (see, e.g., Thorndike 1953), but only recently formalized (Tibshirani et al. 2001). A “gap” is defined as the difference between the observed decay rate of the dispersion and the decay from a surrogate distribution of features. Then, the most likely number of clusters is found when the gap is largest (Tibshirani et al. 2001).

### 3.5.2 Akaike and Bayesian information criteria

Other approaches are better suited for models with a likelihood function, such as the Gaussian mixture in Section 3.3. Again, the idea is to let the number of clusters vary, but with a cost for each new cluster. If no penalty existed, the number of clusters would be the number of data points. A penalty incorporates a trade-off in the model, where the gains from better explaining the data must be considered against the costs of creating new clusters. More formally, given a cost function  $F(K, N)$ , a new likelihood is defined as

$$\log \mathcal{L}'(\theta_K) = \log \mathcal{L}(\theta_K) - F(K, N) , \quad (3.26)$$

where  $\log \mathcal{L}(\theta_K)$  is the original model likelihood, with parameters collected in  $\theta_K$ , and the cost is a function of how many clusters ( $K$ ) and data points ( $N$ ) are in the dataset.

In statistics, this is known as a problem of model selection (see, e.g., Hastie et al. 2009; Barber 2012); that is – among different models, which is better at explaining the data? Two measures are often used. Defining  $\#(K) = \dim(\theta_K)$  as the number of parameters required to fit a model with  $K$  clusters, the Akaike information criterion (AIC) is given (Akaike 1974) by

$$\text{AIC}(\theta_K) = -2 \{ \log \mathcal{L}(\theta_K) - \#(K) \} , \quad (3.27)$$

and the Bayesian information criterion (BIC) is defined (Schwarz 1978) as

$$\text{BIC}(\theta_K) = -2 \left\{ \log \mathcal{L}(\theta_K) - \frac{\#(K)}{2} \log N \right\} . \quad (3.28)$$

The “best” model will then be the one which minimizes either the AIC or BIC, which is the same as maximizing the likelihood with different costs. But which of the two? While the costs of both AIC and BIC are linear on the number of parameters, the BIC penalizes large datasets more. As more data is accumulated, the BIC favors models which are simpler than the ones given by AIC. However, there is no consensus on whether AIC or BIC gives a better model.

Nevertheless, because the BIC will estimate fewer clusters than AIC, one can use AIC and BIC together to obtain a bound on the number of clusters.

### 3.5.3 Eigenvalues of the graph Laplacian

In spectral clustering, the eigenvectors of the graph Laplacian (Equation 3.17) were used to partition the similarity graph, thus clustering the data. But the eigenvalues of the Laplacian matrix can be useful too: they indicate how many clusters one should expect in a dataset. For the *unnormalized* graph Laplacian, the number of null eigenvalues gives the number of connected components in the graph. For a block-diagonal similarity matrix, this is an estimate for the number of clusters. For other datasets, the number of clusters  $K$  is estimated by finding the first large gap  $|\lambda_{K+1} - \lambda_K|$ , where  $\lambda_{1,2,\dots,K+1}$  are the  $K + 1$  *smallest* eigenvalues (Luxburg 2007).

An example of this method can be seen on the top right of Figure 3.5. There, the *largest* eigenvalues of the *normalized* graph Laplacian start decreasing after  $K = 3$ , the true number of clusters in the data. If the number of clusters were unknown, an estimate of  $K = 6$  based on the gap between the sixth and seventh eigenvalues would be reasonable.



FUNCTIONAL TYPES OF RETINAL GANGLION CELLS

---

*The concept of a neuronal type can be quite slippery. Just when you think you've got it in hand, it can jump out of your grasp like the soap in the shower.*

— JEREMY COOK, *Getting to Grips with Neuronal Diversity*

For classifying retinal ganglion cells, a few strategies are commonly employed. As shown in Chapter 1, ganglion cells can be classified by using genetic markers, morphological aspects, or light-response properties. In this chapter, I investigate the classification of ganglion cells in the axolotl retina based on their response to a simple stimulus, a spatiotemporal uncorrelated noise (white-noise).

While simple, a spatiotemporal white-noise can be used, via reverse correlation, to find the average spike-causing stimulus for a cell (spike-triggered average, STA; see Section 2.5.2). The STA provides a rich description of a ganglion cell's receptive field. Besides capturing the spatial extent of a receptive field, the STA gives an approximation for the fine temporal filtering properties of that receptive field. The STA has been useful for classifying ganglion cells in the rabbit (DeVries and Baylor 1997), monkey (Field and Chichilnisky 2007), and tiger salamander (Segev et al. 2006; Marre et al. 2012).

Here, I investigate a classification of ganglion cells based on their receptive field features from the STA and the temporal structure of their spike trains (represented by the spike-train autocorrelation). These features are obtained for each cell. The cells are then grouped based on their similarities via a spectral clustering algorithm (Section 3.4). At least three groups were consistently found between experiments.

Before delving into the results of cell classification, however, it is important to understand the signature of a cell type. How to recognize that a group of cells forms a type? For ganglion cells of the same type, a pattern is often observed in their somas. This pattern, an apparent repulsion between cell bodies, resembles a mosaic whose occurrence is referred to as tiling. Tiling is used in morphological studies as a tell-tale sign of single cell types (Wässle, Peichl, et al. 1981; Shamim et al. 1999; Zhang et al. 2012) and was often observed in the receptive fields of functionally classified ganglion cells (DeVries and Baylor 1997; Field and Chichilnisky 2007). Tiling is considered a gold-standard for confirming retinal cell types (Cook and Chalupa 2000; Sanes and Masland 2015). I will briefly review the importance

of tiling for classifying cell types, and methods to measure the mosaic formed by the receptive fields of a putative type.

#### 4.1 ASSESSING CLASSIFICATION QUALITY WITH TILING

Retinal cells of a single type are not just randomly located in the retina, but their somas form a seemingly regular pattern – akin to a frustrated lattice – with an apparent local (but not global) regularity (Wässle and Riemann 1978; Wässle, Peichl, et al. 1981; Wässle, Boycott, and Illing 1981; Rockhill et al. 2000). This pattern was observed as a minimum distance between somas of cells of the same type, often compared to a repulsion. Because of this local structure, this spatial organization is described as a mosaic; the cells which form a mosaic are then said to tile (Cook 2004).

Tiling is likely not just an artifact of the retinal development, and is expected to play a role in visual encoding (see, e.g., Cook 1998). Receptive fields were found to tile in the primate (Field and Chichilnisky 2007) and rabbit (DeVries and Baylor 1997) retinas. As cell types are expected to encode independent features of the visual scene, tiling reduces redundancy (DeVries and Baylor 1997; Masland 2001). By respecting a minimum distance, cells avoid encoding the same feature at the exact same visual location. However, to avoid a perceptual gap, the separation between cells is not expected to be arbitrarily large. This interplay between reducing redundancy and avoiding gaps has been observed in receptive fields of ganglion cells, and may depend on the functions that a cell exerts (DeVries and Baylor 1997; Field et al. 2007; Gauthier et al. 2009).<sup>1</sup>

Because of its near ubiquity, tiling is often taken as the defining property of cell types and used for compensating the unknowns in cell classification (Cook 1998). When describing a cell type, it is often unclear which properties of a retinal cell should be considered. Moreover, the variance of a property inside a type may not be known a priori, and could indeed be as large as the variance across types. Some properties may overlap between types, requiring the combination of features to disambiguate a neural type (Rowe and Stone 1980). However, most of the uncertainty vanishes if a group of retinal cells is found to tile (Cook and Chalupa 2000; Cook 2004; Sanes and Masland 2015).

Whether one “defines” or “discovers” a type, the observation of tiling cells is a strong evidence for the existence of a cell type (Cook 1998). Violations of tiling have been used in morphological studies to guide the detection of new cell types,

<sup>1</sup> A population of ganglion cells with Gaussian-shaped receptive fields, when packed at a distance smaller than the linear size of a receptive field, has a uniform spatial sensitivity to stimuli. This would imply that this *population* could equally respond to a spot flashed anywhere in the aggregated visual field, avoiding perceptual gaps (DeVries and Baylor 1997). Gauthier et al. (2009) has further shown, in the primate retina, that receptive fields interlock as “puzzle pieces”, with the irregularities of a receptive field being compensated by the irregularities of its neighbors.



as features could be selected in order to distinguish overlapping cells. Then, by using the distinguishing features, cell types can be disambiguated and shown to tile (Cook and Sharma 1995; Shamim et al. 1999; Cook 2004).

Therefore, tiling was considered in this work as a benchmark for a cell type. If a group of cells was found to tile, the hypothesis was that they belonged to the same bona-fide type. Because ganglion cells of a type may be collected by a clustering algorithm into two or more groups, groups with similar features were tested on whether they independently tiled the retina.

#### 4.1.1 *Measuring tiling*

To make the detection of tiling less subjective, one must measure how cells are spatially distributed in a retina (for a review, see Cook 2004). Given a group of cells, how to tell whether they indeed tile?

##### *Nearest-neighbor distance method*

The use of the nearest-neighbor distances (Clark and Evans 1954) was one of the first, and perhaps most intuitive, methods to be proposed for assessing tiling (Wässle and Riemann 1978). This method is based on measuring the distance of a cell to its closest neighbor; the average nearest-neighbor distance, then, is an estimate of how closely packed cells are and, if a significance test is desired, the distribution of distances itself can be analyzed (Cook 1996).

However, while simple, the nearest neighbor method may be misleading for incompletely recorded populations, as the average distance increases when neighboring cells are missing (Cook 1996; Cook 2004). Because recordings are rarely complete, the nearest neighbor method should be cautiously employed.

##### *Spatial autocorrelation*

A second method, the spatial autocorrelation, measures not only how close cells in a group are, but also whether their cell bodies (or receptive fields) repel one another (Rodieck 1991). After choosing a reference cell from the group, all other cells are plotted relative to this reference cell. By repeating the procedure for all cells, one at a time as reference cell and overlaying the plots, one obtains what is called a spatial autocorrelogram.

For a group of cells, the spatial autocorrelogram provides a clear visualization of their spatial organization. If the cells repel one another, there will be a region close to the center of the autocorrelogram which is empty – the size of this area is the minimum distance between cells. If the cells are distributed in a regular pattern, such as a lattice, this regularity will also be represented in the autocorrelogram.

As an example, the center columns of Figures 4.1B-C show the autocorrelogram for receptive field mosaics (left column of the same figure) created from a simple model of a mosaic. The model is based on displacing cells from an underlying hexagonal lattice and is described in detail in Section 4.1.2. In Figures 4.1B, the mosaic is close to a regular lattice (small displacements), which is reflected in the autocorrelogram; notice how the cells – represented as black dots – are grouped in a hexagonal pattern. In Figures 4.1C, the displacements are larger and no clear pattern is observed. For both mosaics, an empty region is observed in the center of the autocorrelogram, showing that the receptive fields indeed tile (which comes from the repulsion rule of the model, see Section 4.1.2).

The spatial autocorrelogram is not only a visual representation of the spatial distribution, but can also provide a quantitative measure. By counting the cells inside circular bins around the center, it is possible to observe a gap in the distribution of tiling cells below some distance. If the count of cells is normalized by the area of each circular bin (which increases linearly with the radius), the distribution is referred to as a density recovery profile (Rodieck 1991). The name is because the density of cells (if they tile) will increase with distance, eventually “recovering” an average density for large distances.

Compared to the nearest neighbor distance, the existence of an empty region in the center of the autocorrelogram (“exclusion zone”) is a more robust measure of tiling; this is especially true for recorded populations whose cells are (uniformly) missing (Cook 1996; Cook 2004).

#### 4.1.2 *Modeling a mosaic*

To illustrate the spatial autocorrelogram method, a mosaic was simulated using a simplified model. Similar (but more complex) models have been proposed in the literature, showing how local rules lead to the mosaic pattern observed in cell types (see, e.g., Galli-Resta et al. 1997; Reese 1999; Eglén and Ooyen 1999).

Here, a regular hexagonal lattice was used as substrate, from where the receptive fields were randomly displaced (Figure 4.1A). The displacement was independent for each cell and chosen from a symmetric 2D-Gaussian distribution with standard deviations of either 20% (Figure 4.1B) or 100% (Figure 4.1C) of the receptive field size. For mimicking repulsion, the displacement of a cell was re-sampled whenever the chosen position would cause a large overlap with an already existing receptive field (i.e., centers having a distance less than a receptive field diameter). The receptive field size and orientation for every simulated cell was the same. For simulating an incomplete mosaic, cells were randomly removed with a probability of 20%.

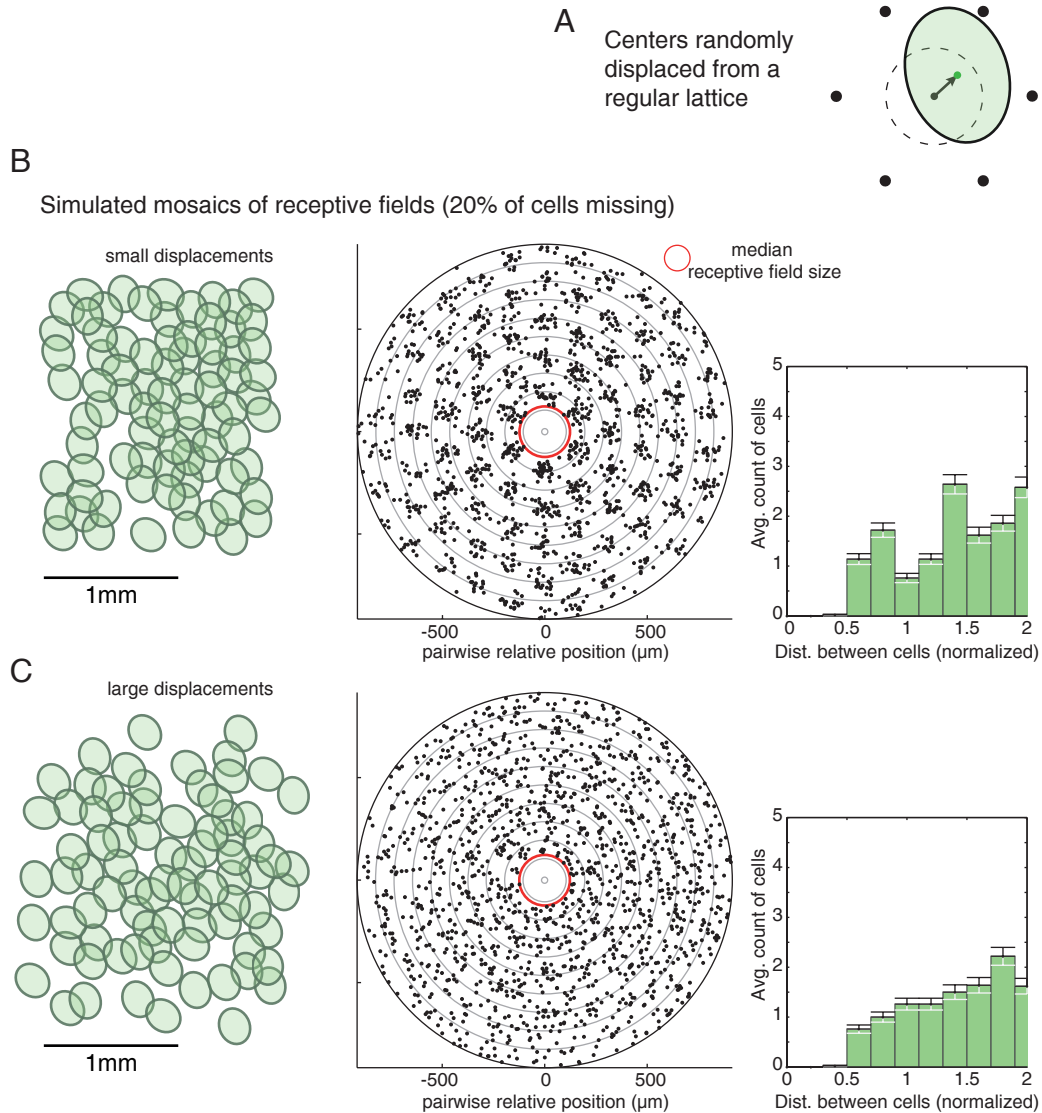


Figure 4.1: MOSAICS OF RECEPTIVE FIELDS. One of the tell-tale signs of a single cell type is the apparent repulsion between receptive fields (tiling). (A) Mosaics are simulated by randomly displacing center locations from an underlying hexagonal lattice; a displacement is re-sampled if the chosen location is closer to another cell than a receptive field size. To simulate an incomplete mosaic, 20% of cells are randomly excluded. (B,C) Autocorrelation of the receptive field locations (center; Rodieck 1991) for simulated mosaics (left); for each pair of cells, a point is placed at the location of the second cell, relative to the first. The reduced number of centers at a distance less than the median receptive field size (red ring) suggests tiling, which can also be seen as a gap in the cell count (right; mean $\pm$ std. error). A gap below a distance of 0.5 indicates that the centers are separated by at least one receptive field size.

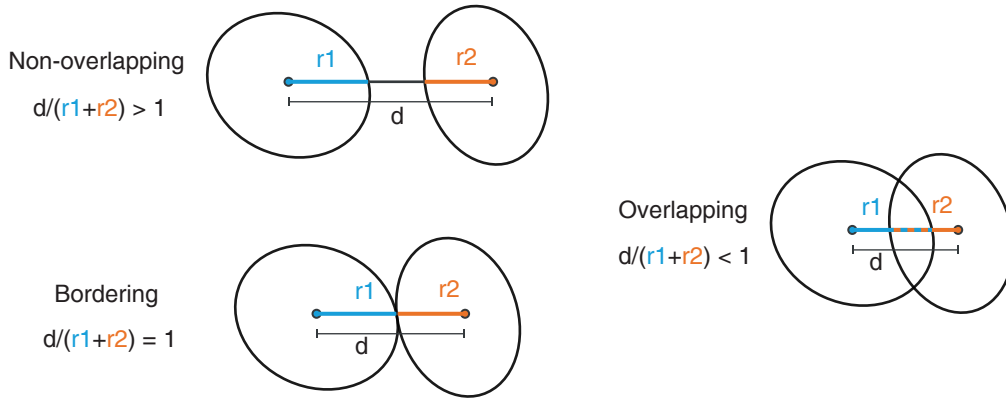


Figure 4.2: **NORMALIZED DISTANCE BETWEEN RECEPTIVE FIELDS.** To account for differences in receptive field sizes, the distance between a pair of receptive field centers ( $d$ ) is normalized by the receptive field radii ( $r_1$  and  $r_2$ ), in the direction of the line connecting their centers (DeVries and Baylor 1997). The receptive field radius of a cell, in a specific direction, is defined as the line segment from the center to the border of the one standard deviation ellipse.

#### 4.1.3 Normalizing distances

Because receptive field sizes may vary (within or between experiments), the distance  $d$  between two receptive field centers was normalized by the distance from each center to its respective border,  $r_1$  and  $r_2$ , measured along the line connecting both centers (DeVries and Baylor 1997). The normalized distance is then

$$d' = \frac{d}{r_1 + r_2} \quad (4.1)$$

and is a measure of receptive field overlap, as shown in Figure 4.2. For receptive fields that do not overlap,  $d' > 1$ . Once the border of the receptive fields touch,  $d' = 1$ . Finally, if the receptive fields overlap, then  $d' < 1$ .

Note, however, that small overlaps are not necessarily a violation of tiling. A normalized distance of  $d' = 0.5$ , for instance, shows that centers are away by a distance of about a receptive field size. While overlaps increase the redundancy, the receptive fields are still considered to tile if a minimum gap is observed in the distribution of cell distances (DeVries and Baylor 1997).

## 4.2 PHYSIOLOGICAL CLASSIFICATION OF GANGLION CELLS

For classifying ganglion cells based on how they respond to light, an experimenter has at their disposal an abundance of features which can be measured from those cells: contrast adaptation (Kastner and Baccus 2011), direction selectivity (Farrow and Masland 2011), spike-train statistics (Zeck and Masland 2007), receptive field shape and filtering properties (DeVries and Baylor 1997; Segev et al. 2006; Field et al. 2007), among others. One must still account, however, for how well a given feature distinguishes ganglion cells from different classes (Carcieri et al. 2003) – if at all – and how long an experiment must last for recording all the desired features.

An isolated retina does not remain viable for long, therefore a classification method is more useful when it uses a smaller set of features, recorded in the least amount of time. If the recording duration is short, one does not need to perform an experiment exclusively for identifying cell types. Rather, one can use the classification method as a tool to achieve further scientific goals, a tool to constrain the variability of the recorded cells. Better yet if these features can be extracted from a simple and commonly employed stimulus.

Uncorrelated noise (white-noise) is often used to estimate, via reverse correlation, the receptive field properties of ganglion cells (Chichilnisky 2001; see also Section 2.5.2). This stimulus allows the estimation of ganglion cell features such as the receptive field extent and its temporal filtering properties, features which can be useful for cell classification (DeVries and Baylor 1997; Segev et al. 2006; Field et al. 2007).

Besides recovering the receptive field properties, white-noise stimulation can be used for classifying ganglion cells based on statistical properties of the evoked spike-trains (Zeck and Masland 2007). The autocorrelation of the spike-trains, in mammalian retinas, has been useful for finding ganglion cell types which tile (DeVries and Baylor 1997; Field et al. 2007).

For tiger salamanders, Segev et al. (2006) suggested that only the temporal filters should be considered for cell classification. They reported that receptive field sizes and autocorrelation functions – while individually successful for separating cells into few types – blurred the distinction between ganglion cell types when taken together. However, the classification based on temporal components alone led to a single tiling type (Segev et al. 2006; Marre et al. 2012).

## 4.3 FEATURES OF GANGLION CELLS

To improve on the current classification for salamander ganglion cells, I investigated whether ganglion cell types in the axolotl retina could be found based on features obtained from spatiotemporal white noise stimulation: receptive field size, temporal dynamics, and autocorrelation function of the spike-trains.

In Section 4.4, these features are combined and a clustering algorithm is applied to study whether these features, when combined, can differentiate between ganglion cell types. But first, I will show how these features are distributed for ganglion cells from a single axolotl retina, show how – in contrast to the mammalian retina – the axolotl ganglion cells are not easily distinguished by a single feature, as similarly observed by Segev et al. (2006) for the tiger salamander.

#### *Multi-electrode recordings*

Retinal ganglion cells were recorded from an isolated axolotl retina using 252-electrode arrays (see Section 2.2). The retina was stimulated via an OLED display, which projected a computer-generated stimulus on the photoreceptor layer. Electrical activity from the ganglion cells was band-pass filtered (300 Hz to 5 KHz) and recorded from the multi-electrode array at 10 KHz. Spike-sorting was performed off-line and only the best units considered (i.e., those with well-separated spike shapes and assumed non-duplicate, as in Section 2.4).

#### *Binary white-noise*

The isolated retina was stimulated with an uncorrelated spatiotemporal noise, with a refresh rate of 30 Hz. For each pixel in each frame, the pixel brightness was randomly and independently chosen as dark or bright with equal probabilities (binary white-noise). Each stimulus pixel had a projected size of  $75 \times 75 \mu\text{m}$  on the retina.

#### *Temporal white-noise*

The retina was also stimulated with a temporal uncorrelated noise, with the same refresh rate of 30 Hz. This stimulus is sometimes referred as a full-field stimulation, because all pixels on the screen are set to the same brightness. For each frame, the screen brightness was independently sampled from a Gaussian distribution. The standard deviation of the stimulus was 30% of the average screen brightness (30% contrast).

#### 4.3.1 *Autocorrelation function*

For each cell, the spikes evoked from the binary white-noise stimulation were binned in 2 ms bins and the spike-train autocorrelated. The autocorrelation function of each cell was normalized so that the peak at zero-lag had unit amplitude. This normalized autocorrelation is related to the probability of a cell to spike, and is an estimate of how often a spike will occur after a certain delay from a reference

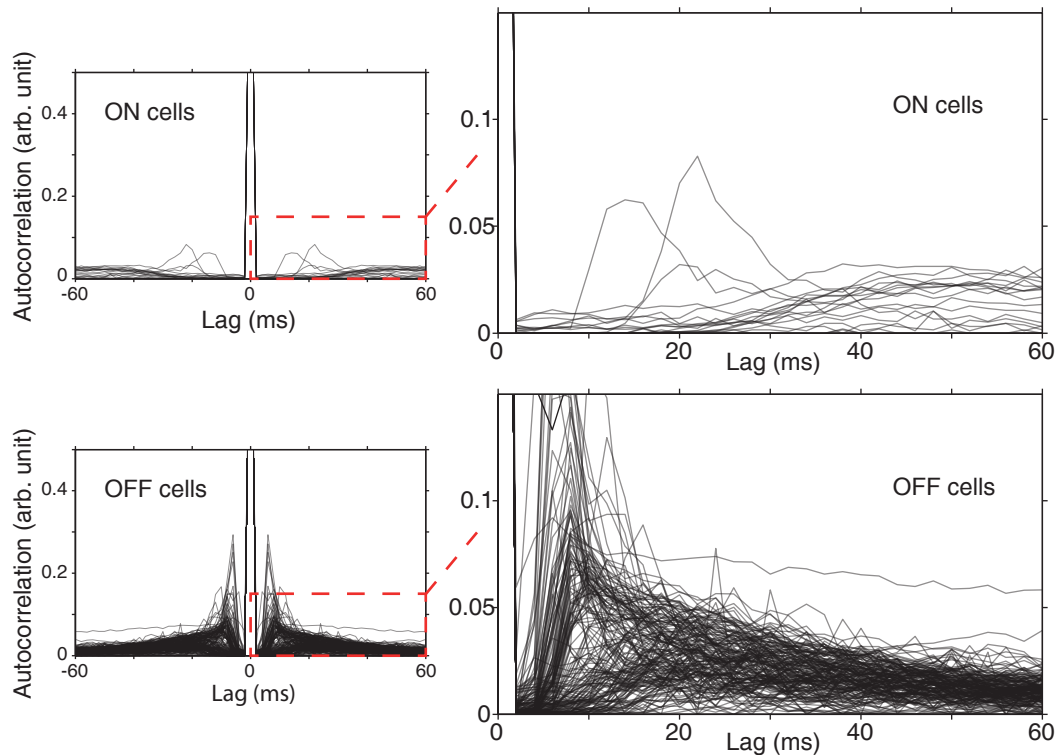


Figure 4.3: SPIKE-TRAIN AUTOCORRELATIONS FROM A SINGLE EXPERIMENT. Autocorrelation of the spike-trains for cells from a single experiment, with spikes binned into 2 ms bins. The autocorrelation function was normalized to unit amplitude. Observe the difference between ON (top) and OFF-cell (bottom) autocorrelations. The ON cells showed more sparse activity, with longer timer intervals between spikes. For the OFF cells at least three kinds of activity were observed, depending on the time course of the autocorrelation function (see text).

spike (regardless of how many spikes happened in-between; see, e.g., Rieke et al. 1999).

The autocorrelation of the spike-trains from a single experiment are shown in Figure 4.3. From the autocorrelation function, one observes that ON cells have more sparsely distributed spikes, with few spikes in the first 20 – 30 ms after a spike. The autocorrelation function increased to a constant value for longer time intervals, suggesting a return to an average firing rate from a sustained activity.

By visual inspection, at least three kinds of OFF cells could be distinguished based on the time course of their autocorrelation functions. The first kind showed a very strong peak in activity at 5 – 10 ms after a spike. For the second kind, activity rose sharply, but less pronounced than the first, at about 15 ms after a spike. The

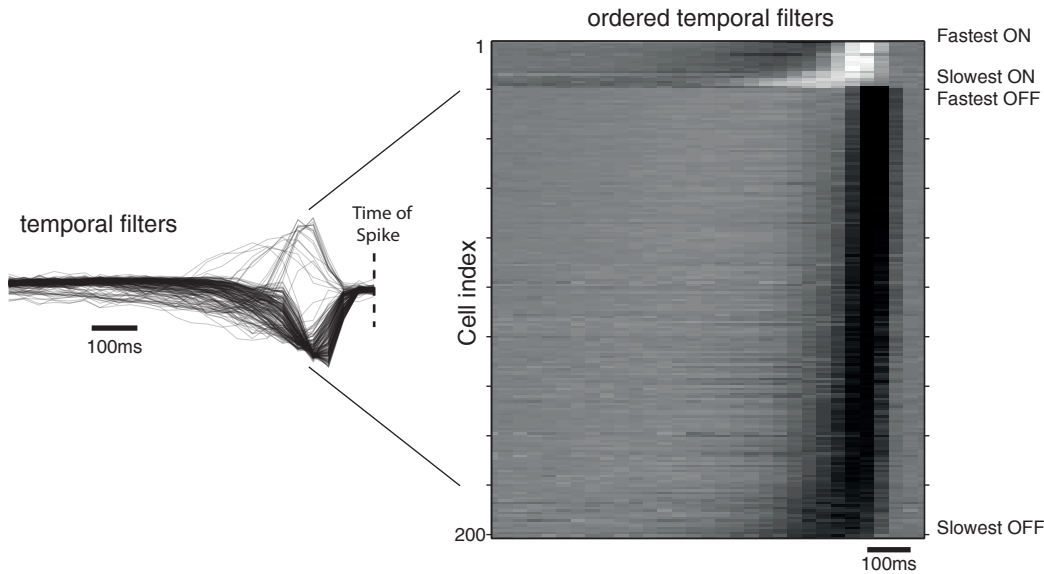


Figure 4.4: DIVERSITY OF TEMPORAL FILTERS FROM A SINGLE EXPERIMENT. A temporal filter provide a fine description of how a receptive field integrates a visual stimulus over time. The peak is used to determine the latency of the cell and whether it responds preferentially to an ON or OFF stimuli. In a single experiment there is a rich diversity of temporal filters. (left) Super-imposed temporal filters from a single experiment. (right) Temporal filters ordered by their polarity (ON, OFF) and latencies (fast to slow), based on their angle in the principal component space (see Figure 4.5).

third kind increased its activity, until a maximum activity at about 25 ms after a spike, but showed no sharp peak. The activity after a spike for the three kinds decreased at a similar rate for longer time intervals.

#### 4.3.2 Spatiotemporal receptive field

The spatiotemporal receptive fields of the recorded cells were estimated by reverse correlating the evoked spikes to the stimulus (see Section 2.5.2). For each ganglion cell, the spatiotemporal receptive field was approximated into separable spatial and temporal components using singular value decomposition (SVD, see Section 2.6). The re-composed spatiotemporal filters (obtained by multiplying the temporal and spatial components) were observed to be similar to the original spatiotemporal filters.



### 4.3.3 Receptive field size

The spatial receptive fields were approximated by a 2D-Gaussian function, with the ellipse at one standard deviation considered as the extent of the receptive field center. The receptive field radius  $r$  was defined as the geometric average of the semi-axes  $\sigma_1$  and  $\sigma_2$  of the ellipse, given by

$$r = \sqrt{\sigma_1 \sigma_2}, \quad (4.2)$$

and the receptive field size then defined as the diameter  $D_{RF} = 2r$ . This is the size of an equivalent circle that occupies the same area as the receptive field.

The distribution of receptive field sizes for a single experiment is shown in the bottom left of Figure 4.5. In a single experiment, the receptive field sizes ranged from 100 – 400  $\mu\text{m}$ ; however, no clear separation was observed between cells based on the receptive field size alone.

### 4.3.4 Temporal filters

A temporal filter provides a fine description of how a receptive field integrates a stimulus over time. It shows if a cell responds preferably to an increase (ON) or a decrease (OFF) of brightness, and how fast. In a typical experiment, temporal filters were observed to be very diverse (see Figure 4.4), with different latencies and waveforms. The majority of cells was observed to be OFF cells (183 out of 201, or 91% of the recorded cells). Possible groupings of cells based on temporal components were observed for ON cells. Manually, one could assign ON cells into at least three types according to their latencies: fast, medium and slow ON cells. For OFF cells, however, a manual classification would be hindered by the difficulty to distinguish between filters.

To gain insight on possible groupings of cells using principal component analysis (PCA), the temporal filters were projected onto their first two principal components, as shown in the top left of Figure 4.5. The first principal component was related to the amplitude (and sign) of the filter peak, clearly separating ON cells from the OFF cells. The second component was related to the latency of a cell, yet with opposite trend for ON and OFF cells. That is, for ON cells, the projection onto the second component was *largest* for the *slowest* ON cells. For OFF cells, the projection was *largest* for the *fastest* OFF cells. Conversely, the *slowest* OFF cells (and the *fastest* ON cells) had the *smallest* second component projection.

If the principal component space is described in polar coordinates, the angle  $\varphi$  of a cell represents both its latency and the sign of its peak. Moving counter-clockwise, for  $-\pi/2 < \varphi < \pi/2$ , the cells are ON and become *faster* with increasing angles; for  $\pi/2 < \varphi < 3\pi/2$ , the cells are OFF and become *slower* with increasing angles.

FUNCTIONAL TYPES OF RETINAL GANGLION CELLS

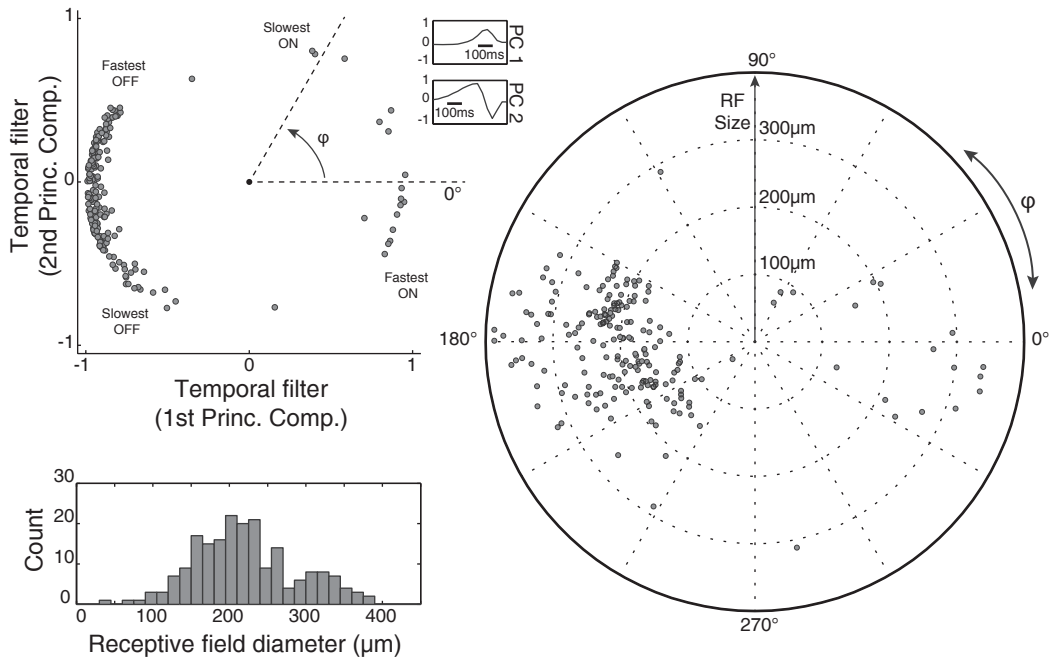


Figure 4.5: RECEPTIVE FIELD FEATURES. Features of the receptive field used for classification. (left column) Neither receptive field size nor the principal component projections of the temporal components alone show clear separations. (right column) Polar plot shows the receptive field size together with the angle in the principal component space. This visualization increases the apparent separation between ganglion cells, most noticeably in the 150–180° range.

Regions of apparent higher density were observed in the principal component space, but no clear separation could be obtained apart from the one between ON and OFF cells.

4.3.5 Combined temporal and spatial components

Based on their temporal and spatial components alone, cells could not be easily distinguished. One may consider, however, what happens if those components are taken together. The cells were represented in a polar plot with the angular coordinate given by the angle in the principal component space ( $\varphi$ ), and the radial coordinate given by receptive field size ( $D_{RF}$ ). This representation is shown on the right in Figure 4.5.

The combined data increased the apparent separation between ganglion cells. While visual inspection alone was not yet enough to find groupings of similar

cells, the differences of receptive field sizes between cells with similar temporal components (small angular differences) were large. Note for example the lower density of cells in a region between  $150\text{--}180^\circ$  in the polar plot. In that region, OFF cells with similar temporal components – the fastest OFF cells – may be separated based on their receptive field sizes.

#### 4.4 FINDING PUTATIVE TYPES

Manual classification of ganglion cells is not easy: differences which are clear for one researcher may not be as clear for another, and it is hard to draw a line between possible types. Specially so in the salamander retina, where the distinctions appear to be blurred. As discussed in Chapter 3, methods of unsupervised learning can find patterns in unlabeled data, such as the ganglion cells recorded here. In particular, cells which share similar features can be grouped using objective criteria, based on a clustering method (Zeck and Masland 2007; Farrow and Masland 2011).

For individual features, Segev et al. (2006) have shown that groups of ganglion cells in a tiger salamander retina could be distinguished by individually applying K-means (see Chapter 3) to each of the available features. K-means was found, however, unable to separate ganglion cells when all features were combined (Segev et al. 2006). Indeed, for grouping cells, clustering methods which assume convex and compact clusters may be a poor choice. This is especially true for the salamander retina, whose ganglion cells have few distinctive features and may not always form convex clusters in the feature space (see, for example, the projection of the temporal filters onto their principal components in Figure 4.5).

##### *Grouping ganglion cells with spectral clustering*

To account for the possibility of non-convex clusters, I used the spectral clustering algorithm as defined by Ng et al. (2002). A detailed explanation of the algorithm can be found in Section 3.4. Briefly, spectral clustering takes into account the local structure of the feature space, mapping the clustering problem into a graph partitioning problem. A graph is built using each cell as a node, with an edge created between two cells with a weight proportional to their pairwise similarity. The algorithm then partitions the nodes so that the least amount of connections are broken (measured by the sum of the edge weights), relative to the connections inside each group. That is, edges within strongly connected nodes will remain, while weak edges between distinct groups will be cut away.

*Gaussian similarity*

The similarity between two cells  $i$  and  $j$  was given by the Gaussian similarity

$$w_{ij} = \exp\left(-\frac{\|\vec{X}_i - \vec{X}_j\|^2}{\sigma^2}\right), \quad (4.3)$$

where  $\sigma$  is a parameter to be adjusted, and  $\vec{X}_i$  is an  $n$ -dimensional vector representing the coordinates of a cell  $i$  in the feature space. The similarity is unity when the two cells have exactly the same features, and decreases as the differences (measured with the Euclidean distance) increase (see Section 3.4.1).

4.4.1 *Representing ganglion cells in a feature space*

One must be careful when representing the features of a ganglion cell. The larger the dimensionality of the feature space is, the less meaningful will the distance between two cells become; for sufficiently large  $n$ , a cell can be almost as far from its nearest neighbor as it is from its farthest neighbors (Marimont and Shapiro 1979; Beyer et al. 1999).<sup>2</sup>

For the cell features considered here, the autocorrelation function alone is 61-dimensional, while the temporal filter is 40-dimensional. Including the receptive field size, one would require a 102-dimensional space to represent the ganglion cells. Disregarding the uneven number of coordinates (61, 40 and 1), which may unduly favor similarities within a single feature, remember that not more than a few hundred cells are simultaneously recorded in a single experiment. When spread over 102 dimensions, those cells would be sparsely distributed and unlike to cluster – especially in the presence of noise. However, one may not need all those dimensions.

To avoid the dimensionality curse, the number of dimensions required to represent the temporal filters and autocorrelation functions were reduced via principal component analysis (PCA). The temporal filters were projected onto their *first* and *second* principal components (about 88% of explained variance), resulting in the scores  $T_i^{(1)}$  and  $T_i^{(2)}$  for each cell  $i$ . The autocorrelation functions were projected onto their *first* principal component (about 60% of explained variance), resulting in the score  $A_i$ .<sup>3</sup>

In total, four scores were used to describe each ganglion cell  $i$ . The first three scores were based on the projections  $T_i^{(1)}$ ,  $T_i^{(2)}$ , from the temporal filters, and  $A_i$

<sup>2</sup> This is one instance of the infamous “curse of dimensionality”, which often afflicts high-dimensional spaces (see Hastie et al. 2009).

<sup>3</sup> The second principal component of the autocorrelation function, while increasing the explained variance to 82%, did not significantly improve the quality of classification for the datasets considered here.

from the autocorrelation function. The fourth score,  $D_i$ , was the receptive field diameter. To compensate for differences in scale, all scores were normalized to unit variance. Each cell was then represented by the feature vector

$$\vec{X}_i = \begin{bmatrix} T_i^{(1)} \\ T_i^{(2)} \\ A_i \\ D_i \end{bmatrix}, \quad (4.4)$$

where all four scores had equal weight.<sup>4</sup>

#### 4.4.2 Putative types of ganglion cells

With every ganglion cell represented by the four scores, 201 ganglion cells from the same retina were grouped according to their similarity. The similarity matrix  $W = \{w_{ij}\}$  was built from the pairwise Gaussian similarities  $w_{ij}$  between all cells  $i$  and  $j$  (from Equation 4.3, see also Section 3.4.1). The similarity was close to unity when the Euclidean distance between scores was low, and vanished when the distance between scores was large. Using the similarity matrix  $W$ , the spectral clustering algorithm (see Section 3.4.4) partitioned the ganglion cells into  $K = 14$  clusters (putative types). The resulting clusters were labeled from 1 to 14, ordered by their median latency (slowest to fastest) and polarity of response (OFF to ON).

The number of clusters  $K = 14$  was chosen via a collection of heuristics. An increase in the number of clusters led to new clusters with few cells each, while a decrease led to the grouping of seemingly distinct cells. The heuristics were used to estimate a range of appropriate values (see Section 3.5). The eigenvalues of the graph Laplacian (shown on the bottom left in Figure 4.6) suggested a number of clusters between 11–20, a range which was consistent with both Akaike and Bayesian information criteria (AIC, BIC). The heuristics had no clear optima, but were useful to restrict the number of clusters.

## 4.5 PROPERTIES OF THE PUTATIVE TYPES

### 4.5.1 Sorted similarity matrix

The elements of the similarity matrix were re-ordered according to their cluster label, with the sorted matrix shown on the right in Figure 4.6. The sorted similarity

<sup>4</sup> The relative weight of each feature, which represents its importance for the classification, could in principle be tweaked. For the datasets considered here, however, tweaking the weights did not improve the classification. To the best of my knowledge, none of the features shown here should be favored when classifying ganglion cells; the equal weights represent this fact.

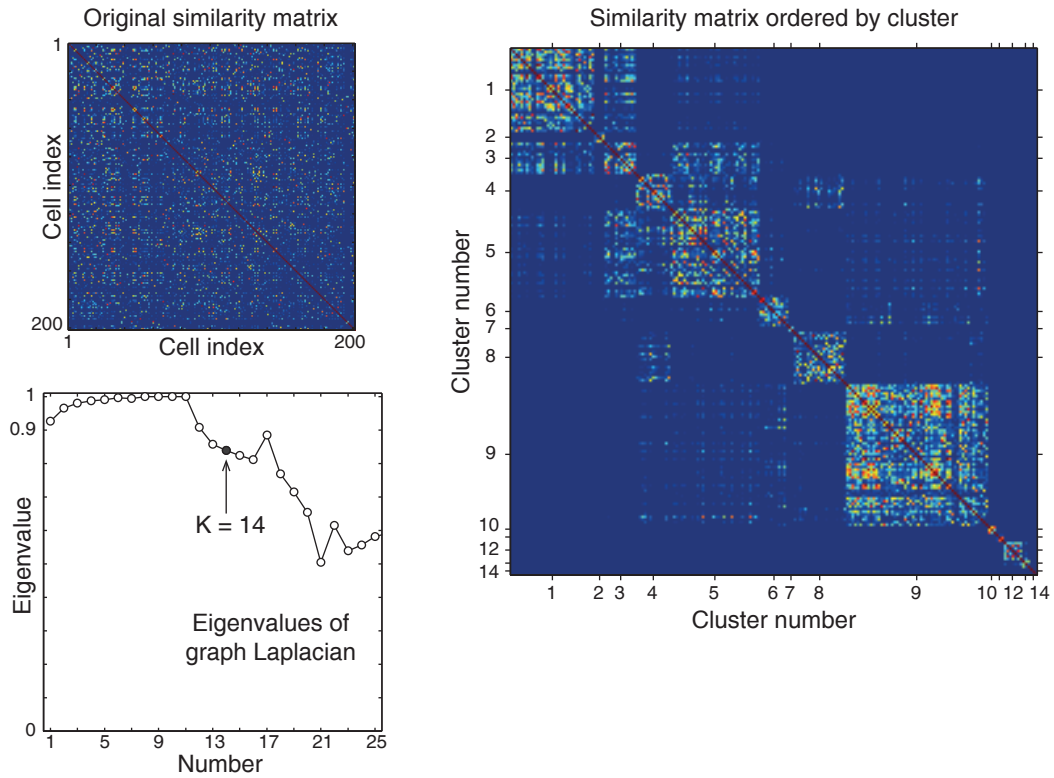


Figure 4.6: SIMILARITY MATRIX AND EIGENVALUES OF GRAPH LAPLACIAN.

(top left) A similarity matrix was built from the pairwise Gaussian similarities between cells from a single experiment. Dark blue means no similarity, brighter pixels indicate higher similarity. (top right) After spectral clustering ( $K = 14$ ), the similarity matrix was ordered by clusters. Blocks of similarity were observed within clusters, with little similarity across clusters. (bottom left) Eigenvalues of the normalized graph Laplacian, whose eigenvectors are used by spectral clustering for grouping the cells (see Figure 3.5).

matrix shows blocks of similarity composed of elements from the same cluster. The blocks indicate that the similarity of cells within a cluster was larger than between clusters, as expected from the spectral clustering algorithm. The similarity matrix gives an overview of the overall cluster quality. Cluster 9, for example, was a large cluster with barely any similarity to other clusters, suggesting that cells in it were well separated from the others. Cells in Cluster 8 shared similarities to cells in Cluster 4; and the same occurred between Clusters 4 and 5. This similarity across clusters often indicated that cells in those clusters had mostly similar features, yet they could be distinguished on at least one of the features.

#### 4.5.2 *Receptive field properties*

In Figure 4.7, the receptive field components from all cells are overlaid, showing the diversity of sizes and temporal filters of the unsorted cells. The temporal (top) and spatial (bottom) components of the receptive fields for the 14 clusters are then arranged and color-coded according to their assigned clusters. The spatial components are represented by their ellipses at one standard deviation of the 2D-Gaussian fit. The clusters are arranged from 1 (top left, red) to 14 (bottom right, gray) from left-to-right and top-to-bottom.

The first 9 clusters were composed of OFF cells with increasing latencies (top of Figure 4.7). Cluster 1 had the slowest OFF cells (latency of  $170 \pm 17$  ms; mean  $\pm$  std.dev.), while Cluster 9 had the fastest OFF cells ( $121 \pm 10$  ms). The next 4 clusters (10–13) were composed of ON cells. Cluster 10 had the slowest ON cells ( $237 \pm 20$  ms), while Clusters 12 and 13 had the fastest ON cells (respectively  $155 \pm 7$  ms and  $139 \pm 2$  ms). Finally, Cluster 14 collected singular cells which were not similar to any other in the dataset.

The clustered receptive fields spread over the visual space with few apparent overlaps (see bottom of Figure 4.7). Some clusters (2, 6, 7, 10 and 11) were observed to sparsely cover the visual space, with large gaps between ganglion cells. These large gaps may, however, be due to the low number of cells in those clusters – a result of a possibly uneven sampling of cell types in the recording. Clusters 8 and 9 were noteworthy, as they were composed of many ( $n_8 = 20$ ,  $n_9 = 50$ ) cells and densely covered the visual space with almost no overlaps (only a single overlap was observed in Cluster 9). Cluster 8 cells also had the largest receptive field sizes ( $337 \pm 27 \mu\text{m}$ ).

#### 4.5.3 *Differences between the putative types*

Ganglion cells were not easily separated by a single feature (see Section 4.3), and this is reflected in the clusters. The four scores used for the classification are shown in Figure 4.8, where each cell was colored according to its assigned cluster. To

FUNCTIONAL TYPES OF RETINAL GANGLION CELLS

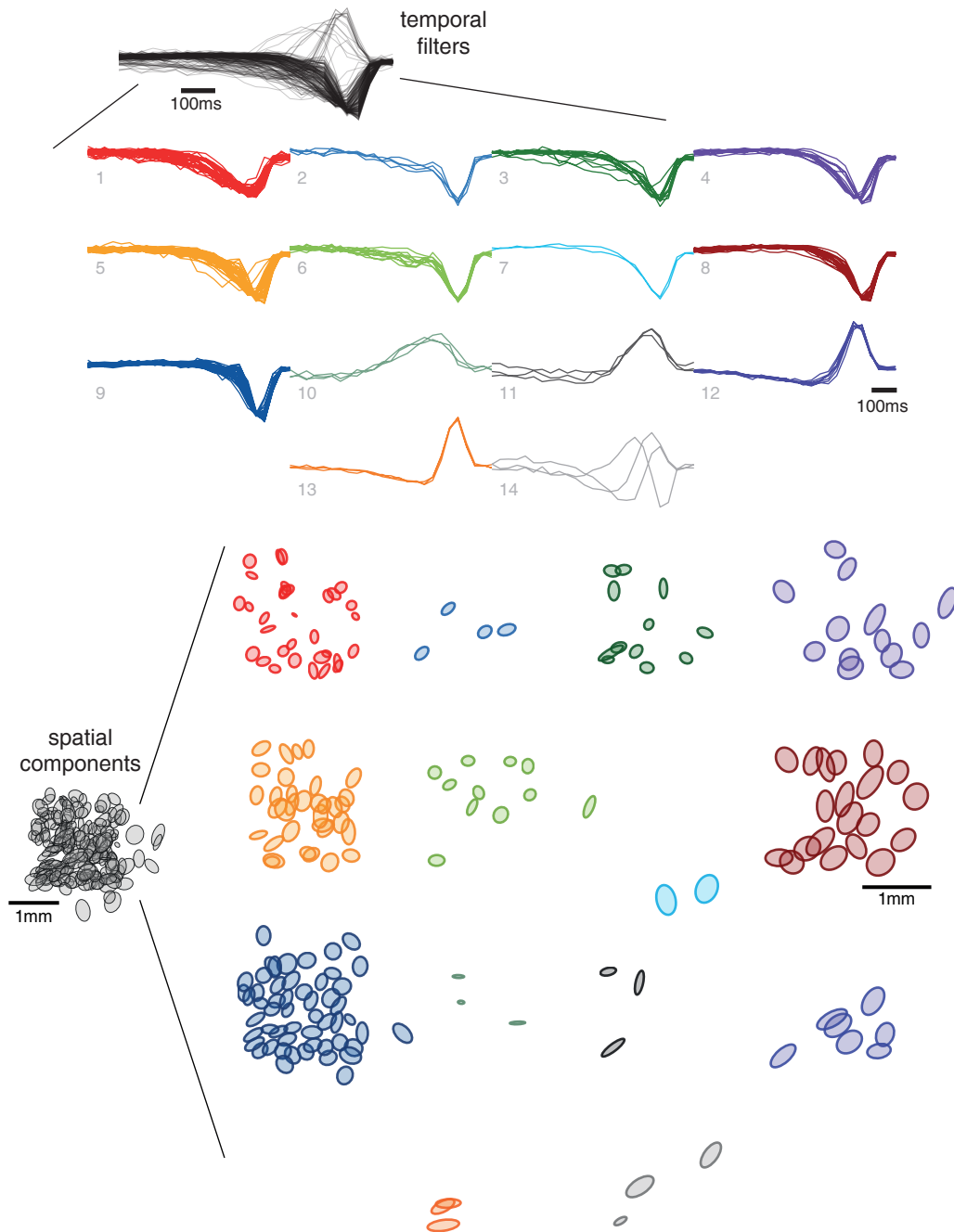


Figure 4.7: GROUPED CELLS FROM A SINGLE RETINA. Temporal and spatial components of receptive fields from ganglion cells ( $n = 201$ ) recorded from the same retina. The cells were grouped into  $K = 14$  clusters based on the similarity of their receptive field sizes, temporal filters and auto-correlation of the spike trains, using the spectral clustering algorithm (see text). Ellipses represent the extent of the receptive field center (one std.dev. of the Gaussian fit).



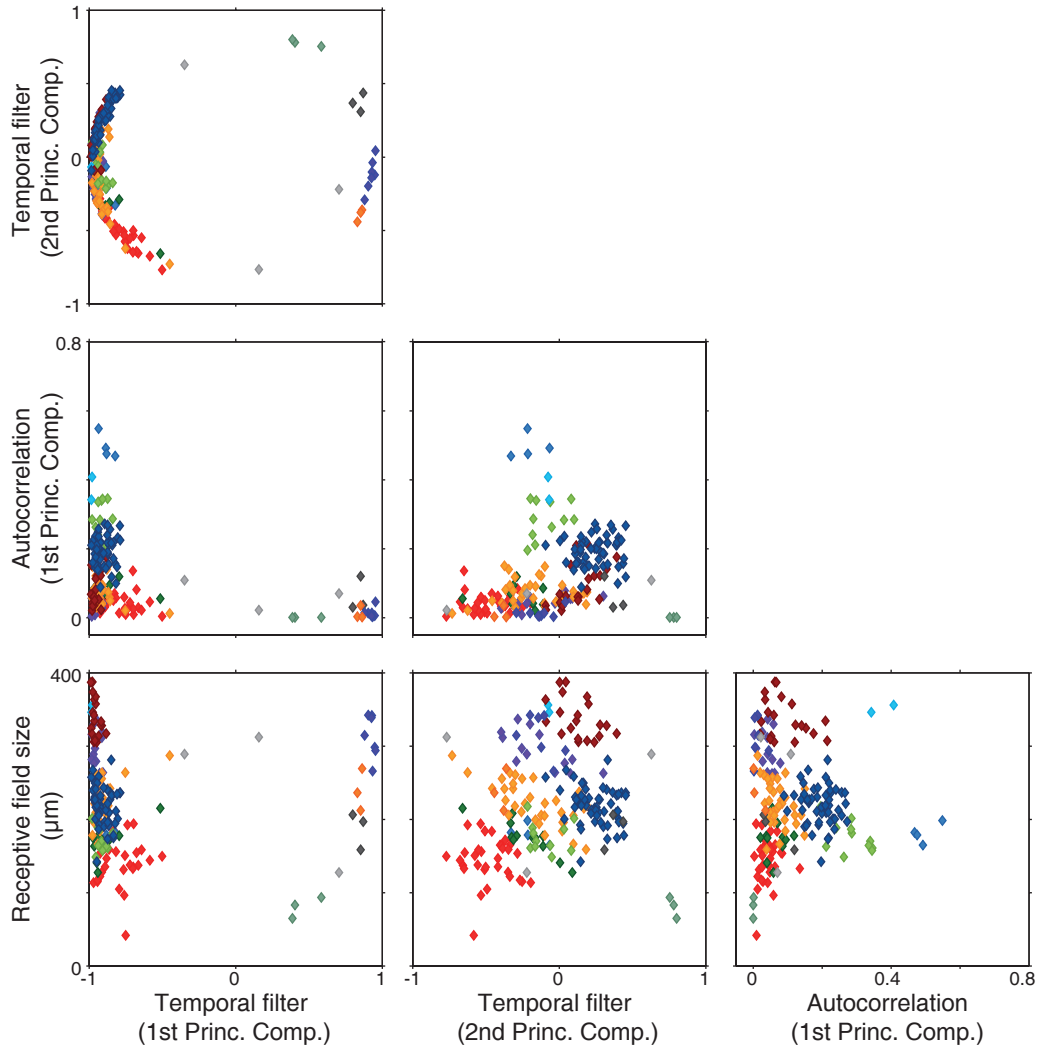


Figure 4.8: MATRIX OF CLASSIFICATION FEATURES. Projection of the features used for classification, for every cell (diamonds) from the same retina. While no single feature clearly separates the cells, the combination of features can be used for teasing out clusters with a spectral clustering algorithm. Cells are colored according to their clusters ( $K = 14$ ).

visualize the distribution of scores for each cluster, the cells were projected onto two scores at a time. The use of the combined scores allowed ganglion cells to be separated. Pairs of clusters with similar properties were often observed, but were separable by at least one of the scores.

For instance, cells in Clusters 5 and 9 (yellow and blue) had similar receptive field sizes but differed both in their autocorrelation functions (Figure 4.8, bottom-right) and temporal components (bottom-center). Clusters 2 and 6 (light blue and light green) had very similar temporal components, but distinct autocorrelation functions. Likewise, Cluster 8 (dark red) and Cluster 9 (blue) had cells with very similar temporal components, but distinct receptive field sizes ( $337 \pm 27 \mu\text{m}$  and  $219 \pm 25 \mu\text{m}$ ).

#### 4.6 COMPARING THREE OFF TYPES

Those differences between clusters were intriguing, and one might wonder whether those similar-but-different clusters were in fact composed of a single natural cell type; a cell type that was split, by chance, into many clusters. To investigate this possibility, I focused on three OFF clusters: Clusters 5, 8 and 9, which had a large population of cells each. Those were named respectively Medium Small OFF,<sup>5</sup> Fast Large OFF, and Fast Small OFF. The three clusters were compared qualitatively in Figure 4.9 and quantitatively in Figure 4.11.

##### 4.6.1 Differences between functional properties

The Fast Large OFF and Fast Small OFF had very similar temporal components (top-left of Figure 4.9), with barely any difference in speeds, but the Fast Small OFF cells were biphasic (see also Figure 4.10). The autocorrelation functions of the Fast Small OFF cells showed a pronounced peak at about 10ms, while the Fast Large OFF cells showed a smaller autocorrelation (Figure 4.11A). The striking difference between the two cell types, as also noticed in the previous section, was the size of their receptive fields (Figure 4.11B).

The Medium Small OFF cells were slower than the Fast Small OFF cells. This was seen in their temporal components (bottom-left of Figure 4.9), which had clearly distinct waveforms – with the Medium cells shifted to the left (slower). This tardiness of the Medium Small OFF cells could also be measured in their latencies ( $148 \pm 25 \text{ms}$  and  $121 \pm 10 \text{ms}$ ). The autocorrelation functions of the Medium Small OFF cells were smaller than the ones for Fast Small OFF cells. Indeed, the autocorrelation functions of the Medium Small OFF were almost the same amplitude as

<sup>5</sup> Note that “Medium” here refers to their latency and not their size.

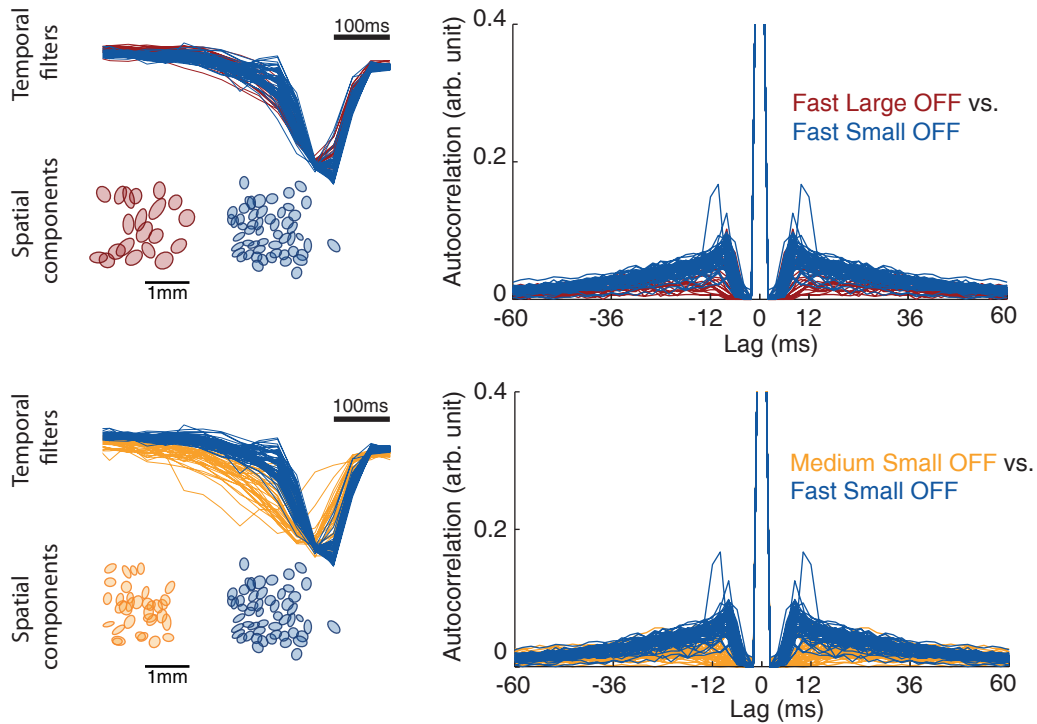


Figure 4.9: COMPARING THREE SIMILAR OFF TYPES. The autocorrelation function for Fast Small OFF cells was larger than both Fast Large OFF (top-right) and Medium Small OFF cells (bottom-right). The temporal filters were very similar between Fast Large OFF and Fast Small OFF cells (top-left). Medium Small OFF cells were slower than the Fast Small OFF (bottom-left). For a quantitative comparison, see Figure 4.11.



Figure 4.10: TEMPORAL FILTERS FROM TEMPORAL WHITE-NOISE. Temporal filters are shown for the Fast Large OFF and Fast Small OFF cells. The filters were obtained from temporal white-noise stimulation (Gaussian, 30% contrast, full-screen). The full field stimulation emphasized the biphasicness of the Fast Small OFF cells, while the Fast Large OFF cells remained monophasic (compare to Figure 4.9).

FUNCTIONAL TYPES OF RETINAL GANGLION CELLS

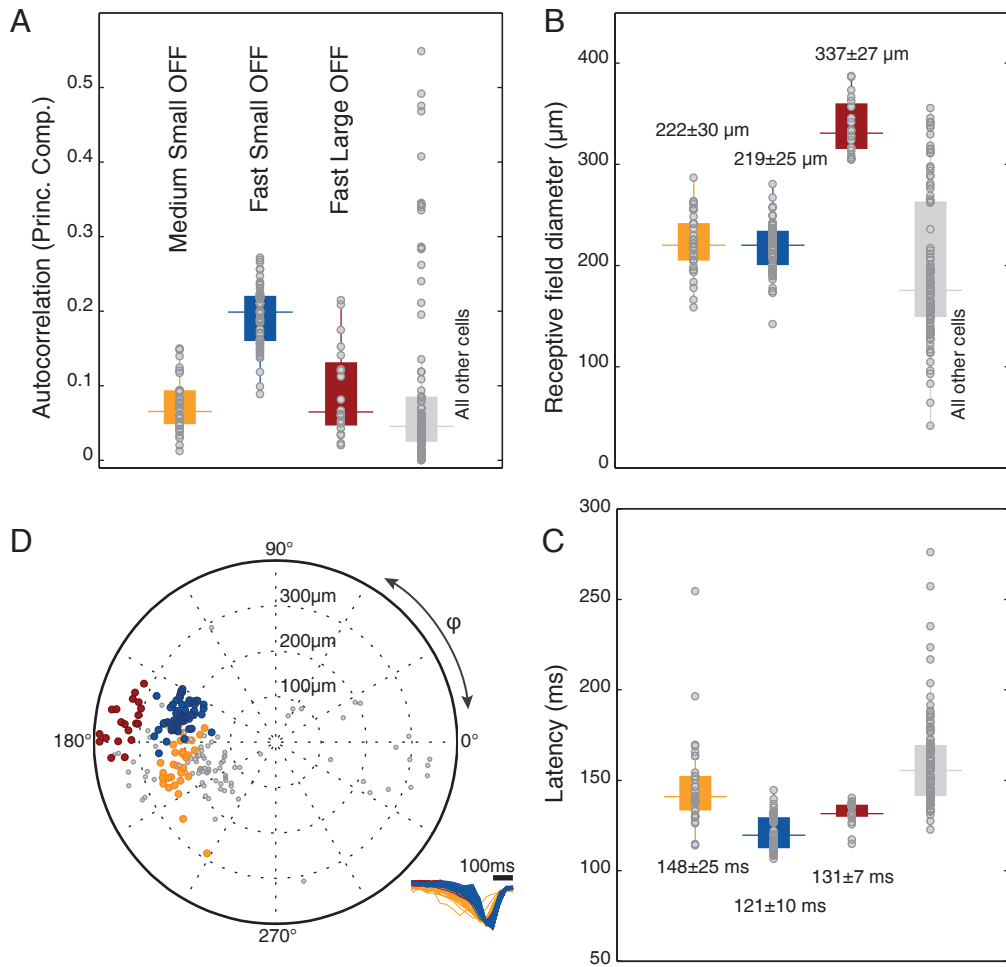


Figure 4.11: DIFFERENCES BETWEEN THREE OFF TYPES. Autocorrelation of the spike trains (A; projected onto its first principal component) and receptive field properties (B, C, D) are shown for different cells (filled circles), grouped by type. (A, B, C) Filled boxes span the range from the first to the third quartile of the distribution, with the median indicated by an horizontal line. Unconnected points (outside the vertical line) are outliers. Average receptive field sizes (B) and latencies (C) are given as mean  $\pm$  std.dev. (D) Temporal filters (in the first and second principal components space) and receptive field size for every cell (filled circle, colored by type; see Figure 4.5).

the ones of the Large Fast OFF (Figure 4.11A). The receptive fields of the Medium Small OFF and Fast Small OFF cells were, however, similar in size (Figure 4.11B).

#### 4.6.2 *Mosaics which independently tiled the retina*

For a putative cell type, a good test of its quality is to observe whether its cells repulse one another, creating a mosaic which tiles the retina (Section 4.1). The three OFF types considered here had indications of tiling. Their receptive fields were spread over the visual space, with only few violations of tiling (overlapping cells) observed: two in the Medium Small OFF, and one in the Fast Small OFF. The Fast Large OFF cells had no observed overlaps.

From the three types, two showed a rather clear evidence of tiling – the Fast Large OFF and the Fast Small OFF cells. In Figure 4.12, tiling was measured for the Fast Large OFF and Fast Small OFF cells via the histogram of normalized distances and the spatial autocorrelogram.

The histogram (bars in Figure 4.12) counted how many cells from the same group were in a circular bin at a normalized distance from a reference cell, averaged over all cells in the group. The gray area in the background is the histogram for a surrogate group of cells, a group with the same number of cells but whose cluster labels were randomly shuffled; the surrogate histogram was averaged over 1000 independent repetitions. A gap in the count of cells below a certain distance is evidence of tiling. The spatial autocorrelogram showed the relative position between pairs of cells from the same group, where each pair of cells was represented as a black dot. Absence of cells in the spatial autocorrelogram below a certain distance (e.g., a receptive field size) indicated tiling. Both measures are equivalent, but complement each other in assessing whether a group of cells tile (see Section 4.1).

Both Fast Large OFF and Fast Small OFF had a clear gap in the distance histogram and spatial autocorrelogram (top of Figure 4.12) – indicating that they tiled the retina. This raised the question, however, of whether this observed tiling was caused by a single tiling ganglion cell type which is (however unlikely) split into two groups. That is, did the two groups *independently* tile the retina, or were they just different shards of the same mosaic?

To investigate whether the Fast Large OFF and Fast Small OFF cells independently tiled the retina, the two types were combined into a single group. This combined group, however, had many more overlapping cells. Indeed, no gaps were observed: neither in the histogram of distances, nor in the spatial autocorrelogram (bottom of Figure 4.12). This suggested that both types not only tiled the retina, but did so independently.

FUNCTIONAL TYPES OF RETINAL GANGLION CELLS

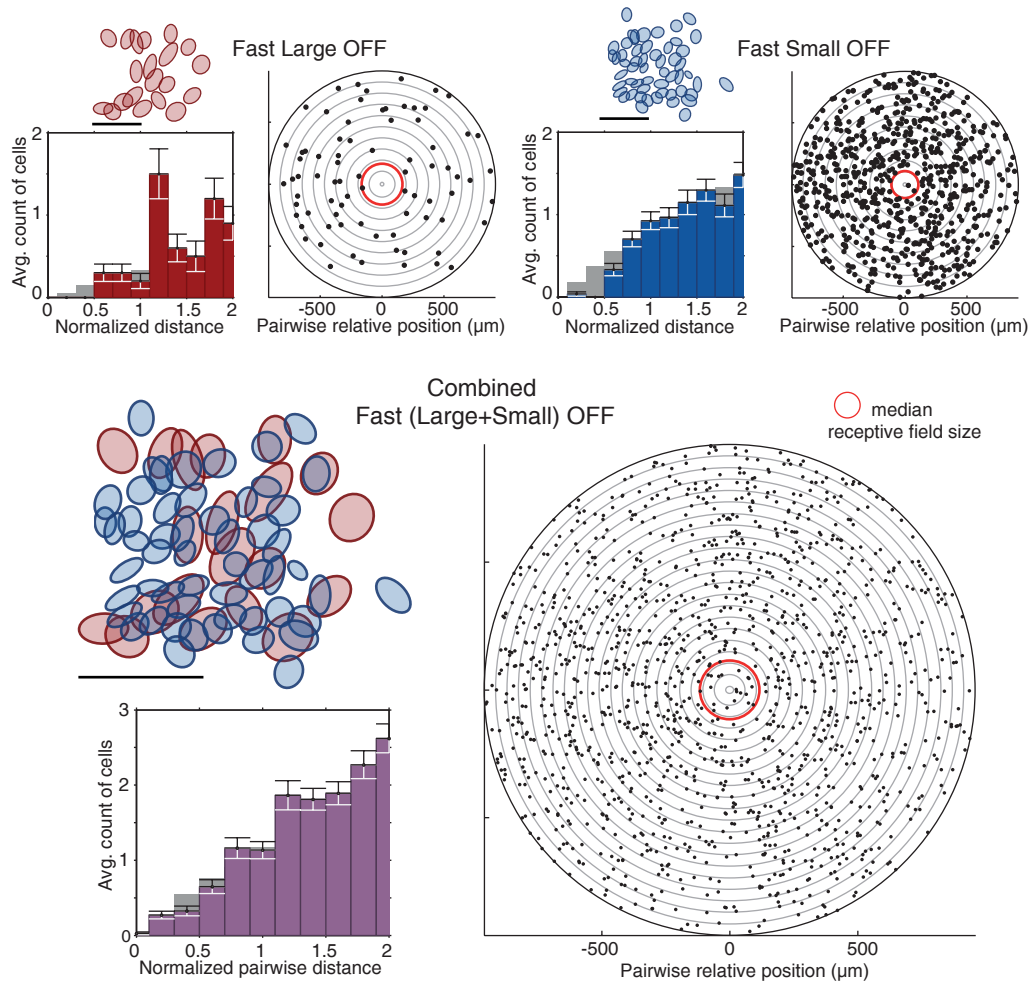


Figure 4.12: COMBINING CLUSTERS INCREASES OVERLAPS. The large (left) and small (right) fast OFF cells individually tile the retina, shown here for a single experiment. However, when combined (bottom), the number of overlaps increases, indicating that they both individually tile the retina. Autocorrelogram is calculated as in Figure 4.1, and shows a reduced number of cells of the same group at a distance smaller than the median receptive field size. Histogram shows the average number of cells, from the same group, at a given distance (bars: mean  $\pm$  std. error); the gray area in the histogram shows the expected average of cells at a given distance, if cells are randomly grouped from the dataset (same number of cells, averaged over 1000 repeats). Scale bars are 1 mm.

## 4.7 HOMOGENEITY OF PROPERTIES IN A CLUSTER

For the remaining putative types, it was not straightforward to assess whether they all tiled. Though most clusters had few or no overlapping cells, most clusters also had only a few cells each. To assess the quality of the classification for those clusters, one may hypothesize that a natural cell type should be homogeneous in other properties, properties that were not used for the classification. Here, I briefly consider the regularity of the spike-trains and the direction-selectivity of the ganglion cells in each cluster.

4.7.1 *Regularity of the spike-trains*

Spikes from a single cell can come in bursts, with many spikes being fired in short intervals, followed by longer intervals of silence. Spikes can also come regularly spaced, with small differences in the interval between the spikes (inter-spike interval, ISI). The spikes were recorded during stimulation with spatiotemporal white-noise. To assess the regularity of the spike-trains, I measured the coefficient of variation ( $C_v$ ) and the local variation coefficient ( $L_v$ ) of the inter-spike intervals for each cell (see Section 2.8).

Briefly, the coefficient of variation  $C_v$  measures the standard deviation of the inter-spike intervals relative to their mean ( $C_v = \sigma_{ISI} / \mu_{ISI}$ ). If the spikes were generated by a homogeneous Poisson process,  $\sigma_{ISI} = \mu_{ISI}$  and  $C_v = 1$ . If the spikes were perfectly regular,  $\sigma_{ISI}$  is small and  $C_v$  vanishes. If the spikes would come in bursts,  $C_v > 1$ . The local variation coefficient

$$L_v = \frac{1}{N-1} \sum_{i=1}^{N-1} \frac{3(\Delta_i - \Delta_{i+1})^2}{(\Delta_i + \Delta_{i+1})^2}, \quad (4.5)$$

where  $\Delta_i$  is the  $i$ -th inter-spike interval, behaves similarly to  $C_v$ . However, differently from  $C_v$ , the local variation coefficient measures the *local* regularity and is less affected by *global* changes, caused for example by the stimulus or cell adaptation. Without being confused by stimulus-caused variances, the local variation coefficient may better capture the intrinsic properties of a cell. (Shinomoto et al. 2003).

The two variation coefficients were compared in Figure 4.13 against the auto-correlation of the spike-trains (projected onto its first principal component); the coefficient of variation  $C_v$  is shown on the bottom and the local variation coefficient  $L_v$  on the top. To better visualize the distributions of the coefficients, the clusters were divided into ON (left) and OFF (right) clusters. Each cell (diamond) was colored by its assigned cluster.

The variation coefficients for ON cells were small, suggesting a more regular spike-train. For OFF cells, variation coefficients were larger than unity, indicating

a more bursty spike-train. Apart from the difference between ON and OFF cells, small differences in burstiness could be noticed between the clusters. For the OFF cells, the variation coefficients distinguished Clusters 2 and 6 as being more bursty ( $L_v = 2.0 \pm 0.2$ , measured together) than the other OFF cells ( $L_v = 1.5 \pm 0.2$ , together). Even though their autocorrelation functions were distinct, there were no differences in burstiness measured between any of the Medium Small OFF, Fast Large OFF, and Fast Small OFF types (each had  $L_v = 1.5 \pm 0.2$ ).

#### 4.7.2 Direction selectivity

Direction selectivity is an asymmetry in the response of a cell to moving stimuli (see Section 2.7). For measuring the direction-selectivity of the ganglion cells, black-white gratings (100% contrast) were presented with a bar width of  $300 \mu\text{m}$  on the retina. The gratings moved in the directions  $\theta_d = (d - 1)\frac{\pi}{4}$ , with  $d = 1$  to 8, with a speed of  $225 \mu\text{m/s}$ , such that each cell observed a complete black-white cycle in  $4/3$  s. Defining  $R_d$  as the average firing rate of a cell when the gratings were moved in the direction  $\theta_d$ , then

$$\text{DSI} = \frac{1}{\sum_d R_d} \left| \sum_d R_d e^{i\theta_d} \right| \quad (4.6)$$

was the direction selectivity index (DSI) of that cell. A direction bias is also defined as the vector pointing towards the preferred direction, normalized to have norm equal to the DSI. The DSI was unity only if a cell responded exclusively to gratings moving in a single direction, and the DSI vanished if there was no preference (by construction,  $0 \leq \text{DSI} \leq 1$ ).

In Figure 4.14, the direction bias for every ganglion cell (top-left) is shown together with the distribution of DSIs (middle-left). Cells were considered direction-selective (DS) whenever their  $\text{DSI} > 0.4$ . On the bottom-left, the fraction of direction-selective (DS) cells in each cluster is shown. On the bottom-right, the total number of cells (DS and non-DS) in each cluster. Clusters with at least one DS cell (Clusters 1, 3, 4 and 5) were represented on the top-right in Figure 4.14.

Only OFF clusters were observed to have DS cells. The majority of cells in Cluster 4 (53%) were DS cells, and Cluster 4 also had 39% of the DS cells in the experiment. Cluster 5 had 33% of the DS cells in the experiment, but they were only a minority (18%) of Cluster 5 itself. Cluster 1 had slow temporal filters, when compared to Clusters 3, 4 and 5, which suggested that at least two populations of direction-selective cells may exist (DS Slow and DS Medium OFF cells).



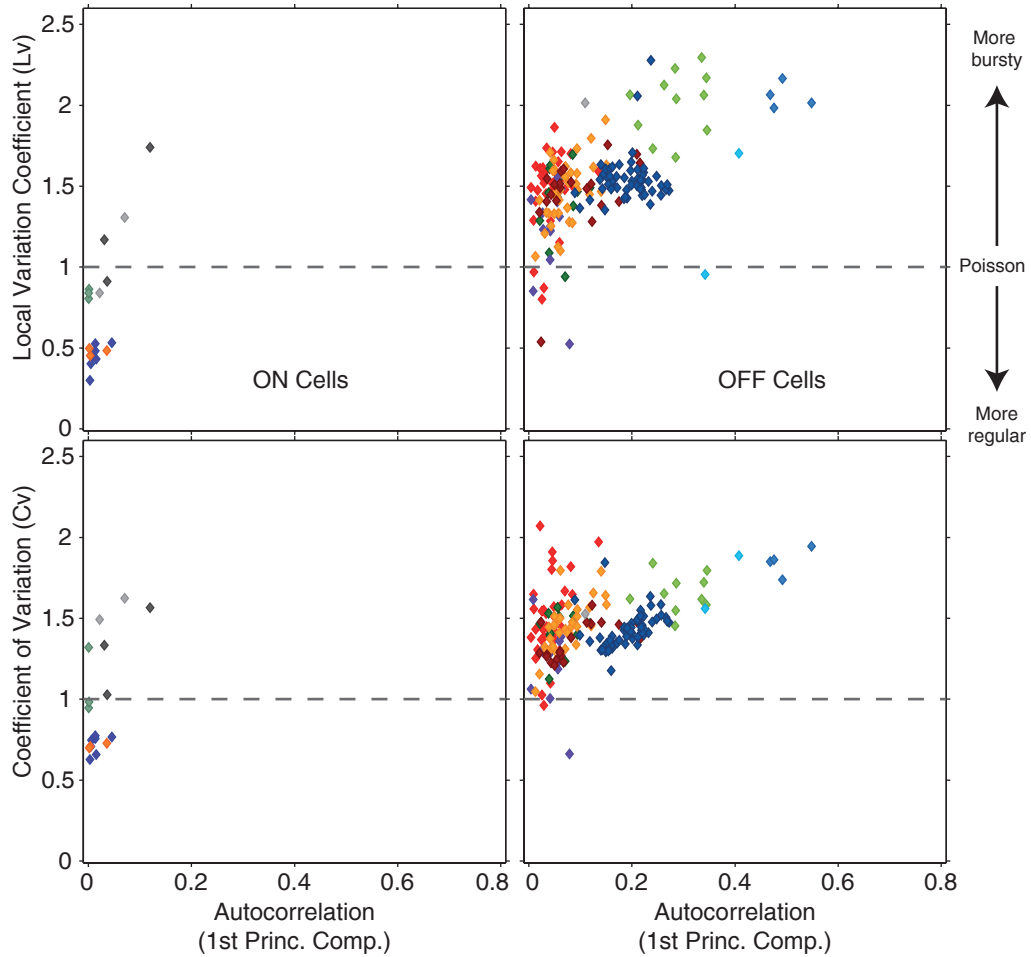


Figure 4.13: MEASUREMENTS OF SPIKE-TRAIN REGULARITY. Local variation coefficient ( $L_v$ , top) and coefficient of variation ( $C_v$ , bottom) for the spike-trains of each cell were compared to the autocorrelation function of the same spike-trains (projected onto its first principal component). Both  $C_v$  and  $L_v$  are unity when the spike-train is Poisson-distributed. The spike-trains from ON cells (left) were more regular than Poisson, while the ones from OFF cells (right) were more bursty. The clusters were homogeneous in the variability of their spike-trains. Differences in autocorrelation were not always captured by the variability coefficients.

FUNCTIONAL TYPES OF RETINAL GANGLION CELLS

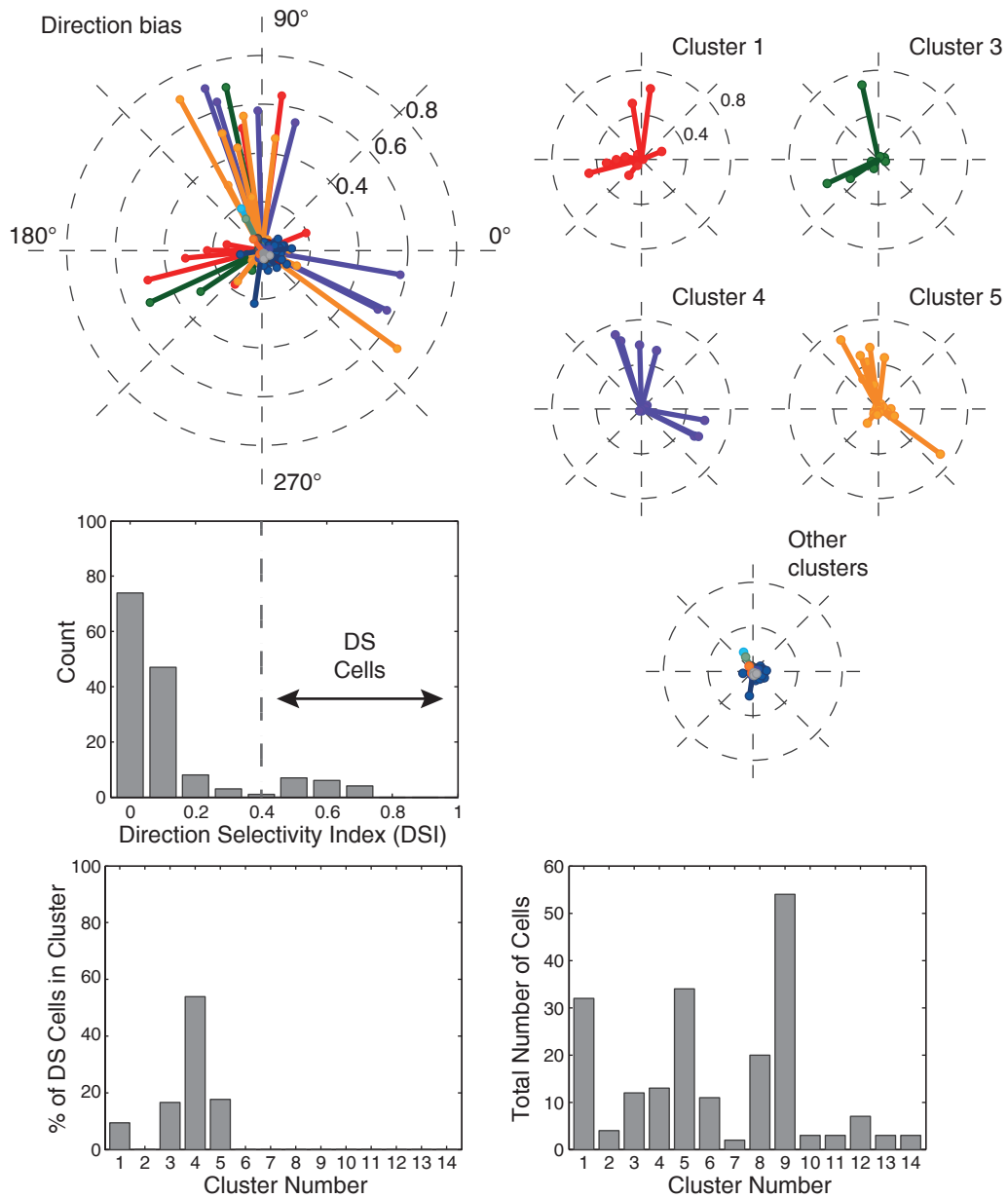


Figure 4.14: DIRECTION SELECTIVITY. Direction bias for all cells (top left) and for clusters with direction-selective (DS) cells (top right). The direction bias points toward the preferred stimulus direction with norm equal to the DSI (Equation 2.10), which vanishes if the cell has no preferred direction ( $0 \leq \text{DSI} \leq 1$ ). The DS cells ( $\text{DSI} > 0.4$ , 18 in total; center left) were observed in few clusters (1, 3, 4 and 5). All observed DS cells were OFF cells. Cluster 4 was mostly (53%) composed of DS cells (bottom left). Cluster 4 and 5, together, collected 72% of all observed DS cells (respectively 39% and 33%). DS cells were, however, a minority in Cluster 5 (18% of total cells).

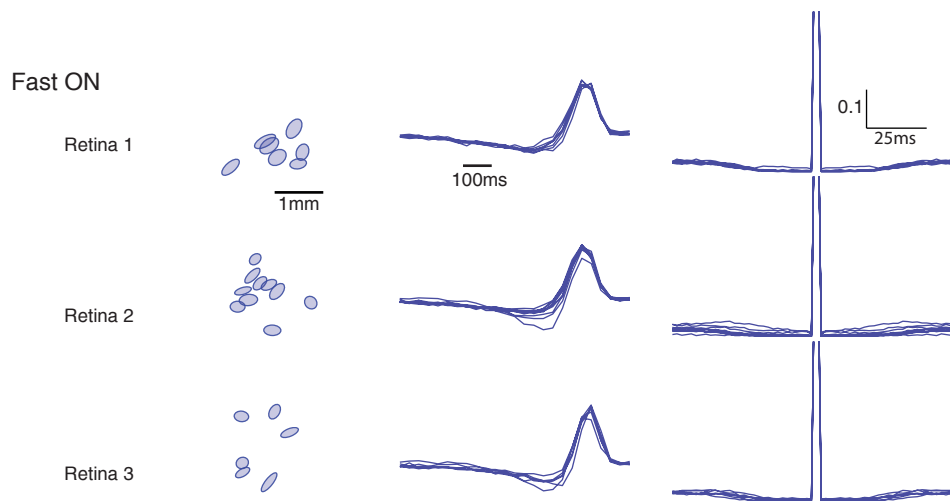


Figure 4.15: FAST ON TYPE ACROSS RETINAS. Fast ON cells were identified across retinas. Here they are shown for three retinas with their spatial components (left), temporal components (center) and autocorrelation functions (right).

#### 4.8 COMPARING TYPES ACROSS RETINAS

One remaining question was, of course, how to identify the same cell types across retinas. Could cells coming from different retinas be pooled together, and classified using the same method used for the single retina? Properties of ganglion cells do change for different preparations, as experimental conditions change. Animal size, health, room temperature, and preparation quality may all affect the cell responses. Indeed, pooled experiments had an increased variance in the data; many clusters separated cells according to which retina they come from instead of grouping them into cell types. Hence, pooling was not found to be useful for identifying types across experiments.

However, while individual cell types had different properties across retinas, the relative order of these types in a retina was conserved (DeVries and Baylor 1997). By clustering cells from each retina individually, the clusters could be ordered by the latency and receptive field size of their cells. Finally, by comparing the autocorrelation functions, it was possible to match similar types across retinas.

Across three retinas, at least five types could be matched. A Fast ON type (Cluster 12 in the first retina) is shown in Figure 4.15. The Fast Small OFF and Fast Large OFF cells are shown in Figure 4.16. Similarly, the Medium Small OFF and the Bursty Medium OFF (Cluster 6) are shown in Figure 4.17.

FUNCTIONAL TYPES OF RETINAL GANGLION CELLS

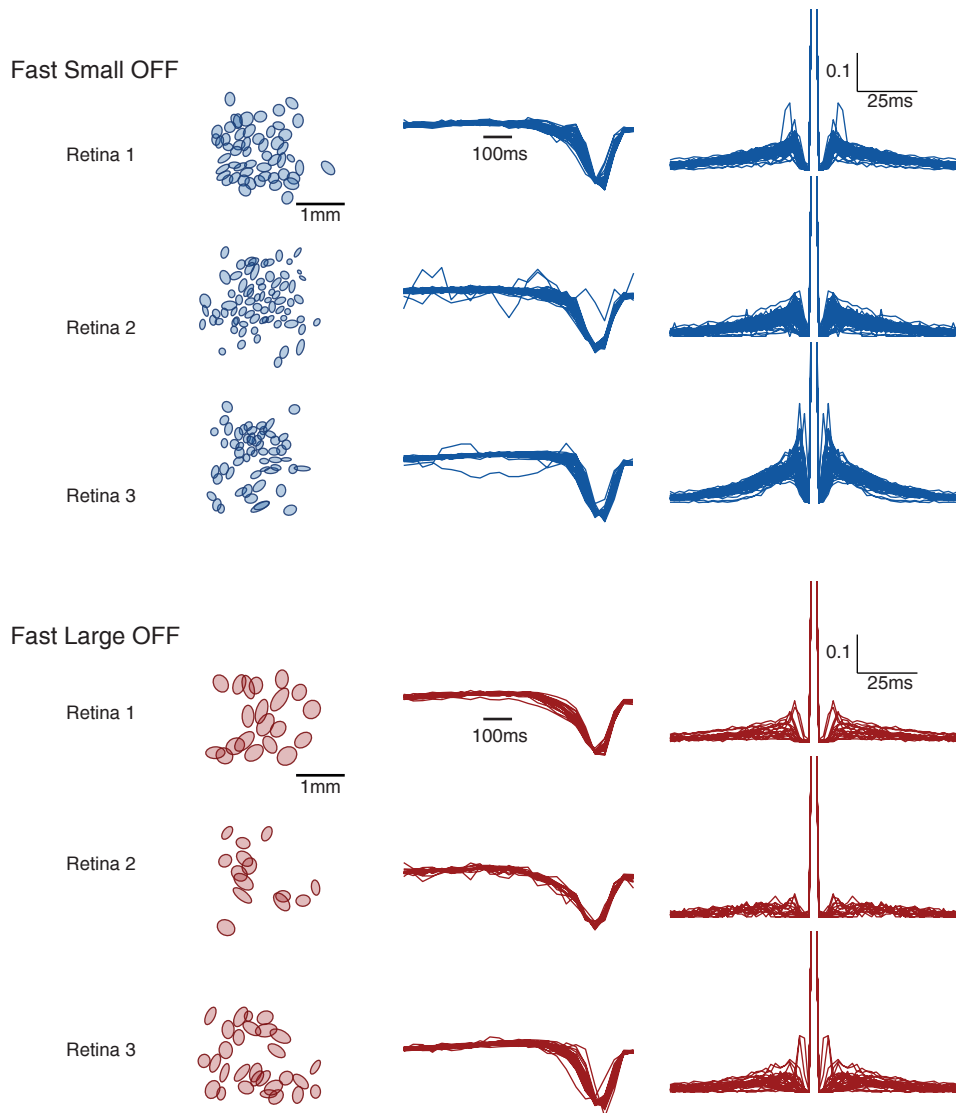


Figure 4.16: FAST OFF TYPES ACROSS RETINAS. Fast Small OFF (top) and Fast Large OFF (bottom) were identified across retinas. Here they are shown for three retinas with spatial components (left), temporal components (center) and autocorrelation functions (right). Note how the time-courses of the temporal filters and autocorrelation functions changed across retinas. For example, the autocorrelation functions from cells in Retina 3 were higher for both cell types.

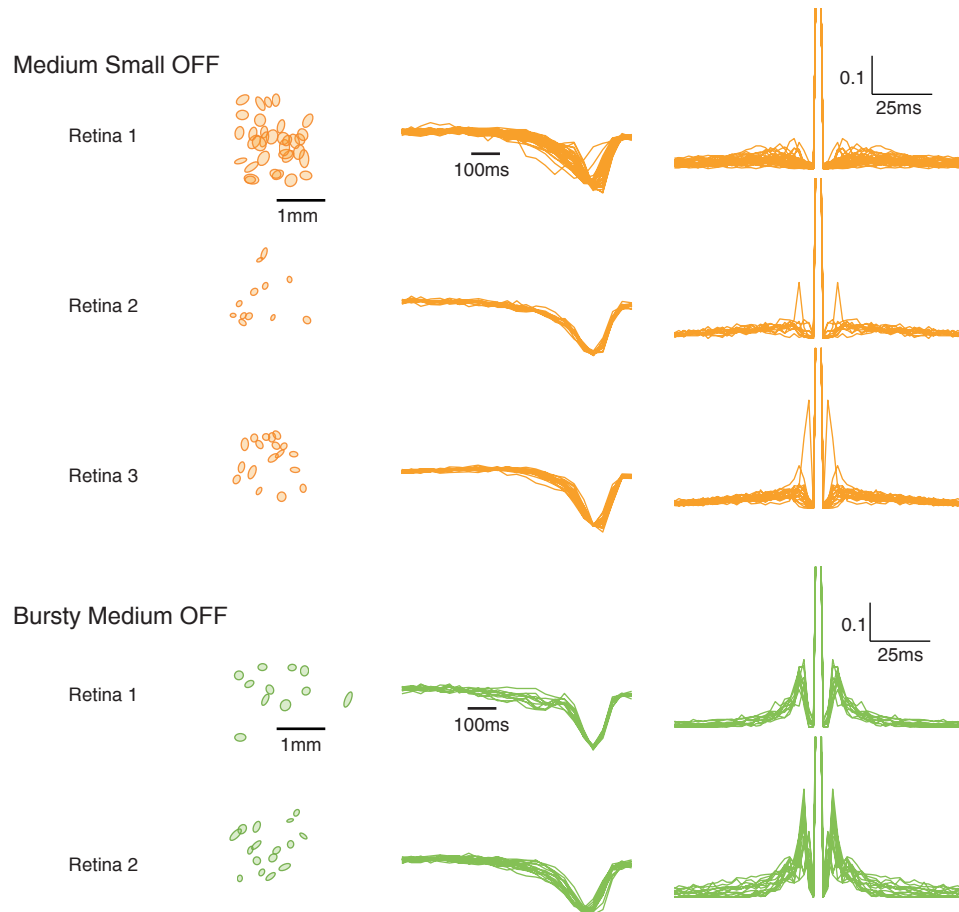


Figure 4.17: MEDIUM OFF TYPES ACROSS RETINAS. Medium-latency OFF cells (Medium Small OFF, top; Bursty Medium OFF, bottom) are shown for three retinas with their spatial components (left), temporal components (center) and autocorrelation functions (right).

Table 4.1: POSSIBLE DIRECTION-SELECTIVE TYPES. Direction selectivity was observed in four clusters (1, 3, 4 and 5); from those, one cluster (Cluster 4) had the majority of direction-selective cells. Two direction-selective cell types were postulated.

Tentative name	Cluster	Observed characteristics
DS Slow OFF	1	Direction-selective cells with slow temporal filters. They formed, however, only a small fraction (9%) of Cluster 1 (Figure 4.14).
DS Medium OFF	3-5	Direction-selective cells were found mostly in Cluster 4, with Medium-latency temporal filters. They were also present in Clusters 3 and 5, but as a minority (respectively 17% and 18% of those clusters; see Figure 4.14).

#### 4.9 SUMMARY

Salamander retinal ganglion cells were recorded and analyzed to obtain their receptive field sizes, temporal filters, and autocorrelation of their spike-trains. While individual features were hazy, without a clear separation into cell types, the combination of features led to an improvement on the separation of ganglion cells. Before applying a clustering algorithm, to avoid the dimensionality curse, the temporal filters and autocorrelation functions were projected onto their principal components. The projections together with the receptive field size were used as scores to represent the ganglion cells in a feature space. After the similarity between every ganglion cell pair was calculated, a spectral clustering algorithm partitioned the dataset into  $K = 14$  clusters. As expected from the algorithm, the cells in each cluster were mostly similar between themselves, with few similarity to cells in other clusters. Those 14 clusters were taken as putative types.

Putative types were observed to share similarities with one another. Specifically, three OFF types (Medium Small OFF, Fast Large OFF, Fast Small OFF) were observed to have similar temporal filters, receptive field sizes, and autocorrelation functions – only not all simultaneously. While similar in a few properties, the three types could still be distinguished by taking another of their properties into account.

Despite observing a separation between clusters, one could still wonder if the putative types do have any relation to natural cell types. That is, whether the identified clusters would tile or, perhaps, show homogeneity in their properties. Two types were observed to individually tile the retina (Fast Large OFF and Fast Small OFF). Moreover, these two types independently tiled the retina – an evidence that they were indeed distinct cell types.

Table 4.2: SUMMARY OF OBSERVED TYPES. Observed types and their tentative names, the clusters in which they were found (see Figure 4.7), and their defining characteristics.

Tentative name	Cluster	Observed characteristics
Fast ON	12	Fast cells with large receptive fields; their autocorrelation functions showed sparse but sustained activity (Figure 4.15).
Medium Small OFF	5	These cells were slower than the Fast OFF cells; they have small receptive field sizes, similar in size to the Fast Small OFF cells. The time-course of their autocorrelation functions were similar to the Fast Large OFF cells (Figure 4.11, Figure 4.17).
Bursty Medium OFF	6	These cells had similar temporal filters as the Medium Small OFF cells, but had a peak in the autocorrelation function. Their peaks were larger than the peaks observed for the Fast Small OFF cells (Figure 4.17). These cells were more bursty than most other OFF cells (as measured with the local variation coefficient $L_v$ , Figure 4.13).
Fast Large OFF	8	Almost as fast as the Fast Small OFF, these cells had monophasic temporal filters. The large receptive fields were its most distinctive property. The autocorrelation functions of these cells reached an amplitude smaller than the ones from Fast Small OFF cells – with no clear peak. They independently tiled the retina (Figure 4.12).
Fast Small OFF	9	Largest population in the dataset. These cells had a sharp peak in their autocorrelation functions and small receptive field sizes. The fastest OFF cells, cells of this type had biphasic temporal filters (Figure 4.10). They independently tiled the retina (Figure 4.12).

Most types had only few violations of tiling, but many of those types had also only few cells each, which hindered the analysis of their mosaic. Therefore, the homogeneity of those cell types was tested using properties not used for classification, such as the regularity of their spike-trains and direction-selectivity. The spike-trains of ON ganglion cells were more regularly spaced than the ones from OFF cells. Most OFF clusters were equally irregular in their spike-trains, with the exception of two more bursty clusters (one of which was tentatively named Bursty Medium OFF). Direction-selectivity was observed only in OFF cells. Four clusters contained direction-selective (DS) cells, but DS cells were a minority (less than 20% of the cells) in three of those. One cluster collected most DS cells. Because of the different temporal filters of the DS cells, two types of OFF DS cells could be postulated and are shown in Table 4.1.

In total, three different retinas were analyzed. Due to differences in experimental conditions, their data could not be pooled together. However, types were matched across retinas by their relative order in latency and size, together with the autocorrelation functions. At least five types were consistently identified across retinas. All five types had few or no violations of tiling. Moreover, two types showed strong evidence of tiling: the Fast Large OFF and Fast Small OFF. The five identified types, together with their characteristics, are summarized in Table 4.2.



DISCUSSION

---

*The White Rabbit put on his spectacles. 'Where shall I begin, please your Majesty?' he asked. 'Begin at the beginning,' the King said gravely, 'and go on till you come to the end: then stop.'*

— LEWIS CARROLL, *Alice's Adventures in Wonderland*

The main goal of this work was to improve on the classification of ganglion cells in the salamander retina. The salamander is useful not only because of its history in vision science and ease of recording, but also due to the challenges involved in the functional classification of its retinal ganglion cells. Salamander ganglion cells were suggested to be highly redundant (Puchalla et al. 2005), and not easily separable based on their functional properties (Segev et al. 2006; Marre et al. 2012). A method which can identify ganglion cell types in the salamander would be expected to also work well for other species. The classification method developed here, based on a simple stimulus, offers an improved view of the salamander retina. While not every putative type was reliably found across retinas, at least five were. This suggests that the salamander retina may have more structure than was previously thought.

### 5.1 CELL TYPES IN THE SALAMANDER RETINA

Ganglion cells in the salamander retina were characterized based on their receptive field sizes, temporal filters, and autocorrelation of spike-trains. These properties were chosen because of their success in distinguishing ganglion cell types in the rabbit (DeVries and Baylor 1997) and monkey (Field et al. 2007) retinas. Surprisingly, ganglion cells had few clear groupings when these properties were individually considered (Segev et al. 2006), which was also observed here. However, by considering the functional properties in tandem, putative cell types could be teased out here. For example, cells with similar temporal filters were distinguished by their receptive field sizes (Fast Large OFF vs Fast Small OFF), and those with similar receptive field sizes were distinguished by their temporal filters and autocorrelation functions (Medium Small OFF vs Fast Small OFF). This suggests that a combination of features is not only helpful, but required if one expects to separate ganglion cell types.

In contrast, Segev et al. (2006) observed putative types to be less distinct when grouped according to combined features. Instead, Segev et al. (2006) proposed six broad classes based on the temporal filters alone: Fast ON, Slow ON, Biphasic OFF,

Table 5.1: OBSERVED CELL TYPES AND THEIR TEMPORAL COUNTERPARTS.

This work	Segev et al. (2006)
Fast ON	Fast ON
Fast Small OFF	Biphasic OFF
Fast Large OFF	Monophasic OFF
Medium Small OFF	Medium OFF
Bursty Medium OFF	

Monophasic OFF, Medium OFF and Slow OFF. The matching between this temporal classification and the clusters found in this work is straightforward, but not always one-to-one, as is shown in Table 5.1. Here, Medium ON and Slow ON cell types were observed, but not consistently across retinas; most other types could be matched. Both Bursty Medium OFF and Medium Small OFF types, however, would fall into the same Medium OFF type. Indeed, Segev et al. (2006) reported that except for the Biphasic OFF, most of the proposed types showed a diversity of receptive field sizes and autocorrelation functions – suggesting that the temporal filters may in fact not be sufficient for cell classification. This may also explain why only the Biphasic OFF cells had been observed to tile in the salamander retina (Segev et al. 2006; Marre et al. 2012), as tiling is considered a tell-tale of a single cell type (Section 4.1).

Consistent with being the Biphasic OFF type, the Fast Small OFF cells did tile the retina. However, they were not the only type to do so – the Fast Large OFF cells showed a mosaic which was consistent with tiling. Could both cell types actually come from the same natural type? Not likely. The Fast Small OFF and Fast Large OFF did not belong in a single mosaic, as combining cells from the two groups increased the receptive field overlap. Hence, by *independently* tiling the retina, there is a strong evidence that each forms an individual cell type.

Indeed, a similar split of the Fast OFF types was recently described in the salamander retina. By presenting the retina with temporal noise that alternated from high to low-contrast, Fast OFF cells could be separated depending on whether they adapted or sensitized to the high-contrast conditions. The Adapting Fast OFF population had small receptive field sizes, with likely biphasic temporal filters. The Sensitizing Fast OFF had large receptive field sizes, with monophasic temporal filters (Kastner and Baccus 2011). While sensitization and adaptation were not measured here, it is tempting to consider the Adapting Fast OFF as analogous to the Fast Small OFF cells, and the Sensitizing Fast OFF to the Fast Large OFF cells. If this correspondence is true, it would suggest a role for having two cell populations with so similar filtering properties; the two populations would compensate each other for the loss of visual information when changing to a low-contrast condition, before short-term adaptation has a chance to act (Kastner and Baccus 2011). This

parallel also suggests higher-order functionality for those cell types. For example, that the Fast Small OFF cells should preferably encode for the local motion of objects in the visual scene (object-motion sensitivity, see Ölveczky et al. 2003; Kastner and Baccus 2013).

The question still remains, however, on whether the other observed types were indeed composed of single natural types. Most reliably identified cell types (see Table 4.2) contained very few violations of tiling. These identified types were also homogeneous in their properties. Even when types were divided based on their direction-selectivity, this sub-division was limited to few clusters with similar temporal filters (only 3 of the 18 direction-selective cells were Slow OFF, all others were Medium OFF). The direction-selective Slow OFF cells, for example, may correspond to a recently proposed subtype of direction-selective cells, which focus on local movement (Kühn and Gollisch 2012; Kühn, personal communication).

It is important to note that the number of putative types, as suggested by the cluster heuristics, may not necessarily give the correct number of natural cell types. However, the number of types used here closely matched those observed in morphological studies in the salamander (Toris et al. 1995; Costa and Velte 1999). There, ganglion cells were separated mainly on their dendritic area of influence and on the complexity of their branching patterns into 5 coarse types. These coarse types, then, were found to further sub-divide depending on where they branched within the inner-plexiform layer – which is assumed to define the ON or OFF characteristics of a ganglion cell (Hare et al. 1986). In total, about 10 ganglion cell types were identified based on their morphology and possible polarity (Toris et al. 1995).

Taken together, the results suggest that the classification method presented here successfully grouped ganglion cells according to their functional similarities. As evidenced by the homogeneity of their properties, and few overlaps, ganglion cells may have been classified into groups likely composed of similar natural types. This work complements the current physiological view of the salamander retina by Segev et al. (2006), indicating that functional ganglion cell properties should be considered simultaneously. Moreover, the discovery of a second tiling type implies that tiling may be a fundamental feature of ganglion cells also in the salamander retina.

## 5.2 SCOPE FOR IMPROVEMENTS

While tiling types were observed, it is likely that the classification may be incomplete, and one will eventually find sub-divisions in a few of the proposed types. For example, because direction selectivity was not taken into account for the classification, the direction-selective cells were outliers between the Medium and Slow OFF cells, instead of forming their own class. It could be worth investigating which sub-divisions may still exist by considering further functional properties. A good

## DISCUSSION

first candidate is the difference between sensitizing and adapting cells (Kastner and Baccus 2011). While a parallel exists between the Fast OFF types identified here and the ones from Kastner and Baccus (2011), it has yet to be tested. Moreover, the dichotomy between sensitizing and adapting cells was not restricted to the Fast OFF cells, and was also observed for Medium and Slow OFF cells (Kastner and Baccus 2011).

Another interesting problem is in how to combine data from multiple retinas. Without pooling data, one may not be able to find rare cell types. Pooling data, however, decreases the quality of clustering due to the differences in cell properties between retinas. This was compensated by individually classifying each dataset, matching the types according to their relative properties (DeVries and Baylor 1997). An improvement could come from using easily identifiable cell types, such as the Fast Small OFF cell, as a reference to normalize the remaining cell types.

### 5.3 TILING IN PHYSIOLOGICAL CLASSIFICATIONS

The observation of tiling ganglion cells is key for confirming (Wässle, Peichl, et al. 1981; Zhang et al. 2012) or discovering (Cook and Sharma 1995; Shamim et al. 1999) a retinal cell type (Cook and Chalupa 2000). Tiling has been useful in morphological studies, for example, to define which properties should be used to disambiguate between ganglion cells (Shamim et al. 1999; Cook 2004). If tiling is a general feature of retinal cells (Rockhill et al. 2000), one would expect tiling to be similarly helpful in the physiological classification of ganglion cells.

Due to the low number of cells in physiological experiments, it is often difficult to assess tiling for every functional type (Sanes and Masland 2015). While tiling receptive fields had been observed in the rabbit (DeVries and Baylor 1997) and monkey (Field et al. 2007) retinas, it was unclear whether the same organization could be found in salamander retinas (Segev et al. 2006; Marre et al. 2012). In this work, the observation of tiling in the salamander reinforces tiling as a general principle in the organization of the vertebrate retina, which is useful for demonstrating the existence of a cell type (Cook 1998).

As the number of simultaneously recorded cells increase (Stevenson and Kording 2011), one can only expect the importance of tiling for the physiological classification of ganglion cells to grow. Indeed, it may be possible – given enough cells – to use tiling not only as a tool for confirming putative cell types, but as an active tool for their discovery. As suggested for morphological studies by Cook (2004), violations of tiling can be a guide for feature selection. Whenever overlapping cells are observed, one may search for features that disambiguate them – and use those features for improving on the classification, repeating as needed.

## 5.4 IMPORTANCE OF CLASSIFICATION

The most accepted view of the retina considers the ganglion cells to form a diverse population of cells, which however can be grouped into discrete types based mainly on their morphology. Each type is expected to encode a different aspect of the visual scene, working as parallel channels of information (see Masland 2012). However, the retina is also known to extract specific features of an image which can be behaviorally significant to an animal, performing computation already at the level of the retina (see Gollisch and Meister 2010). The functional classification of ganglion cells is an important tool to grasp how visual information is encoded, aggregating cells into populations which are expected to have a more homogeneous response, linking physiological behavior to morphology.

The distinction of types has been used, for example, to explore how much information is encoded by each ganglion cell type (Koch et al. 2006), the shape of receptive field mosaics from a single type (Gauthier et al. 2009) and how ganglion cell types change their response with age (Samuel et al. 2011). The classification of ganglion cells provides an important view into the retinal circuitry, allowing one to map the functional connections between different retinal cell types (Asari and Meister 2014; Field and Chichilnisky 2007) and to target specific cell types. Much of the classification has however been performed coarsely, which may lose fine information on types, or manually, which may not scale as the number of recorded cells grow (Stevenson and Kording 2011; Armañanzas and Ascoli 2015).

The retina is however not the only area of the brain to struggle with neuronal classification. In other areas of the brain, neuronal identification has been a growing problem (Stevens 1998; Armañanzas and Ascoli 2015). Because retinal cells are so easily accessible and have well studied morphological properties, the retina may be uniquely suited for developing and testing methods for neuronal classification (Masland 2004; Sanes and Masland 2015). The tiling observed in retinal cells may be a fundamental advantage for the fine-tuning of classification methods, but it may also provide insights into the variety of neuronal types in higher areas of the brain (Stevens 1998). Hence, by using the retina as a testbed for classification methods, one may eventually not only understand the retinal circuitry, but also illuminate aspects of the general organization of the brain.



## BIBLIOGRAPHY

---

- Adrian, E. D. and Matthews, R. (1927). "The action of light on the eye: Part I. The discharge of impulses in the optic nerve and its relation to the electric changes in the retina." *J. Physiol.* 63.4, pp. 378–414 (cit. on p. 3).
- Akaike, H. (1974). "A new look at the statistical model identification". *IEEE Trans. Automat. Contr.* 19.6, pp. 716–723 (cit. on p. 38).
- Armañanzas, R. and Ascoli, G. a. (2015). "Towards the automatic classification of neurons". *Trends Neurosci.* 38.5, pp. 307–318 (cit. on pp. 6, 23, 79).
- Asari, H. and Meister, M. (2014). "The Projective Field of Retinal Bipolar Cells and Its Modulation by Visual Context". *Neuron* 81.3, pp. 641–652 (cit. on pp. 10, 79).
- Attwell, D., Mobbs, P., Tessier-Lavigne, M., and Wilson, M. (1987). "Neurotransmitter-induced currents in retinal bipolar cells of the axolotl, *Ambystoma mexicanum*." *J. Physiol.* 387, pp. 125–161 (cit. on p. 10).
- Baccus, S. A. and Meister, M. (2002). "Fast and slow contrast adaptation in retinal circuitry." *Neuron* 36.5, pp. 909–19 (cit. on p. 10).
- Barber, D. (2012). *Bayesian Reasoning and Machine Learning*. Cambridge University Press (cit. on pp. 23, 27, 38).
- Bar-Gad, I., Ritov, Y., and Bergman, H. (2001). "The neuronal refractory period causes a short-term peak in the autocorrelation function". *J. Neurosci. Methods* 104.2, pp. 155–163 (cit. on p. 21).
- Barlow, H. B. (1953). "Summation and inhibition in the frog's retina." *J. Physiol.* 119.1, pp. 69–88 (cit. on pp. 4, 5).
- Barlow, H. B. (1961). "Possible Principles Underlying the Transformation of Sensory Messages". *Sens. Commun.* (Cit. on p. 5).
- Barlow, H. B., Hill, R. M., and Levick, W. R. (1964). "Retinal Ganglion Cells Responding Selectively To Direction and Speed of Image Motion in the Rabbit." *J. Physiol.* 173, pp. 377–407 (cit. on pp. 5, 20).
- Barlow, H. B. and Hill, R. M. (1963). "Selective sensitivity to direction of movement in ganglion cells of the rabbit retina". *Science* 139.2, pp. 412–414 (cit. on pp. 5, 20).
- Barlow, H. B. and Levick, W. R. (1965). "The mechanism of directionally selective units in rabbit's retina." *J. Physiol.* 178.3, pp. 477–504 (cit. on p. 20).
- Beyer, K., Goldstein, J., Ramakrishnan, R., and Shaft, U. (1999). "When is "nearest neighbor" meaningful?" In: *Database Theory—ICDT'99*, pp. 217–235 (cit. on p. 54).

## Bibliography

- Bölinger, D. and Gollisch, T. (2012). "Closed-Loop Measurements of Iso-Response Stimuli Reveal Dynamic Nonlinear Stimulus Integration in the Retina". *Neuron* 73, pp. 333–346 (cit. on p. 10).
- Boycott, B. B. and Wässle, H. (1974). "The morphological types of ganglion cells of the domestic cat's retina." *J. Physiol.* 240.2, pp. 397–419 (cit. on p. 5).
- Brew, H. and Attwell, D. (1987). "Electrogenic glutamate uptake is a major current carrier in the membrane of axolotl retinal glial cells." *Nature* 327.6124, pp. 707–709 (cit. on p. 10).
- Brown, P. K., Gibbons, I. R., and Wald, G. (1963). "the Visual Cells and Visual Pigment of the Mudpuppy, *Necturus*." *J. Cell Biol.* 19.2, pp. 79–106 (cit. on p. 10).
- Carcieri, S. M., Jacobs, A. L., and Nirenberg, S. (2003). "Classification of retinal ganglion cells: a statistical approach." *J. Neurophysiol.* 90.3, pp. 1704–13 (cit. on p. 47).
- Chichilnisky, E. J. (2001). "A simple white noise analysis of neuronal light responses." *Network* 12.2, pp. 199–213 (cit. on pp. 16, 17, 47).
- Clark, P. J. and Evans, F. C. (1954). "Distance to Nearest Neighbor as a Measure of Spatial Relationships in Populations". *Ecol. Soc. Am.* 35.4, pp. 445–453 (cit. on p. 43).
- Cook, J. E. (1996). "Spatial properties of retinal mosaics: an empirical evaluation of some existing measures." *Vis. Neurosci.* 13.1, pp. 15–30 (cit. on pp. 43, 44).
- Cook, J. E. and Sharma, S. C. (1995). "Large retinal ganglion cells in the channel catfish (*Ictalurus punctatus*): Three types with distinct dendritic stratification patterns form similar but independent mosaics". *J. Comp. Neurol.* 362.3, pp. 331–349 (cit. on pp. 43, 78).
- Cook, J. E. (1998). "Getting to Grips with Neuronal Diversity". English. In: *Development and Organization of the Retina*. Ed. by L. M. Chalupa and B. L. Finlay. Vol. 299. NATO ASI Series. Springer US, pp. 91–120 (cit. on pp. 42, 78).
- Cook, J. E. (2004). "Spatial regularity among retinal neurons". In: *Vis. Neurosci.* Ed. by L. M. Chalupa and J. S. Werner. Vol. 1. 2004. MIT Press. Chap. 29, pp. 463–477 (cit. on pp. 42–44, 78).
- Cook, J. E. and Chalupa, L. M. (2000). "Retinal mosaics: New insights into an old concept". *Trends Neurosci.* 23.1, pp. 26–34 (cit. on pp. 6, 41, 42, 78).
- Costa, L. d. F. and Velte, T. J. (1999). "Automatic characterization and classification of ganglion cells from the salamander retina". *J. Comp. Neurol.* 404.1, pp. 33–51 (cit. on pp. 10, 77).
- Custer, N. V. (1973). "Structurally specialized contacts between the photoreceptors of the retina of the axolotl." *J. Comp. Neurol.* 151.1, pp. 35–56 (cit. on p. 10).
- DeVries, S. H. and Baylor, D. A. (1997). "Mosaic arrangement of ganglion cell receptive fields in rabbit retina." *J. Neurophysiol.* 78.4, pp. 2048–2060 (cit. on pp. 6, 41, 42, 46, 47, 69, 75, 78).



- Donoho, D. L. and Johnstone, I. M. (1994). "Ideal Spatial Adaption by Wavelet Shrinkage". *Biometrika* 81.3, pp. 425–455 (cit. on p. 14).
- Dowling, J. E. (1987). *The Retina: An Approachable Part of the Brain*. Cambridge, MA: Harvard University Press (cit. on pp. 1, 2).
- Dowling, J. E. and Werblin, F. S. (1969). "Organization of retina of the mudpuppy, *Necturus maculosus*. I. Synaptic structure." *J. Neurophysiol.* 32.3, pp. 315–338 (cit. on p. 10).
- Eglen, S. and Ooyen, A. van (1999). "Modelling retinal mosaic development with dendritic outgrowth and lateral cell movement". In: *9th Int. Conf. Artif. Neural Networks ICANN '99*. Vol. 1, pp. 377–382 (cit. on p. 44).
- Enroth-Cugell, C. and Robson, J. G. (1966). "The contrast sensitivity of retinal ganglion cells of the cat." *J. Physiol.* 187.3, pp. 517–552 (cit. on p. 4).
- Farrow, K. and Masland, R. H. (2011). "Physiological clustering of visual channels in the mouse retina." *J. Neurophysiol.* 105.4, pp. 1516–1530 (cit. on pp. 47, 53).
- Field, G. D. and Chichilnisky, E. J. (2007). "Information processing in the primate retina: circuitry and coding." *Annu. Rev. Neurosci.* 30, pp. 1–30 (cit. on pp. 41, 42, 79).
- Field, G. D., Sher, A., Gauthier, J. L., Greschner, M., Shlens, J., Litke, A. M., and Chichilnisky, E. J. (2007). "Spatial properties and functional organization of small bistratified ganglion cells in primate retina." *J. Neurosci.* 27.48, pp. 13261–72 (cit. on pp. 6, 15, 42, 47, 75, 78).
- Galli-Resta, L., Resta, G., Tan, S. S., and Reese, B. E. (1997). "Mosaics of islet-1-expressing amacrine cells assembled by short-range cellular interactions." *J. Neurosci.* 17.20, pp. 7831–7838 (cit. on p. 44).
- Garvert, M. M. and Gollisch, T. (2013). "Local and global contrast adaptation in retinal ganglion cells". *Neuron* 77.5, pp. 915–928 (cit. on p. 10).
- Gauthier, J. L., Field, G. D., Sher, A., Greschner, M., Shlens, J., Litke, A. M., and Chichilnisky, E. J. (2009). "Receptive fields in primate retina are coordinated to sample visual space more uniformly". *PLoS Biol.* 7.4, pp. 0747–0755 (cit. on pp. 6, 19, 42, 79).
- Gollisch, T. and Meister, M. (2010). "Eye Smarter than Scientists Believed: Neural Computations in Circuits of the Retina". *Neuron* 65.2, pp. 150–164. arXiv: NIHMS150003 (cit. on pp. 1, 79).
- Gordon, A. D. (1990). "Constructing dissimilarity measures". *J. Classif.* 7.2, pp. 257–269 (cit. on pp. 24, 29).
- Grabowski, S. R., Pinto, L. H., and Pak, W. L. (1972). "Adaptation in retinal rods of axolotl: intracellular recordings." *Science* 176.40, pp. 1240–1243 (cit. on p. 10).
- Hare, W. A., Lowe, J. S., and Owen, G. (1986). "Morphology of physiologically identified bipolar cells in the retina of the tiger salamander, *Ambystoma tigrinum*." *J. Comp. Neurol.* 252.1, pp. 130–138 (cit. on p. 77).

## Bibliography

- Hartline, H. K. (1938). "The response of single optic nerve fibers of the vertebrate eye to illumination of the retina". *Am J Physiol*, pp. 400–415 (cit. on pp. 3, 4, 9).
- Hartline, H. K. (1940a). "The effects of spatial summation in the retina on the excitation of fibers of the optic nerve". *Am. J. Physiol.* 130, pp. 700–711 (cit. on p. 9).
- Hartline, H. K. (1940b). "The receptive fields of optic nerve fibers". *Am. J. Physiol.* 130, pp. 690–699 (cit. on p. 9).
- Hastie, T., Tibshirani, R., and Friedman, J. (2009). *The Elements of Statistical Learning: Data Mining, Inference, and Prediction*. 2nd ed. Springer (cit. on pp. 23–28, 38, 54).
- Hochstein, B. S. and Shapley, R. M. (1976). "Quantitative analysis of Retinal Ganglion Cell Classifications". *J. Physiol.* Pp. 237–264 (cit. on p. 4).
- Hurley, J. B. (2002). "Shedding light on adaptation." *J. Gen. Physiol.* 119.2, pp. 125–128 (cit. on p. 1).
- Kastner, D. B. and Baccus, S. A. (2011). "Coordinated dynamic encoding in the retina using opposing forms of plasticity." *Nat. Neurosci.* 14.10, pp. 1317–22 (cit. on pp. 10, 47, 76, 78).
- Kastner, D. B. and Baccus, S. A. (2013). "Spatial segregation of adaptation and predictive sensitization in retinal ganglion cells". *Neuron* 79.3, pp. 541–554. arXiv: NIHMS150003 (cit. on pp. 10, 77).
- Koch, K., McLean, J., Segev, R., Freed, M. A., Berry, M. J., Balasubramanian, V., and Sterling, P. (2006). "How Much the Eye Tells the Brain". *Curr. Biol.* 16.14, pp. 1428–1434 (cit. on p. 79).
- Kuffler, S. W. (1953). "Discharge Patterns and Functional Organization of Mammalian Retina". *J. Neurophysiol.* 16.1, pp. 37–68 (cit. on p. 4).
- Kühn, N. K. and Gollisch, T. (2012). "The encoding of object motion and motion direction in the retina". *Frontiers in Computational Neuroscience Conference Abstract: Bernstein Conference 2012* (cit. on p. 77).
- Lasansky, A. (1973). "Organization of the outer synaptic layer in the retina of the larval tiger salamander." *Philos. Trans. R. Soc. Lond. B. Biol. Sci.* 265.872, pp. 471–489 (cit. on p. 10).
- Lettvin, J. Y., Maturana, H. R., McCulloch, W. S., and Pitts, W. H. (1959). "What the frog's eye tells the frog's brain". *Proc. Inst. Radio Eng.* 47, pp. 1940–1951 (cit. on p. 5).
- Levick, W. R. (1967). "Receptive Fields and Trigger Features of Ganglion Cells in the Visual Streak of the Rabbit's Retina". *J. Physiol.* 188, pp. 285–307 (cit. on p. 5).
- Lewicki, M. S. (1998). "A review of methods for spike sorting: the detection and classification of neural action potentials." *Network* 9.4, pp. R53–R78 (cit. on p. 13).
- Li, P. H., Gauthier, J. L., Schiff, M., Sher, A., Ahn, D., Field, G. D., Greschner, M., Callaway, E. M., Litke, A. M., and Chichilnisky, E. J. (2015). "Anatomical Identi-

- fication of Extracellularly Recorded Cells in Large-Scale Multielectrode Recordings". *J. Neurosci.* 35.11, pp. 4663–4675 (cit. on p. 14).
- Liao, S. H. (2005). "Expert system methodologies and applications-a decade review from 1995 to 2004". *Expert Syst. Appl.* 28.1, pp. 93–103 (cit. on p. 23).
- Luxburg, U. von (2007). "A tutorial on spectral clustering". *Stat. Comput.* 17.4, pp. 395–416. arXiv: 0711.0189 (cit. on pp. 28–33, 39).
- Marimont, R. B. and Shapiro, M. B. (1979). "Nearest Neighbour Searches and the Curse of Dimensionality". *IMA J. Appl. Math.* 24.1, pp. 59–70 (cit. on p. 54).
- Marre, O., Amodei, D., Deshmukh, N., Sadeghi, K., Soo, F., Holy, T. E., and Berry, M. J. (2012). "Mapping a Complete Neural Population in the Retina". *J. Neurosci.* 32.43, pp. 14859–14873 (cit. on pp. 10, 41, 47, 75, 76, 78).
- Masland, R. H. (2001). "The fundamental plan of the retina." *Nat. Neurosci.* 4.9, pp. 877–86 (cit. on p. 42).
- Masland, R. H. (2004). "Neuronal cell types." *Curr. Biol.* 14.13, pp. R497–R500 (cit. on p. 79).
- Masland, R. H. (2012). "The Neuronal Organization of the Retina". *Neuron* 76.2, pp. 266–280 (cit. on pp. 1, 3, 7, 79).
- McCusker, C. and Gardiner, D. M. (2011). "The axolotl model for regeneration and aging research: A mini-review". *Gerontology* 57.6, pp. 565–571 (cit. on p. 9).
- Meila, M. and Shi, J. (2001). "Learning Segmentation by Random Walks". In: *Adv. Neural Inf. Process. Syst.* 13. Ed. by T. K. Leen, T. G. Dietterich, and V. Tresp. MIT Press, pp. 873–879 (cit. on pp. 29–33).
- Miller, R. F. and Dacheux, R. F. (1976). "Synaptic organization and ionic basis of on and off channels in mudpuppy retina. III. A model of ganglion cell receptive field organization based on chloride-free experiments." *J. Gen. Physiol.* 67.6, pp. 679–690 (cit. on p. 10).
- Mobbs, P., Brew, H., and Attwell, D. (1988). "A quantitative analysis of glial cell coupling in the retina of the axolotl (*Ambystoma mexicanum*)." *Brain Res.* 460.2, pp. 235–245 (cit. on p. 10).
- Ng, A. Y., Jordan, M. I., and Weiss, Y. (2002). "On Spectral Clustering: Analysis and an Algorithm". *Adv. Neural Inf. Process. Syst.* 14. Ed. by T. G. Dietterich, S. Becker, and Z. Ghahramani, pp. 849–856 (cit. on pp. 29, 32–34, 53).
- Ölveczky, B. P., Baccus, S. A., and Meister, M. (2003). "Segregation of object and background motion in the retina." *Nature* 423.6938, pp. 401–408 (cit. on pp. 10, 77).
- Paninski, L. (2003). "Convergence properties of three spike-triggered analysis techniques." *Network* 14.3, pp. 437–64 (cit. on pp. 16, 17).
- Paninski, L., Pillow, J., and Lewi, J. (2007). "Statistical models for neural encoding, decoding, and optimal stimulus design". *Prog. Brain Res.* 165, pp. 493–507 (cit. on p. 17).

## Bibliography

- Peichl, L. and Wässle, H. (1981). "Morphological Identification of on- and off-Centre Brisk Transient (Y) Cells in the Cat Retina". *Proc. R. Soc. Lond. B. Biol. Sci.* 212.1187, pp. 139–153 (cit. on p. 5).
- Pillow, J. W., Shlens, J., Chichilnisky, E. J., and Simoncelli, E. P. (2013). "A Model-Based Spike Sorting Algorithm for Removing Correlation Artifacts in Multi-Neuron Recordings". *PLoS One* 8.5, pp. 1–14 (cit. on p. 13).
- Pouzat, C., Mazor, O., and Laurent, G. (2002). "Using noise signature to optimize spike-sorting and to assess neuronal classification quality." *J. Neurosci. Methods* 122.1, pp. 43–57 (cit. on p. 14).
- Puchalla, J. L., Schneidman, E., Harris, R. A., and Berry, M. J. (2005). "Redundancy in the population code of the retina." *Neuron* 46, pp. 493–504 (cit. on pp. 6, 75).
- Quiroga, R. Q., Nadasdy, Z., and Ben-Shaul, Y. (2004). "Unsupervised spike detection and sorting with wavelets and superparamagnetic clustering." *Neural Comput.* 16.8, pp. 1661–87 (cit. on p. 14).
- Reese, B. E. (1999). "Modelling the mosaic organization of rod and cone photoreceptors with a minimal-spacing rule". *Eur. J. Neurosci.* 11.4, pp. 1461–1469 (cit. on p. 44).
- Rieke, F., Warland, D., Ruyter van Steveninck, R. de, and Bialek, W. (1999). *Spikes: Exploring the Neural Code*. Cambridge, MA, USA: MIT Press (cit. on pp. 21, 49).
- Rockhill, R. L., Euler, T., and Masland, R. H. (2000). "Spatial order within but not between types of retinal neurons." *Proc. Natl. Acad. Sci. U. S. A.* 97.5, pp. 2303–2307 (cit. on pp. 6, 42, 78).
- Rodieck, R. W. (1965). "Quantitative analysis of cat retinal ganglion cell response to visual stimuli". *Vision Res.* 5.12, pp. 583–601 (cit. on p. 4).
- Rodieck, R. W. (1979). "Visual pathways." *Annu. Rev. Neurosci.* 2, pp. 193–225 (cit. on p. 5).
- Rodieck, R. W. (1991). "The density recovery profile: a method for the analysis of points in the plane applicable to retinal studies." *Vis. Neurosci.* 6.2, pp. 95–111 (cit. on pp. 43–45).
- Rodieck, R. W. (1998). *The First Steps in Seeing*. Sunderland, MA: Sinauer Associates, Inc. (cit. on pp. 1–3).
- Rodieck, R. W. and Stone, J. (1965a). "Analysis of receptive fields of cat retinal ganglion cells." *J. Neurophysiol.* 28.5, pp. 832–849 (cit. on p. 4).
- Rodieck, R. W. and Stone, J. (1965b). "Response of cat retinal ganglion cells to moving visual patterns". *J. Neurophysiol.* 28.5, pp. 819–832 (cit. on p. 4).
- Rowe, M. H. and Stone, J. (1980). "The interpretation of variation in the classification of nerve cells." *Brain. Behav. Evol.* 17.2, pp. 123–151 (cit. on p. 42).
- Samuel, M. A., Zhang, Y., Meister, M., and Sanes, J. R. (2011). "Age-Related Alterations in Neurons of the Mouse Retina". *J. Neurosci.* 31.44, pp. 16033–16044 (cit. on p. 79).

- Sanes, J. R. and Masland, R. H. (2015). "The Types of Retinal Ganglion Cells: Current Status and Implications for Neuronal Classification". *Annu. Rev. Neurosci.* 38.1, pp. 221–246 (cit. on pp. 1, 3, 41, 42, 78, 79).
- Schwartz, O., Pillow, J. W., Rust, N. C., and Simoncelli, E. P. (2006). "Spike-triggered neural characterization." *J. Vis.* 6, pp. 484–507 (cit. on pp. 16, 17).
- Schwarz, G. (1978). "Estimating the Dimension of a Model". *Ann. Stat.* 6.2, pp. 461–464 (cit. on p. 38).
- Segev, R., Puchalla, J., and Berry, M. J. (2006). "Functional organization of ganglion cells in the salamander retina." *J. Neurophysiol.* 95.4, pp. 2277–2292 (cit. on pp. 6, 7, 10, 41, 47, 48, 53, 75–78).
- Shamim, K. M., Tóth, P., Becker, D. L., and Cook, J. E. (1999). "Large retinal ganglion cells that form independent, regular mosaics in the bufonoid frogs *Bufo marinus* and *Litoria moorei*." *Vis. Neurosci.* 16.5, pp. 861–879 (cit. on pp. 41, 43, 78).
- Sharpee, T., Rust, N. C., and Bialek, W. (2004). "Analyzing neural responses to natural signals: maximally informative dimensions." *Neural Comput.* 16.2, pp. 223–250. arXiv: 0212110 [physics] (cit. on p. 17).
- Shi, J. and Malik, J. (2000). "Normalized Cuts and Image Segmentation". *IEEE Trans. Pattern Anal. Mach. Intell.* 22.8, pp. 888–905. arXiv: 0703101v1 [cs] (cit. on pp. 29–33).
- Shinomoto, S., Shima, K., and Tanji, J. (2003). "Differences in spiking patterns among cortical neurons." *Neural Comput.* 15.12, pp. 2823–2842 (cit. on pp. 22, 65).
- Stevens, C. F. (1998). "Neuronal diversity: too many cell types for comfort?" *Curr. Biol.* 8.20, pp. R708–R710 (cit. on p. 79).
- Stevenson, I. H. and Kording, K. P. (2011). "How advances in neural recording affect data analysis." *Nat. Neurosci.* 14.2, pp. 139–142. arXiv: NIHMS150003 (cit. on pp. 6, 78, 79).
- Stone, J. and Fukuda, Y. (1974). "Properties of cat retinal ganglion cells: a comparison of W-cells with X-and Y-cells". *J. Neurophysiol.* 37.4, pp. 722–748 (cit. on p. 5).
- Takeshita, D. and Gollisch, T. (2014). "Nonlinear spatial integration in the receptive field surround of retinal ganglion cells." *J. Neurosci.* 34.22, pp. 7548–61 (cit. on p. 10).
- Taurog, A. (1974). "Effect of TSH and long-acting thyroid stimulator on thyroid <sup>131</sup>I-metabolism and metamorphosis of the Mexican axolotl (*Ambystoma mexicanum*)." *Gen. Comp. Endocrinol.* 24.3, pp. 257–266 (cit. on p. 9).
- Taurog, A., Oliver, C., Eskay, R. L., Porter, J. C., and McKenzie, J. M. (1974). "The role of TRH in the neoteny of the Mexican axolotl (*Ambystoma mexicanum*)." *Gen. Comp. Endocrinol.* 24.3, pp. 267–279 (cit. on p. 9).

## Bibliography

- Tessier-Lavigne, M., Attwell, D., Mobbs, P., and Wilson, M. (1988). "Membrane Currents in Retinal Bipolar Cells of the Axolotl". *J. Gen. Physiol.* 91.1, pp. 49–72 (cit. on p. 10).
- Thorndike, R. L. (1953). "Who belongs in the family?" *Psychometrika* 18.4, pp. 267–276 (cit. on p. 38).
- Tibshirani, R., Walther, G., and Hastie, T. (2001). "Estimating the number of clusters in a data set via the gap statistic". *J. R. Statist. Soc. B* 63, pp. 411–423 (cit. on p. 38).
- Toris, C. B., Eiesland, J. L., and Miller, R. F. (1995). "Morphology of ganglion cells in the neotenus tiger salamander retina". *J. Comp. Neurol.* 352.4, pp. 535–559 (cit. on p. 77).
- Vaney, D. I., He, S., Taylor, W. R., and Levick, W. R. (2001). "Direction-selective ganglion cells in the retina". In: *Motion Vision - Computational, Neural, and Ecological Constraints*. Ed. by J. M. Zanker and J. Zeil (cit. on p. 20).
- Wässle, H. and Boycott, B. B. (1991). "Functional architecture of the mammalian retina." *Physiol. Rev.* 71.2, pp. 447–480 (cit. on pp. 5, 6).
- Wässle, H., Boycott, B. B., and Illing, R. B. (1981). "Morphology and mosaic of on- and off-beta cells in the cat retina and some functional considerations." *Proc. R. Soc. Lond. B. Biol. Sci.* 212.1187, pp. 177–195 (cit. on pp. 5, 42).
- Wässle, H., Peichl, L., and Boycott, B. B. (1981). "Morphology and topography of on- and off-alpha cells in the cat retina." *Proc. R. Soc. Lond. B. Biol. Sci.* 212.1187, pp. 157–175 (cit. on pp. 5, 41, 42, 78).
- Wässle, H. and Riemann, H. J. (1978). "The Mosaic of Nerve Cells in the Mammalian Retina". *Proc. R. Soc. Lond. B. Biol. Sci.* 200.1141, pp. 441–461 (cit. on pp. 5, 42, 43).
- Wässle, H. (2004). "Parallel processing in the mammalian retina." *Nat. Rev. Neurosci.* 5.10, pp. 747–757 (cit. on pp. 1, 3).
- Werblin, F. S. and Dowling, J. E. (1969). "Organization of the retina of the mudpuppy, *Neturus maculosus*. II. Intracellular recording." *J. Neurophysiol.* 32, pp. 339–355 (cit. on p. 10).
- Wong-Riley, M. T. (1974). "Synaptic organization of the inner plexiform layer in the retina of the tiger salamander." *J. Neurocytol.* 3.1, pp. 1–33 (cit. on p. 10).
- Wunk, D. F. and Werblin, F. S. (1979). "Synaptic inputs to the ganglion cells in the tiger salamander retina." *J. Gen. Physiol.* 73.3, pp. 265–286 (cit. on p. 10).
- Zeck, G. M. and Masland, R. H. (2007). "Spike train signatures of retinal ganglion cell types." *Eur. J. Neurosci.* 26.2, pp. 367–80 (cit. on pp. 21, 47, 53).
- Zhang, Y., Kim, I.-J., Sanes, J. R., and Meister, M. (2012). "The most numerous ganglion cell type of the mouse retina is a selective feature detector". *Proc. Natl. Acad. Sci.* 109.36, pp. E2391–E2398 (cit. on pp. 41, 78).

## ACRONYMS

---

AIC	Akaike information criterion
BIC	Bayesian information criterion
DS	direction-selective
DSI	direction selectivity index
EM	expectation maximization algorithm
ISI	inter-spike interval
LNP	linear-nonlinear-Poisson model
MEA	multi-electrode array
PCA	principal component analysis
RGC	retinal ganglion cell
STA	spike-triggered average
SVD	singular value decomposition





## CURRICULUM VITAE

---

FERNANDO OHLWEILER ROZENBLIT

08.10.1987 Born in Recife, Pernambuco (Brazil)

### EDUCATION:

2005–2008 Bachelor's degree in Physics,  
at the Federal University of Pernambuco (UFPE), Brazil

2009–2011 Master's degree in Physics,  
with Prof. Dr. Mauro Copelli (advisor)  
at the Federal University of Pernambuco (UFPE), Brazil  
Thesis title: "Collective oscillations in networks of probabilistic excitable cellular automata"  
(orig.: "Oscilações coletivas em redes de autômatos celulares probabilísticos excitáveis")

2011–2015 Doctoral degree in Natural Sciences,  
with Prof. Dr. Tim Gollisch (advisor)  
in the program of Theoretical and Computational Neuroscience (GGNB)  
at the Georg-August-Universität Göttingen, Germany

### COURSES:

01/2010 III Latin American School on Computational Neuroscience – LASCON,  
Ribeirao Preto, SP, Brazil

03/2012 4th G-Node Winter Course in Neural Data Analysis,  
Munich, Germany  
(Sponsored by a GGNB Travel Grant)

07/2013 Berkeley Summer Course in Mining and Modeling of Neuroscience Data,  
Berkeley, USA  
(Partly sponsored by a GGNB Travel Grant)

### PUBLICATIONS:

2011 "Collective oscillations of excitable elements: order parameters, bistability  
and the role of stochasticity", F. Rozenblit and M. Copelli.  
*J. Stat. Mech*, P01012

#### COLOPHON

This document was typeset in L<sup>A</sup>T<sub>E</sub>X using the typographical look-and-feel classicthesis.  
The bibliography is typeset using biblatex.